NBSIR 88-3690
Report No. 14

Dynamic Mechanical Properties of Two AAR M128 and One ASTM A212-B Steel Tank Car Head Plates

J.G. Early, C.G. Interrante, S.R. Low, III, and B.A. Fields

U.S. DEPARTMENT OF COMMERCE
National Bureau of Standards
Institute for Materials Science and Engineering
Gaithersburg, MD 20899

February 1988

Issued June 1988

Prepared for:
Federal Railroad Administration
Department of Transportation

NBS-114A (REV. 2-8C)

U.S. DEPT. OF COMM. BIBLIOGRAPHIC DATA SHEET (See instructions)	1. PUBLICATION OR REPORT NO. NBSIR 88-3690	2. Performing Organ. Report No.	3. Publication Date JUNE 1988

4. TITLE AND SUBTITLE

Dynamic Mechanical Properties of Two AAR M128 and One ASTM A212-B Steel Tank Car Head Plates

5. AUTHOR(S)

J.G. Early, C.G. Interrante, S.R. Low III, and B.A. Fields

6. PERFORMING ORGANIZATION *(If joint or other than NBS, see instructions)*

NATIONAL BUREAU OF STANDARDS
U.S. DEPARTMENT OF COMMERCE
GAITHERSBURG, MD 20899

7. Contract/Grant No.

8. Type of Report & Period Covered

9. SPONSORING ORGANIZATION NAME AND COMPLETE ADDRESS *(Street, City, State, ZIP)*

Federal Railroad Administration
Department of Transportation
Washington, D.C.

10. SUPPLEMENTARY NOTES

☐ Document describes a computer program; SF-185, FIPS Software Summary, is attached.

11. ABSTRACT *(A 200-word or less factual summary of most significant information. If document includes a significant bibliography or literature survey, mention it here)*

Instrumented precracked Charpy impact testing and dynamic teat testing were carried out on steel plate samples taken from three railroad tank cars. Two of the samples were given as AARM128, a high strength carbon manganese steel, while the third was reported to be ASTM A212-65, a high strength carbon silicon steel. Values were found for the ranges of transition temperatures and for the energies absorbed, including crack initiation energy, crack propagation energy and total energy.

12. KEY WORDS *(Six to twelve entries; alphabetical order; capitalize only proper names; and separate key words by semicolons)*

crack initiation; crack propagation; dynamic mechanical properties; high strength steel; impact fracture; railorad tank car; transition temperature

13. AVAILABILITY

☒ Unlimited

☐ For Official Distribution. Do Not Release to NTIS

☐ Order From Superintendent of Documents, U.S. Government Printing Office, Washington, D.C. 20402.

☒ Order From National Technical Information Service (NTIS), Springfield, VA. 22161

14. NO. OF PRINTED PAGES

98

15. Price

$13.95

NBSIR 88-3690
Report No. 14

DYNAMIC MECHANICAL PROPERTIES OF TWO AAR M128 AND ONE ASTM A212-B STEEL TANK CAR HEAD PLATES

J.G. Early, C.G. Interrante, S.R. Low, III, and B.A. Fields

U.S. DEPARTMENT OF COMMERCE
National Bureau of Standards
Institute for Materials Science and Engineering
Gaithersburg, MD 20899

February 1988

Issued June 1988

Prepared for:
Federal Railroad Administration
Department of Transportation

U.S. DEPARTMENT OF COMMERCE, C. William Verity, *Secretary*
NATIONAL BUREAU OF STANDARDS, Ernest Ambler, *Director*

ABSTRACT

Instrumented precracked Charpy impact testing and dynamic tear testing were carried out on steel plate samples taken from three railroad tank cars. Two of the samples were given as AAR M128, a high strength carbon manganese steel, while the third was reported to be ASTM A212-65, a high strength carbon silicon steel. Values were found for the ranges of transition temperatures and for the energies absorbed, including crack initiation energy, crack propagation energy and total energy.

It should be noted that some of the transition temperatures obtained were within normal tank car service temperature ranges.

TABLE OF CONTENTS

Abstract

1. INTRODUCTION....1

2. PURPOSE....1

3. SIGNIFICANCE....1

3.1 Instrumented Charpy Impact Test....1
3.2 Precracked Charpy Specimen Tests....1

4. EXPERIMENTAL PROCEDURE....2

4.1 Instrumented Precracked Charpy Tests....2
4.1.1 Specimens....2
4.1.2 Test Method....2
4.1.3 Absorbed Energy Calculation....2
4.1.4 True Energy Calculation....3
4.1.5 Total Energy Absorbed....4
4.1.6 Calculation of Dynamic Fracture Toughness....4
4.1.6.1 Linear Elastic Fracture Toughness....4
4.1.6.2 Post General Yield Fracture Toughness.5
4.1.7 Calculation of Dynamic Yield Stress....5
4.2 Dynamic Tear Tests 5

5. PREVIOUS RESULTS....5

5.1 Compositions and Properties....5
5.2 Charpy V-notch Tests....5

6. RESULTS AND DISCUSSION....6

6.1 Instrumented Precracked Charpy Tests....6
6.1.1 Energy Absorption-Raw Data Values....6
6.1.2 Transition Temperatures....7
6.1.3 Normalized Energy....7
6.1.3.1 Total Energy....7
6.1.3.2 Initiation Energy....7
6.1.3.3 Propagation Energy....7
6.1.3.4 Transition Temperatures....7
6.1.4 Dynamic Fracture Toughness....8
6.1.5 Dynamic Yield Stress....8
6.2 Dynamic Tear Tests....8

7. CONCLUSIONS....9

8. ACKNOWLEDGEMENTS....10

REFERENCES....11

TABLE OF CONTENTS (cont.)

TABLES.....12

APPENDIX A.....17

APPENDIX B.....18

APPENDIX C.....19

APPENDIX D.....20

FIGURES.....43

TABLES

1. Chemical Compositions of Plates G and U

2. Chemical Compositions of Plate S

3. Tensile Properties of Plates G and U

4. Tensile Properties of Plate S

5. Charpy V-notch Impact and Drop Weight Transition Temperatures for Plates G, U, and S

APPENDICES

A. Limitations Required for a Valid Instrumented Precracked Charpy Test.

B. Compliance Calculations

C. Values of the Function h(a/W) Used to Calculate K_{ID}.

D. Instrumented Precracked Charpy Impact Test Results.

Table D1. Raw Data for LT Orientation, Plate G.

Table D2. Results of Evaluation for LT Orientation, Plate G.

Table D3. Compliance Values for LT Orientation, Plate G.

Table D4. Raw Data for TL Orientation, Plate G.

Table D5. Results of Evaluation for TL Orientation, Plate G.

Table D6. Compliance Values for TL Orientation, Plate G.

Table D7. Raw Data for LT Orientation, Plate U.

Table D8. Results of Evaluation for LT Orientation, Plate U.

Table D9. Compliance Values for LT Orientation, Plate U.

Table D10. Raw Data for TL Orientation, Plate U.

Table D11. Results of Evaluation for TL Orientation, Plate U.

Table D12. Compliance Values for TL Orientation, Plate U.

Table D13. Raw Data for LT Orientation, Plate S.

Table D14. Results of Evaluation for LT Orientation, Plate S.

Table D15. Compliance Values for LT Orientation, Plate S.

Table D16. Raw Data for TL Orientation, Plate S.

Table D17. Results of Evaluation for TL Orientation, Plate S.

Table D18. Compliance Values for TL Orientation, Plate S.

FIGURES

Figure 1. Idealized Load-Time Record for a Three Point Bend Specimen.

Figure 2. Charpy V-notch-Energy Absorption Results for Plate G.

Figure 3. Charpy V-notch-Energy Absorption Results for Plate U.

Figure 4. Charpy V-notch-Energy Absorption Results for Plate S.

Figure 5. Charpy V-notch-Lateral Expansion Results for Plate G.

Figure 6. Charpy V-notch-Lateral Expansion Results for Plate U.

Figure 7. Charpy V-notch-Lateral Expansion Results for Plate S.

Figure 8. Charpy V-notch-Shear Fracture Appearance Results for Plate G.

Figure 9. Charpy V-notch-Shear Fracture Appearance Results for Plate U.

Figure 10. Charpy V-notch-Shear Fracture Appearance Results for Plate S.

Figure 11. Precracked Charpy-Total Energy Absorption Results for Plate G.

Figure 12. Precracked Charpy-Total Energy Absorption Results for Plate U.

Figure 13. Precracked Charpy-Total Energy Absorption Results for Plate S.

Figure 14. Comparison of Total Energy Absorbed for Plates G, U, and S.

Figure 15. Precracked Charpy-Energy Absorbed to Maximum Load for Plate G.

Figure 16. Precracked Charpy-Energy Absorbed to Maximum Load for Plate U.

Figure 17. Precracked Charpy-Energy Absorbed to Maximum Load for Plate S.

Figure 18. Comparison of Energy Absorbed to Maximum Load for Plates G, U, and S.

Figure 19. Comparison of Total Energy and Energy Absorbed to Maximum Load for Plate G.

Figure 20. Comparison of Total Energy and Energy Absorbed to Maximum Load for Plate U.

Figure 21. Comparison of Total Energy and Energy Absorbed to Maximum Load for Plate S.

Figure 22. Comparison of Total Energy and Energy Absorbed to Maximum Load for Plates G, U, and S.

Figure 23. Precracked Charpy-Normalized Total Energies for Plate G.

Figure 24. Precracked Charpy-Normalized Total Energies for Plate U.

Figure 25. Precracked Charpy-Normalized Total Energies for Plate S.

Figure 26. Precracked Charpy-Normalized Initiation Energies for Plate G.

Figure 27. Precracked Charpy-Normalized Initiation Energies for Plate U.

Figure 28. Precracked Charpy-Normalized Initiation Energies for Plate S.

Figure 29. Precracked Charpy-Normalized Propagation Energies for Plate G.

Figure 30. Precracked Charpy-Normalized Propagation Energies for Plate U.

Figure 31. Precracked Charpy-Normalized Propagation Energies for Plate S.

Figure 32. Fracture Toughness Values for Plate G.

Figure 33. Fracture Toughness Values for Plate U.

Figure 34. Fracture Toughness Values for Plate S.

Figure 35. Comparison of K_{ID} Values for Plates G, U, and S.

Figure 36. Comparison of K_{JD} Values for Plates G, U, and S.

Figure 37. Dynamic Yield Stresses for Plate G.

Figure 38. Dynamic Yield Stresses for Plate U.

Figure 39. Dynamic Yield Stresses for Plate S.

Figure 40. Dynamic Tear-Energy Absorption Values for Plate G.

Figure 41. Dynamic Tear-Energy Absorption Values for Plate S.

Figure 42. Comparison of Dynamic Tear Results for Plates G and S.

Figure 43. Comparison of Results for CVN, PCI, and DT Tests for Plate G.

Figure 44. Comparison of Results for CVN and PCI Tests for Plate U.

Figure 45. Comparison of Results for CVN, PCI, and DT Tests for Plate S.

TABLE OF SYMBOLS

B	-	thickness of the Charpy specimen
W	-	depth of the Charpy specimen
a	-	length of the notch plus the sharp crack
S	-	support span of the specimen
U	-	energy absorbed during impact
U_o	-	total energy available at impact
U_a	-	energy absorbed at time t
U_M	-	energy absorved at maximum load
E_M	-	true energy absorbed by the specimen at maximum load
v	-	initial impact velocity
m	-	effective mass of the falling weight
P	-	load at time t
P_M	-	maximum load
P_{GY}	-	load at general yield
d	-	displacement
C_S	-	specimen compliance
C_M	-	machine compliance
C_T	-	total compliance
K_{ID}	-	dynamic fracture toughness
K_{JD}	-	dynamic fracture toughness calculated using the J integral
$\dot{K}$	-	stress intensity rate
E	-	Young's modulus
σ_{YD}	-	dynamic yield stress

1. INTRODUCTION

The National Bureau of Standards was requested by the Federal Railroad Administration, Department of Transportation to conduct metallurgical evaluations of three steel plate samples taken from three railroad tank cars. These tank cars were identified as SOEX 3033, GATX 93412 and UTLX 38498. The details and history of the three tank cars were discussed in previous reports[1,2]. For simplicity, the three plate samples will be referred to as S, G and U respectively. Plate S was reported to be ASTM A212-65, a high tensile strength, carbon-silicon steel. Plates G and U were reported to be AAR M128, a high strength carbon manganese steel.

Previous NBS Reports[1,2] have determined that plates G and U met the chemical, tensile strength, and tensile ductility requirements of AAR M128 steel. Plate S, however, while satisfying the chemical and tensile elongation requirements of ASTM A212-65 steel, failed to meet those for minimum yield and tensile strengths.

For plates G, U, and S the nil-ductility transition (NDT) temperatures were determined to be -20°F, -40°F, and 30°F respectively. The 15 ft-lbs energy absorption temperatures were found to be approximately -50°F, -45°F, and 67°F, respectively. The values determined for plate S are of considerable concern as they are well within the normal tank car service temperature range.

2. PURPOSE

The purpose of the present evaluation is to study further the impact test behaviors of these plate samples. Both instrumented precracked Charpy tests and dynamic tear tests were carried out over the temperature range of interest.

3. SIGNIFICANCE

3.1. Instrumented Charpy Impact Test

This test augments the information provided by a standard Charpy impact test. Strain gauges placed on the striking tup are used to sense the load variation with time. A typical load-time plot is shown in Figure 1. Such a plot may be integrated to obtain energies at specified points on the curve, e.g., at yield or maximum load.

3.2. Precracked Charpy Specimen Tests

In a precracked Charpy specimen the standard V notch is extended by fatigue cracking to produce a sharp crack representing the most severe condition found in practice. In a standard Charpy test the energy obtained includes both the energy for initiation of the crack and that for its propagation. The energy required to initiate a crack may be considerably greater than that for its propagation. Thus using only the total energy can mask the fact that in a given material the energy required to propagate a crack already present in the material may be quite low. If a precracked Charpy specimen is used the initiation energy will be a much smaller part of the total energy, thus giving

a more realistic value for propagation energy. This means that a precracked Charpy test more closely simulates the conditions under which an existing crack begins to extend.

Another reason for using precracked specimens is that results for tests where fracture occurs before general yield can be used to calculate a value for dynamic fracture toughness $K_{ID}(t_M)$. This can be correlated with the standard fracture toughness K_{IC}. The time value (t_M) (illustrated in Figure 1) is the time taken to reach maximum load and references the relative testing rate in units of seconds.

4. EXPERIMENTAL PROCEDURES

4.1. Instrumented Precracked Charpy Tests

4.1.1. Specimens

The nominal dimensions of the specimens were those given in ASTM E23-72 (Notched Bar Impact Testing of Metallic Materials)(Figure 4, Charpy type A). These are 0.394 in (10 mm) thick by 0.394 in (10 mm) deep by 2.165 in (55 mm) long. The machined notch was extended about 0.10 in (2.5 mm) by fatigue cycling such that the total depth of the notch plus the crack was between 0.177 (4.5 mm) and 0.217 in (5.5 mm). The fatigue precracking was carried out following the procedure given in ASTM E399-74.

Two orientations of specimens were used. In one the longitudinal specimen axis was aligned parallel to the rolling direction and the plane of notching was in the transverse direction. In the other the longitudinal axis was in the transverse direction while the notch plane in the rolling direction. These two orientations were given the standard notations of LT and TL.

4.1.2. Test method

The specimens were dynamically loaded in three point bending using a standard Charpy machine modified for acquisition of the load-time data. The tests were carried out in accordance with ASTM E23-72.

Additional requirements for acceptable frequency response, inertial oscillation dampening, velocity reduction and electronic curve fitting, as discussed by Server[3] are summarized in Appendix A.

4.1.3. Absorbed Energy Calculation

The energy absorbed (U) at any time (t) during the impact event can be computed from the instrumented tup load-time record as follows [3]

$$U = U_a\left(1 - \frac{U_a}{4U_o}\right) \qquad (1)$$

where U_o is the total available energy at impact, $1/2mV_o^2$, and U_a is determined at time t as follows:

$$U_a = V_o \int_o^t P dt \qquad (2)$$

where V_o is the initial impact velocity, P is the load, and m is the effective mass of the falling weight. The energy absorbed at maximum load, U_M, can be determined from the above expression when $t = t_M$ (see Figure 1).

When comparing energies absorbed in standard Charpy V-notch specimens and precracked specimens it should be noted that the ligament area, B(W-a) (where B is the specimen thickness, W is the depth, and a is the length of the notch plus the crack), will be smaller in the latter case because of the extension of the notch by fatigue cracking. Thus, it is not accurate to directly compare energies for the two types of specimens. A solution is to normalize the energy values by dividing by the fracture ligament area.

4.1.4. True Energy Calculations

The value of the energy calculated from the area under the load-time curve (equation 1) includes contributions due to the deflections of both the specimen and that of the testing machine. A calculation of true energy absorbed, therefore, needs to include a correction for the machine compliance.
For tests when fracture is linear elastic, the normalized value of E_M can be calculated directly from the area under the load-displacement curve:

$$E_M = \frac{P_M d}{2B(W-a)} \qquad (3)$$

where d is displacement. Since the specimen compliance C_S, is defined as

$$C_S = d/P \qquad (4)$$

it follows that

$$E_M = \frac{P_M^2 C_S}{2B(W-a)} \qquad (5)$$

For a calculation of C_S see Appendix B.

When general yield occurs before fracture a correction must be made to equation 1. If the total energy under the load-time curve is U_M, then the true energy absorbed at maximum load, E_M, is given by

$$E_M = U_M - \frac{P_M^2 C_M}{2B(W-a)} \qquad (6)$$

where C_M is the machine compliance and can be calculated from

$$C_M = C_T - C_S \qquad (7)$$

where C_T is the total system compliance. Therefore

$$E_M = U_M - \frac{P_M^2 (C_T - C_S)}{2B(W-a)} \qquad (8)$$

For a calculation of C_T see Appendix B.

The value of E_M obtained is a measure of the initiation energy, i.e. the energy required to initiate cracking.

4.1.5. Total Energy Absorbed

The values of total energy absorbed were obtained from the dial energy recorded. As was described in section 4.1.3. a direct comparison of energies absorbed in different specimens is achieved by normalizing the energy values by the fracture ligament area, i.e. by B(W-a).

4.1.6. Calculations of Dynamic Fracture Toughness

4.1.6.1. Linear Elastic Fracture Toughness

The dynamic fracture toughness, K_{ID} can be calculated from the measured value of maximum load, P_M, and the initial specimen dimensions, in the manner specified by ASTM Method E399-74. The general specimen size requirements of this method appear to be too conservative for dynamic testing [4][5]. It is therefore suggested by Server[3] that as long as general yielding has not occurred, a linear elastic value of fracture toughness can be calculated.

The relationship for K_{ID} in units of psi$\sqrt{in}$ (MPa$\sqrt{m}$), where B=W and S=4W is

$$K_{ID} = P_M h(a/W) \qquad (9)$$

where B is specimen thickness, S is the support span, W is the specimen depth, a is the crack length and the function h(a/W) is given in Appendix C.

The fracture toughness values can be reported as $K_{ID}(t_M)$ where the time value, t_M, references the relative testing rate in units of seconds. The stress intensity rate, $\dot{K}$, can be calculated as

$$\dot{K} = K_{ID}/t_M \qquad (10)$$

For impact loading a minimum value of $\dot{K}$ obtained is of the order of 0.9×10^5ksi.in$^{1/2}$/s (1×10^5MPa$\cdot$m$^{1/2}$/s).

4.1.6.2. Post General Yield Fracture Toughness

When general yielding occurs a valid K_{ID} cannot be determined from a linear elastic analysis. An energy-based value of the J integral can be used to obtain a measure of fracture toughness.[3] When the initiation load can be determined and $a/W \geq 0.5$[6][7]

$$J_{ID} = 2E_M/B(W-a) \tag{11}$$

A dynamic value of the toughness K_{JD} can be given as

$$K_{JD} = (EJ_{ID})^{1/2} \tag{12}$$

where E is Young's Modulus. Therefore

$$K_{JD} = (2EE_M/B(W-a))^{1/2} \tag{13}$$

4.1.7. Dynamic Yield Stress

The dynamic yield stress, σ_{YD}, can be calcuated from an equation of the form[4]

$$\sigma_{YD} = AP_{GY} \frac{W}{B(W-a)^2} \tag{14}$$

where A is a constant. The upper and lower bounds for the value of A are given by Knott[8] to be about 2.5 and 4. For the present work, following Server[9, 10], a value of 3.3 was used.

4.2. Dynamic Tear Tests

Testing procedure followed that given in ASTM Method E604-77. The specimen dimensions were: length 7.125 in (181 mm), width 1.6 in (40.6 mm) and thickness 0.625 in (15.9 mm).

5. PREVIOUS RESULTS

5.1. Compositions and Properties

The chemical compositions, as determined by check chemical analyses of the plate samples, are given in Tables 1 and 2. Results of these analyses along with those for macroscopic observations, metallographic analyses, hardness measurements, bend behavior and inclusion contents were given and discussed in the two previous reports [1, 2]. Also given previously, and reproduced here, were the tensile properties (Tables 3 and 4) for all three plates.

5.2. Charpy V-notch Tests

Figures 2 - 10 are given for comparison with the present work. They show the results of the previously conducted Charpy V-notch (CVN) impact tests for both longitudinal (LT) and transverse (TL) specimens. These include results for

energy absorption, lateral expansion, shear fracture appearance and nil-ductility temperature. Table 5 shows the transition temperatures for four commonly reported fracture criteria: 15 ft-lbf energy absorption, 15 mil lateral expansion, 50% shear fracture appearance and nil ductility. These results have been discussed in the previous reports. Of note are the transition temperatures for plate S which all fall within the normal tank car service temperature range, e.g., a transition temperature of 67°F (19°C) for the 15 ft-lbs energy absorption. This is cause for concern since it indicates that for temperatures lower than 67°F (19°C) a crack that initiates may propagate in a brittle fashion, possibly leading to fracture.

6. RESULTS AND DISCUSSION

6.1. Instrumented Precracked Charpy Tests

The raw and calculated data for all the precracked tests are given in Appendix D, Tables D1 through D18. The tests from which these results were taken all satisfied the acceptance criteria as discussed in section 4.1.2. and Appendix A.

6.1.1. Energy Absorption - Raw Data Values

Figure 11-13 show the total energy absorbed, E_T, as measured by the dial gauge, for each of the plates, G, U, and S. Results are shown for both LT and TL specimens. Figure 14 compares these results. Figures 15-17 show the energy absorbed up to the point of maximum load, E_M. These values were calculated as described in section 4.1.3. Figure 18 compares the results presented in Figures 15-17. Figures 19-21 compare E_M and E_T for TL specimens taken from each plate. Figure 22 provides a comparison of all data in Figures 19-21.

It should be noted that Figures 11-22 show unnormalized energy absorption data. In order to compare these values with those obtained for standard CVN specimens they may be multiplied by $(W-a_1)/(W-a_2)$ where a_1 is the standard notch length and a_2 is the length of the notch plus the fatigue crack. This corrects for the different ligament areas as discussed in section 4.1.3. Using W = 0.394 in (10 mm), a_1 = 0.10 in (2.5 mm) and assuming that the fatigue crack is of length 0.10 in (2.5 mm), this factor becomes 1.5. Subsequent energy values quoted have been corrected in this fashion.

The value of E_M can be considered as a measure of the energy required to initiate an extension to an existing sharp crack. It can be seen in Figure 22 that these energies, when corrected as described, are very small, of the order of 5-6 ft-lbf (3.7 - 4.4 J) at the upper shelf and of less than 1 ft-lbf (.7 J) at the lower shelf. Thus, as stated earlier, very little energy is needed to initiate an extention of a sharp crack.

The values of E_T are within a range of 22 to 29 ft-lbf (16 - 21 J) for the upper shelf. These should be compared with the energies absorbed in the standard CVN TL specimens which fall in a range of about 37 - 47 ft-lbf (27 - 35 J) on the upper shelf (Figures 2 - 4). It can be seen, therefore, that the energies required to initiate and propagate an existing sharp crack are

considerably less that that needed to fracture a standard notched specimen.

6.1.2. Transition Temperatures

The transition region is the range of temperatures over which a transition from brittle to ductile fracture is observed. At lower temperatures in the range the fracture is predominately of a brittle or cleavage mode, while at higher temperatures fracture is dominated by a ductile or fibrous mode. For plates G and U the transition in precracked specimens occurs over a temperature range of approximately -70 to -10 F (-56 to -23C). For plate S the range is about 30 to 130 F (-1 to 54C). As noted previously for the CVN specimens the latter temperatures are within the range for normal tank car service. This indicates that brittle crack propagation may occur at the lower temperatures of this range.

6.1.3. Normalized Energy

6.1.3.1. Total Energy Absorbed

Figures 23-25 show the values of the E_T, the total energy absorbed for plates G, U, and S respectively. These values were obtained from the dial energy normalized by the ligament area as discussed in section 4.1.3.

6.1.3.2. Initiation Energy

Figures 26-28 show the initiation energies, E_M, for each of the plates. These values were obtained from the energy absorbed up to maximum load, U_M, corrected for the deflection of the testing machine as described in section 4.1.4. In this case 'initiation' means the point of extension of the already existing fatigue crack. It can be seen that on the lower shelf these values are very low - of the order of 57 in-lbf/in^2 (10 KJ/m^2) or less - for each of the plates.

6.1.3.3. Propagation Energy

The energy required for propagation of the crack was calculated as the difference between total energy absorbed and initiation energy. The results are plotted in Figures 29-31. For plates G and S the points are somewhat scattered making it hard to evaluate lower or upper shelf values. However it can be seen that these energies are considerably larger than those for initiation.

6.1.3.4. Transition Temperatures

The transition temperature ranges for total energies absorbed can be seen in Figures 23 - 25. For plate TL specimens of plate G this range is about -40 to 20 F (-40 to -29C), of plate U about -50 to 0F (-46 to -18C) and of plate S up to about 125F (52C). These compare with values found for the 15 ft-lbf energy absorption for TL specimens of -46F (-43C), -41F (-42C) and 67F (19C) for plates G, U, and S respectively.

6.1.4. Dynamic Fracture Toughness

Figures 32-34 show the dynamic fracture toughness versus temperature for each of the plates, G, U, and S. Figure 35 shows a comparison for valid K_{IC} results from the three plates. Figure 36 includes all the K_{JD} values for TL orientation specimens of each plate.

For plate G (Figure 32) valid K_{ID} values are of the order of 50 ksi$\sqrt{}$in (55 MPa$\sqrt{}$m). The highest temperature at which a valid result was obtained was 0F (-18C). The transition temperature range was about -13 to 14F (-25 to -10C). For the upper shelf there was a considerable difference in the toughness, K_{JD}, between the LT and TL orientations. The former had a toughness of the order of 200 ksi$\sqrt{}$in (220 MPa$\sqrt{}$m), while the latter was about 150 ksi$\sqrt{}$in (165 MPa$\sqrt{}$m). This difference between the two orientations was also found in the energy absorption results, see Figures 11 and 15. This is a consequence of a large difference in the times taken to reach maximum load, t_M, for specimens of the two orientations. For the TL specimens t_M is 3 to 5 times greater than for the LT specimens, as can be seen in Table D1.

For plate U (Figure 33) the results are not dependent on orientation. The lower shelf fracture toughness is about 50 ksi$\sqrt{}$m (55 MPa$\sqrt{}$m), while that of the upper shelf is of the order of 180 ksi$\sqrt{}$in (200 MPa$\sqrt{}$m). The transition temperature is around -15F (-26C). The highest temperature at which a valid K_{IC} was recorded was -30F (-34C).

For Plate S (Figure 34) the lower and upper shelves also have values of the order of 40 and 180 ksi$\sqrt{}$in (44 and 200 MPa$\sqrt{}$m) respectively. The most significant difference between Plate S and Plates G and U is that the transition temperature of the former is about 122F (50C), compared to a value of about -13F (-25C) for the latter two plates. A valid K_{ID} of 39 ksi$\sqrt{}$in (43 MPa$\sqrt{}$m) was obtained at a temperature of 125F (52C). This indicates that at temperatures up to around 125F (52C) an existing sharp crack subjected to impact loading could propagate in a brittle fashion, possibly causing failure.

6.1.5. Dynamic Yield Stress

Figures 37-39 show the results for dynamic yield stresses for plates G, U, and S, respectively. For plate G, there is a decrease in σ_{YD} with increasing temperature as would be expected. For plates U and S the results are so scattered that no trend is visible. At least part of this scatter is attributable to the variation in the rate of testing as shown by the values of t_M given in the raw data tables in Appendix D.

6.2. Dynamic Tear Tests

Figures 40 and 41 show the energy absorbed in the dynamic tear tests for plates G and S. No tests were carried out for plate U. Figure 42 compares the data from Figures 40 and 41. The results for plate G are somewhat scattered giving a wide range for the transition temperature of about 0 to 80F (-18 to 27C) which overlaps the range of about 60-80F (16 to 27C) for plate S. It should be noted that for both plates these ranges include normal service temperatures for tank cars.

Figures 43 and 45 show a comparison of energy absorption results for Charpy V-notch (CVN), precracked Charpy (PCI) and dynamic tear (DT) transverse specimens for plates G and S. The energy values are normalized so that the upper shelf energies are all equal to 100 ft-lbf. Figure 44 shows the same results for plate U with the exception of dynamic tear results which were not obtained for this plate. The purpose of these figures is to show the variation in transition temperature ranges for the three different tests.

For plate G the DT tests show a large upward shift of the transition temperature compared to those for CVN and PCI tests. Since the specimens for the DT test are larger than the Charpy specimens it is possible that the greater constraint in the former leads to a higher transition temperature range. As noted previously, this higher range includes normal operating temperatures. For plate U the CVN and PCI results show ranges similar to each other within experimental error. For plate S transition temperature ranges for all three tests are within normal service temperatures.

7. CONCLUSIONS

1. The results of the precracked Charpy tests show that:

   a. The lower shelf for the normalized total energy absorbed is of the order of 600 in-lbf/in^2 (105 KJ/m^2) for plates G and U and about 1000 in-lbf/in^2 (175 KJ/m^2) for plate S.

   b. The upper shelf for the normalized total absorbed energy is about 2300 in-lbf/in^2 (403 KJ/m^2) for TL specimens of G, and 2500 in-lbf/in^2 (438 KJ/m^2) for plate U and for TL specimens of plate S.

   c. The transition temperature range for plate G is approximately -40 to -20F (-40 to -29C), for plate U about -50 to 0F (-46 to -18C), and for plate S of up to 125 F (52C). For a plate containing a sharp crack, brittle propagation may occur at and below the lower end of this range. For plate S this is of concern since these temperatures include those found under normal service conditions.

   d. When a sharp crack is present in a plate the energy to initiate further cracking is of the order of 57 in-lbf/in^2 (10 KJ/m^2) or less for all three plates.

   e. Valid fracture toughness tests give K_{ID} values of about 46 ksi$\sqrt{}$in (50 MPa$\sqrt{}$m) for all three plates.

   f. Upper shelf values of post general yield fracture toughness, K_{JD}, are approximately 137 ksi$\sqrt{}$in (150 MPa$\sqrt{}$m) for all three plates.

   g. The transition temperatures for fracture toughness values are of the order of -13F (-25C) for plates G and U, and 122F (50C) for plate S.

   h. The dynamic yield stresses calculated show a wide scatter believed to be largely caused by differences in the rate of testing.

2. The results of the dynamic tear tests show that:

a. For plate G the transition temperature range is considerably higher than that for the precracked Charpy tests, i.e. about 0 to 120F (-18 to 49C) compared to about -40 to -20F (-40 to -29C). Since the specimens for the dynamic tear tests are larger than the Charpy specimens it is possible that the greater constraint in the former leads to a higher transition temperature range. It should be noted that this higher range includes normal service temperatures.

b. For plate S the transition temperature range for the dynamic tear test is about 60 to 130F (16 to 54C) compared to a precracked Charpy range of up to 125F (52C). Both ranges include normal service temperatures.

8. ACKNOWLEDGEMENTS

The authors wish to express thanks to Mr. D.E. Harne for his contribution to the mechanical testing involved in this project, and to Mrs. J. Vaughan for typing the manuscript and to the Federal Railroad Administration for support and valuable comments and advice.

REFERENCES

1. Early, J.G., "A Metallurgical Analysis of an ASTM A212-B Steel Tank Car Head Plate," Report No. NBSIR-78-1582, National Bureau of Standards, Sept. 1978.

2. Early, J.G., and Interrante, C.G., "A Metallurgical Evaluation of Two AAR M128 Steel tank Car Head Plates Used in Switchyard Imact Tests," Report No. NBSIR-80-2039, National Bureau of Standards, May 1980.

3. Server, W.L., "Impact Three-Point Bend Testing for Notched and Precracked Specimens," Journal of Testing and Evaluation, JTEVA, Vol. 6, No. 1, Jan. 1978, pp 29-34.

4. Server, W.L., Wullaert, R.A., and Sheckherd, J.W., "Verification of the EPRI Dynamic Fracture Toughness Testing Procedures, "Report TR75-42, Effects Technology, Inc., Santa Barbara, California, October 1975.

5. Wullaert, R.A., Oldfield, W., and Server, W.L., "Fracture Toughness Data for Ferritic Nuclear Pressure Vessel Materials: Task A, "Final Report to the Electric Power Research Institute on Research Project PR232-1, EPRI Report NP-121, Palo Alto, California, April 1976.

6. Rice, J.R., "Mathematical Analyses in the Mechanics of Fracture," in Fracture, An Advance Treatise, Vol. 2, H. Liebowitz, Ed., Academic Press, New York 1968.

7. Sumpter, J.D.G. and Turner, C.E., "Method for Laboratory Determination of J_c," in Cracks and Fracture, STP 601, American Society for Testing and Materials, Philadelphia, 1976, pp. 3-18.

8. Knott, J.F., "Fundamentals of Fracture Mechanics," Butterworths, 1973, pp. 37-38.

9. Server, W.L. and Wullaert, R.A., "Dynamic Three-Point Bend Analysis for Notched and Precracked Samples," Fracture Control Corporation, FCC 76-8, Aug. 1976.

10. Server, W.L., "Dynamic Fracture Toughness Determined from Instrumented Precracked Charpy Tests," UCLA-ENG-7267, Aug. 1972.

Table 1. Chemical Compositions of Plates G and U.

Percent by Weight

Element	Specification AAR M128-69 Ladle Analysis Grade A	Specification AAR M128-69 Ladle Analysis Grade B	Tank Car GATX 93412 Check Analysis	Tank Car UTLX 38498(d) (a) Check Analysis
Carbon	0.25 max		0.23	0.24
Manganese	1.35 max		1.15	1.24
Phosphorus	0.04 max		0.01	0.01
Sulfur	0.05 max		0.017	0.014
Silicon	0.30 max		0.19	0.28
Copper	(b)	0.35 max	0.02	0.06
Nickel	(b)	0.25 max	0.20	0.15
Chromium	(b)	0.25 max	0.09	0.06
Molybdenum	(b)	0.07 max	0.05	0.01
Vanadium	0.02 min	(c)	0.026	0.01
Aluminum	(c)		0.02	0.025

(a) Carbon was determined by combustion-conductometric analysis; all other elements were determined by emission spectroscopy.

(b) Element not specified.

(c) Element not specified, fine grain practice is required.

(d) Producers Report: UTLX 38498 plate sample is reported to be Kawasaki heat number 91-7850, AAR M128-B, with the ladle analysis of 0.25 carbon, 1.30 manganese, 0.0015 phosphorus, 0.0019 sulfur, 0.29 silicon, 0.08 copper, 0.15 nickel, 0.05 chromium, and 0.0015 molybdenum; all weight percent.

Table 2. Chemical Compositions of Plate S

Element	Percent by Weight Specification ASTM A212-65-B Ladle Analysis	Check Analysis[a]
Carbon	0.31 max	0.24
Manganese	0.90 max	0.73
Phosphorus	0.04 max	<0.005
Sulfur	0.05 max	0.026
Silicon	0.13/0.33[b]	0.26
Copper	(c)	<0.05
Nickel	(c)	<0.05
Chromium	(c)	0.07
Molybdenum	(c)	<0.05
Vanadium	(d)	<0.01
Aluminum	(d)	<0.01

(a) Carbon was determined by combusion-conductometric analysis; all other elements were determined by emission spectroscopy.

(b) Check analysis

(c) Element not specified

(d) Element not specified, either fine-or coarse-grain practice allowed.

Table 3. Tensile Properties of Plates G and U

Tank Car Identification	Specimen Orientation(a) and Code	Tensile Strength ksi	Yield Strength 0.2% Offset ksi	Yield Point ksi	Elongation Percent in one inch(b)	Reduction of Area Percent	Yield Point Observed
GATX 93412	Longitudinal - GL1	84.6	55.1	58.4	29.7	63.0	Yes, Large
GATX 93412	Longitudinal - GL2	84.1	55.4	58.1	33.7	63.5	Yes, Large
	Average	84.4	55.2	58.3	31.7	63.2	
GATX 93412	Transverse - GT1	90.5	56.5	57.3	26.8	57.3	Yes, Small
GATX 93412	Transverse - GT2	90.0	56.2	57.3	27.0	57.6	Yes, Small
	Average	90.2	56.4	57.3	26.9	57.4	
UTLX 38498	Longitudinal - UL	88.6	58.5	60.0	31.4	61.0	Yes, Large
UTLX 38498	Transverse - UT	88.2	52.8	N/A	33.9	61.0	No
UTLX 38498	45° - U1	88.8	57.9	61.4	30.6	61.0	Yes, Large
UTLX 38498	45° - U2	88.5	56.7	60.2	31.7	60.8	Yes, Large
UTLX 38498	45° - U3	87.9	54.4	55.4	30.1	61.0	Yes, Small
UTLX 39898	45° - U4	88.1	51.9	N/A	30.1	59.8	No
	Average	88.4	55.2	59.5	32.0	60.9	
Specification AAR M128-69		101.0 max (c) 81.0 min		50.0 min	19	(c)	

(a) Although the specification AAR M128-69 does not specify test specimen orientation, ASTM A370-73 does specify that wrought steel products are usually tested in the longitudinal direction but that where size permits and service justifies it, transverse testing is done.

(b) A comparison of elongation data obtained from different sizes of specimens of the same material can be made provided the ratio of the gage length to cross-sectional dimensions is held constant. Since the ratio of the square root of the cross-sectional area to the gage length is the same for the specimen with a 0.500-inch-diameter with a 2-inch-gage and for the specimen with a 0.250-inch-diamter with a 1-inch-gage length, the elongation data from the 1-inch-gage length specimen can be directly compared to the specification requirement based on a 2-inch-gage length.

(c) Not specified.

Table 4. Tensile Properties of Plate S

Specimen Orientation(a) and Code	Tensile Strength ksi	Yield Strength 0.2% Offset ksi	Yield Point ksi	Elongation Percent in one inch(b)	Reduction of Area Percent
Longitudinal - SL1	68.1	33.0	35.0	37.7	61.3
Longitudinal - SL2	67.7	33.0	33.4	37.1	61.5
Average	67.9	33.0	34.2	37.4	61.4
Transverse - ST1	67.7	32.2	34.3	35.5	56.4
Transverse - ST2	67.6	32.2	N/A	36.0	58.0
Average	67.6	32.2	34.3	35.8	57.2
Specification ASTM A212-B-65	85.0 max 70.0 min	(c)	38.0 min	21	(c)

(a) Although the specification ASTM A212-65 does not specify test specimen orientation, ASTM A370-73 does specify that wrought steel products are usually tested in the longitudinal direction but that where size permits and service justifies it, transverse testing is done.

(b) A comparison of elongation data obtained from different sizes of specimens of the same mateial can be made prodived the ratio of the gage length to cross-sectional dimensions is held constant. Since the ratio of the square root of the cross-sectional area to the gage length is the same for the specimen with a 0.500-inch-diameter with a 2-inch-gage and for the specimen with a 0.250-inch-diameter with a 1-inch-gage length, the elongation data from the 1-inch-gage length specimen can be directly compared to the specification requirement based on a 2-inch-gage length.

(c) Not specified.

Table 5. Charpy V-notch Impact and Drop Weight Transition Temperatures for Plates G, U, and S.

Plate	Specimen Orientation	Transition Temperature, F/C 15 ft-lbf Energy Absorption	15 mil Laterial Expansion	50% Shear Fracture	Nil Ductility Temp.
G	LT	-58F	-64	-30	-20
		-50C	-53	-34	-29
G	TL	-46	-50	-17	
		-43	-46	-27	
U	LT	-47	-46	-7	-40
		-44	-43	-22	-40
U	TL	-42	-46	4	
		-41	-43	16	
S	LT	66	50	111	30
		19	10	44	-1
S	TL	67	44	100	
		19	7	38	

APPENDIX A

Limitations Required for a Valid Test

As discussed in detail by Server[3] the following limitations need to be satisfied to ensure acceptable load and available energy values:

1. $t \geq 3\tau$ (A1)

where t is the time of any event being considered, and τ is related to the period of inertial oscillations in the contact load between tup and specimen. τ is predicted empirically for S/W = 4 to be

$$\tau = 3.36(W/S_o)(EBC_S)^{1/2} \quad \text{(A2)}$$

where W is specimen width, S is support span, B is specimen thickness, S_o is speed of sound in the specimen, E is Young's Modulus and C_S is specimen compliance. (See Appendix B.)

2. $t_M \geq 1.1\ T_R$ (A3)

where T_R is the frequency response time of the instrumentation and is given by

$$T_R = 0.35/f_{0.915db} \quad \text{(A4)}$$

where $f_{0.915dB}$ is the frequency at a 0.915db attenuation (10% voltage attenuation) of a sine wave superimposed on the output of the strain gauge bridge circuit.

3. $T_R \geq 1.4\tau$ (A5)

where T_R and τ are defined as in equation A1-A4. Specifying a minimum T_R for the curve fitting of the oscillations reduces the amplitude of the oscillations so that the disparity between tup contact load and the effective minimum load is minimal.

4. $U_o \geq 3E_M$ (A6)

where U_o is the total available energy at impact (section 4.1.3.) and E_M is the energy absorbed by the specimen at maximum load. This requirement is based on minimizing the reduction to hammer velocity during the period needed to reach maximum load.

APPENDIX B

Compliance Calculations

For each test specimen the compliance of the total system (C_T) and that of the specimen (C_S) were calculated. Subtracting C_S from C_T gave the machine compliance (C_M).

Server[3] gives an equation for the total system complicance calculated at general yield and corrected for the decrease in velocity through general yield:

$$C_T = (V_o t_{GY}/P_{GY}) - (V_o^2 t_{GY}/8E_o) \qquad (B1)$$

where V_o is the impact velocity, t_{GY} is time to general yield and P_{GY} is load at general yield. For typical values of V_o, t_{GY}, and E_o used in the present tests the second term of equation B1 is of the order of 0.1% of the first term and is thus not considered significant.

The specimen compliance C_S was calculated from

$$C_S = 72[f(a/W) + 0.215(1 - \nu)]/(EB) \qquad (B2)$$

where E is Young's Modulus, B is specimen thickness and f(a/W) is given by

$$1.86(a/W)^2 - 3.95(a/W)^3 + 16.4(a/W)^4 - 37.2(a/W)^5 + 77.6(a/W)^6$$
$$- 127(a/W)^7 + 173(a/W)^8 - 144(a/W)^9 + 66.6(a/W)^2 \qquad (B3)$$

The machine compliance C_M was obtained from

$$C_M = C_T - C_S \qquad (B4)$$

Values of C_M, C_T, C_S are tabulated in Appendix D, Tables D3, 6, 9, 12, 15, and 18.

APPENDIX C

Values of the Function h(a/W) Used to Calculate K_{ID}

a/W	h(a/W)	a/W	h(a/W)
0.450	36.86	0.520	45.92
0.455	37.41	0.525	46.70
0.460	39.98	0.530	47.49
0.465	38.55	0.535	48.31
0.470	39.15	0.540	49.14
0.475	39.75	0.545	50.00
0.480	40.37	0.550	50.88
0.485	41.01	0.555	51.78
0.490	41.66		
0.495	42.33		
0.500	43.01		
0.505	43.71		
0.510	44.43		
0.515	45.17		

APPENDIX D

Table D1. Raw Data for Instrumented Impact Evaluation of Precracked Charpy Specimens, Plate G, Orientation LT

Specimen Code	Test Temperature F C	Dial Energy ft-lbf J	Loads P_{GY} lbf N	Loads P_M lbf N	Times t_{GY} ms	Times t_M ms	Initiation Energy ft-lbf J	a/W
GL6	-20	14.5	1412	1472	0.19	0.22	0.8	0.48
	-29	19.7	6282	6549			1.0	
GL11	-10	20.4	1338	1422	0.18	0.79	4.8	0.50
	-23	27.7	5951	6324			6.5	
GL4	-10	23.6	1301	1437	0.25	1.12	6.6	0.50
	-23	32.0	5786	6391			8.9	
GL2	0	18.5	1351	1486	0.17	0.74	4.7	0.48
	-18	25.1	6010	6624			6.3	
GL8	15	23.5	1312	1450	0.17	0.80	4.9	0.49
	-9	31.9	5834	6448			6.7	

Table D2. Results of Instrumented Impact Evaluation of Precracked Charpy Specimens, Plate G, Orientation LT

Specimen Code	Test Temp. F C	Dynamic Yield Stress ksi MPa	Normalized Energies in-lbf/in^2 KJ/M^2 Total	Init.	Prop.	Fracture Toughness ksi$\sqrt{in}$ MPa$\sqrt{m}$ K_{ID}	K_{JD}	Stress Intensity Rate ksi$\sqrt{in}$/s MPa$\sqrt{m}$/s
GL6	-20	113.1	2175	56	2119	-	58.5	0.26E6
	-29	779.7	381	10	371	-	64.3	0.29E6
GL11	-10	112.6	3138	689	2449	-	204.2	0.26E6
	-23	776.4	550	121	429	-	224.4	0.28E6
GL4	-10	109.5	3630	908	2722	-	234.4	0.21E6
	-23	754.9	636	159	477	-	257.6	0.23E6
GL2	0	108.2	2776	650	2126	-	198.1	0.27E6
	-18	746.0	486	114	372	-	217.7	0.29E6
GL8	15	107.1	3561	694	2867	-	204.4	0.25E6
	-9	738.7	624	121	502	-	224.7	0.28E6

Table D3. Young's Modulus and Compliance Values for Plate G, Orientation LT

Specimen	Temp F C	YM ksi x 10^3 MPa x 10^3	C_T in-lbf^{-1} x 10^{-6} mN^{-1} x 10^{-8}	C_S in-lbf^{-1} x 10^{-6} mN^{-1} x 10^{-8}	C_M in-lbf^{-1} x 10^{-6} mN^{-1} x 10^{-8}
GL6	-20	30	8.8	4.5	4.3
	-29	207	5.0	2.6	2.5
GL11	-10	30	8.8	4.7	4.1
	-23	207	5.0	2.7	2.3
GL4	-10	30	13.0	4.7	7.9
	-23	207	7.4	2.7	4.5
GL2	0	30	8.2	4.5	3.7
	-17	207	4.7	2.6	2.1
GL8	15	30	8.5	4.6	3.9
	-9	207	4.8	2.6	2.2

Table D4. Raw Data for Instrumented Impact Evaluation of Precracked Charpy Specimens, Plate G, Orientation TL

Specimen Code	Test Temperature F C	Dial Energy ft-lbf J	Loads P_{GY} lbf N	Loads P_M lbf N	Times t_{GY} ms	Times t_M ms	Initiation Energy ft-lbf J	a/W
GT29	-60	4.2	-	912	-	.140	.2	.50
	-51	5.7	-	4057			.3	
GT12	-60	5.3	-	1228	-	.180	.4	.48
	-51	7.2	-	5463			.6	
GT3	-40	14.9	1314	1490	.200	.260	.9	.48
	-40	20.2	5846	6629			1.2	
GT8	-40	6.5	-	1250	-	.180	.5	.48
	-40	8.8	-	5560			.7	
GT30	-30	7.0	-	1174	-	.180	.4	.51
	-34	9.5	-	5224			.6	
GT9	-20	14.7	1301	1423	.210	.260	.8	.48
	-29	19.9	5789	6332			1.1	
GT17	-20	11.5	1274	1344	.220	.290	.8	.50
	-29	15.6	5667	5978			1.1	
GT20	-10	14.4	1325	1325	.210	.210	1.0	.50
	-23	19.5	5895	5895			.14	
GT2	-10	14.7	1242	1342	.170	.210	.8	.50
	-23	19.9	5525	5969			1.1	
GT36	0	13.7	1070	1170	.170	.440	2.1	.53
	-18	18.6	4760	5204			2.8	
GT4	0	15.7	-	1417	-	.190	.8	.48
	-18	21.3	-	6304			1.0	
GT14	15	14.8	1277	1289	.190	.520	2.6	.49
	-9	20.1	5682	5736			3.5	
GT13	15	14.3	1255	1311	.180	.500	2.7	.49
	-9	19.4	5582	5831			3.7	
GT23	60	14.1	1085	1187	.160	.510	2.5	.51
	16	19.1	4827	5281			3.4	

Table D4. Continued.

Specimen Code	Test Temperature F C	Dial Energy ft-lbf J	Loads P_{GY} lbf N	Loads P_M lbf N	Times t_{GY} ms	Times t_M ms	Initiation Energy ft-lbf J	a/W
GT16	90	14.6	1115	1191	.180	.670	3.3	.50
	32	19.8	4959	5297			4.5	
GT5	90	15.5	1182	1280	.156	.464	3.6	.48
	32	21.0	5257	5693			4.9	

Table D5. Results of Instrumented Impact Evaluation of Precracked Charpy Specimens, Plate G, Orientation TL

Specimen Code	Test Temp. F C	Dynamic Yield Stress ksi MPa	Normalized Energies in-lbf/in² KJ/M² Total	Init.	Prop.	Fracture Toughness ksi√in MPa√m K_{ID}	K_{JD}	Stress Intensity Rate ksi√in/s MPa√m/s
GT29	-60	> 76.8	646	23	624	38.8	-	0.28E6
	-51	>529.3	113	4	109	42.7	-	0.30E6
GT12	-60	> 97.4	791	38	754	49.8	-	0.28E6
	-51	>671.5	139	7	132	54.8	-	0.30E6
GT3	-40	104.2	2225	85	2140	-	71.7	0.27E6
	-40	718.5	390	15	375	-	78.8	0.30E6
GT8	-40	> 99.1	970	39	931	50.7	-	0.28E6
	-40	>683.9	170	7	163	55.7	-	0.31E6
GT30	-30	>101.9	1093	40	1054	51.2	-	0.28E6
	-34	>702.7	191	7	185	56.3	-	0.31E6
GT9	-20	103.2	2195	74	2120	-	67.1	0.26E6
	-29	711.5	384	13	371	-	73.7	0.28E6
GT17	-20	108.3	1778	79	1699	-	69.2	0.24E6
	-29	746.9	311	14	298	-	76.1	0.26E6
GT20	-10	112.7	2226	100	2126	-	77.8	0.37E6
	-23	776.9	390	18	372	-	85.5	0.41E6
GT2	-10	104.5	2261	81	2180	-	69.9	0.33E6
	-23	720.8	396	14	382	-	76.8	0.36E6
GT36	0	102.1	2243	295	1948	-	133.5	0.30E6
	-18	703.7	393	52	341	-	146.7	0.33E6
GT4	0	>111.3	2333	50	2283	57.0	-	0.30E6
	-18	>767.3	408	9	400	62.7	-	0.33E6
GT14	15	105.4	2254	349	1905	-	145.0	0.28E6
	-9	726.6	395	61	334	-	159.3	0.31E6
GT13	15	104.6	2189	361	1828	-	147.5	0.29E6
	-9	720.9	383	63	320	-	162.1	0.32E6
GT23	60	97.1	2237	361	1876	-	146.9	0.29E6
	16	669.8	392	63	329	-	161.4	0.32E6

Table D5. Continued.

Specimen Code	Test Temp. F C	Dynamic Yield Stress ksi MPa	Normalized Energies in-lbf/in^2 KJ/M^2 Total	Init.	Prop.	Fracture Toughness ksi$\sqrt{in}$ MPa$\sqrt{m}$ K_{ID}	K_{JD}	Stress Intensity Rate ksi$\sqrt{in}$/s MPa$\sqrt{m}$/s
GT16	90	94.8	2257	458	1800	-	165.1	0.25E6
	32	653.6	395	80	315	-	181.4	0.27E6
GT5	90	92.8	2303	451	1851	-	164.0	0.35E6
	32	639.8	403	79	324	-	180.2	0.39E6

Table D6. Young's Modulus and Compliance Values for Plate G, Orientation TL

Specimen	Temp F C	YM ksi x 10^3 MPa x 10^3	C_T in-lbf^{-1} x 10^{-6} mN^{-1} x 10^{-8}	C_S in-lbf^{-1} x 10^{-6} mN^{-1} x 10^{-8}	C_M in-lbf^{-1} x 10^{-6} mN^{-1} x 10^{-8}
GT29	-60	33	7.7	4.3	3.4
	-51	228	4.4	2.5	1.9
GT12	-60	33	7.4	4.0	3.4
	-51	228	4.2	2.3	1.9
GT3	-40	30	7.7	4.4	3.3
	-40	207	4.4	2.5	1.9
GT8	-40	33	9.4	4.0	5.4
	-40	228	5.4	2.3	3.1
GT30	-30	33	7.7	4.4	3.3
	-34	228	4.4	2.5	1.9
GT9	-20	30	8.1	4.4	3.7
	-29	207	4.6	2.5	2.1
GT17	-20	30	8.7	4.8	4.0
	-29	207	5.0	2.7	2.3
GT20	-10	30	9.6	4.8	4.8
	-23	207	5.5	2.7	2.7
GT2	-10	30	8.9	4.7	4.2
	-20	207	5.1	2.7	2.4
GT36	0	30	10.0	5.4	5.0
	-18	207	5.7	3.1	2.9
GT4	0	33	8.8	4.0	4.7
	-18	228	5.0	2.3	2.7
GT14	15	30	9.0	4.6	4.4
	-9	207	5.1	2.6	2.5
GT13	15	30	9.4	4.7	4.7
	-9	207	5.4	2.7	2.7
GT23	60	30	9.6	5.1	4.5
	16	207	5.5	2.9	2.6
GT16	90	30	11.0	4.8	5.7
	32	207	6.3	2.7	3.2
GT5	90	30	12.0	4.5	8.0
	32	207	6.8	2.6	4.6

Table D7. Raw Data for Instrumented Impact Evaluation of Precracked Charpy Specimens, Plate U, Orientation LT

Specimen Code	Test Temperature F C	Dial Energy ft-lbf J	Loads P_{GY} lbf N	Loads P_M lbf N	Times t_{GY} ms	Times t_M ms	Initiation Energy ft-lbf J	a/W
UL8	-40	7.8	1165	1267	.180	.270	1.0	.51
	-40	10.6	5180	5634			1.3	
UL418	-30	8.7	1084	1428	.140	.250	.9	.48
	-34	11.8	4622	6352			1.2	
UL23	-20	11.8	1336	1400	.190	.360	1.9	.48
	-29	16.0	5943	6227			2.6	
UL417	-15	7.8	1185	1581	.150	.260	1.3	.46
	-26	10.6	5273	7034			1.8	
UL115	0	18.0	1119	1469	.150	.490	2.9	.48
	-18	24.4	4977	6534			3.9	
UL7	40	17.7	1140	1362	.180	.660	3.7	.49
	4	24.0	5071	6058			5.0	
UL822	90	15.9	1287	1531	.250	.610	3.5	.47
	32	21.6	5723	6808			4.8	
UL11	90	18.1	1026	1270	.150	.810	4.3	.50
	32	24.5	4564	5649			5.9	

Table D8. Results of Instrumented Impact Evaluation of Precracked Charpy Specimens, Plate U, Orientation LT

Specimen Code	Test Temp. F C	Dynamic Yield Stress ksi MPa	Normalized Energies in-lbf/in^2 KJ/M^2 Total	Init.	Prop.	Fracture Toughness ksi$\sqrt{in}$ MPa$\sqrt{m}$ K_{ID}	K_{JD}	Stress Intensity Rate ksi$\sqrt{in}$/s MPa$\sqrt{m}$/s
UL8	-40	104.3	1237	118	1120	-	84.6	0.31E6
	-40	718.8	217	21	196	-	92.9	0.34E6
UL418	-30	86.0	1299	95	1204	-	76.0	0.30E6
	-34	592.7	227	17	211	-	83.5	0.33E6
UL23	-20	103.9	1745	221	1523	-	115.8	0.32E6
	-29	716.3	306	39	267	-	127.3	0.35E6
UL412	-15	85.4	1110	124	986	-	86.6	0.33E6
	-26	588.9	194	22	173	-	95.2	0.36E6
UL115	0	87.0	2661	368	2293	-	149.1	0.30E6
	-18	599.9	466	65	402	-	163.9	0.33E6
UL7	40	95.0	2709	494	2215	-	172.3	0.26E6
	4	655.0	474	87	388	-	189.3	0.29E6
UL822	90	97.2	2317	395	1922	-	153.5	0.25E6
	32	670.2	406	69	337	-	168.6	0.27E6
UL11	90	87.2	2798	621	2178	-	192.3	0.24E6
	32	601.5	490	109	381	-	211.3	0.26E6

Table D9. Young's Modulus and Compliance Values for Plate U, Orientation LT

Specimen	Temp F C	YM ksi x 10^3 MPa x 10^3	C_T in-lbf^{-1} x 10^{-6} mN^{-1} x 10^{-8}	C_S in-lbf^{-1} x 10^{-6} mN^{-1} x 10^{-8}	C_M in-lbf^{-1} x 10^{-6} mN^{-1} x 10^{-8}
UL8	-40	30	8.6	5.0	3.6
	-40	207	4.9	2.9	2.1
UL418	-30	30	7.2	4.4	2.7
	-34	207	4.1	2.5	1.5
UL23	-20	30	9.3	4.4	4.9
	-29	207	5.3	2.5	2.8
UL417	-15	30	8.3	4.0	4.2
	-9	207	4.7	2.3	2.4
UL115	0	30	8.8	4.4	4.4
	-18	207	5.0	2.5	2.5
UL7	40	30	10.0	4.7	5.6
	4	207	5.7	2.7	3.2
UL822	90	30	13.0	4.3	8.4
	32	207	7.4	2.5	4.8
UL11	90	30	9.6	4.8	4.7
	32	207	5.5	2.7	2.7

Table D10. Raw Data for Instrumented Impact Evaluation of Precracked Charpy Specimens, Plate U, Orientation TL

Specimen Code	Test Temperature F C	Dial Energy ft-lbf J	Loads P_{GY} lbf N	Loads P_M lbf N	Times t_{GY} ms	Times t_M ms	Initiation Energy ft-lbf J	a/W
UT30	-80	3.5	728	868	.180	.210	.3	.49
	-62	4.7	3237	3949			.4	
UT22	-60	4.5	-	1280	-	.220	.6	.49
	-51	6.1	-	5692			.8	
UT20	-40	7.9	-	1176	-	.200	.5	.49
	-40	10.7	-	5229			.7	
UT45	-40	6.4	-	1095	-	.210	.4	.49
	-40	8.7	-	4871			.5	
UT34	-40	8.3	1025	1027	.150	.170	.4	.50
	-40	11.3	4561	4570			.5	
UT12	-30	8.0	-	1218	-	.190	.4	.49
	-34	10.8	-	5419			.6	
UT10	-20	12.3	1326	1326	.260	.280	.6	.48
	-29	16.7	5899	5899			.8	
UT46	-20	10.1	1109	1191	.240	.510	1.6	.48
	-29	13.7	4932	5297			2.2	
UT31	-20	9.5	1041	1155	.190	.510	1.7	.52
	-29	12.9	4629	5136			2.4	
UT36	-15	13.0	1214	1388	.170	.500	2.8	.49
	-26	17.6	5399	6173			3.8	
UT3	-15	13.1	1240	1382	.180	.440	2.4	.48
	-26	17.8	5517	6148			3.3	
UT47	-15	11.7	1390	1436	.220	.300	1.2	.48
	-26	15.9	6182	6387			1.6	
UT5	0	15.5	1128	1358	.200	.730	3.4	.51
	-18	21.0	5018	6042			4.6	
UT6	0	15.1	1249	1433	.180	.490	2.8	.48
	-18	20.5	5558	6376			3.8	
UT338	0	14.6	1257	1331	.300	.490	2.2	.50
	-18	19.8	5593	5922			3.0	

Table D10. Continued.

Specimen Code	Test Temperature F C	Dial Energy ft-lbf J	Loads P_{GY} lbf N	Loads P_M lbf N	Times t_{GY} ms	Times t_M ms	Initiation Energy ft-lbf J	a/W
UT9	15 -9	15.8 21.4	1103 4908	1271 5655	.170	.650	3.5 4.7	.52
UT17	40 4	17.3 23.5	1178 5239	1408 6262	.188	.504	2.7 3.7	.49
UT7	40 4	17.0 23.0	1160 5158	1360 6048	.180	.660	3.7 5.0	.49
UT1	90 32	18.0 24.4	1493 6643	1493 6643	.504	.504	4.6 6.2	.47
UT32	90 32	17.0 23.0	1313 5840	1313 5840	.504	.504	4.0 5.4	.56
UT16	135 57	17.0 23.0	1339 5957	1339 5957	.498	.498	4.1 5.6	.49
UT8	135 57	15.5 21.0	1172 5212	1172 5212	.500	.500	3.5 4.7	.52

Table D11. Results of Instrumented Impact Evaluation of Precracked Charpy Specimens, Plate U, Orientation TL

Specimen Code	Test Temp. F C	Dynamic Yield Stress ksi MPa	Normalized Energies in-lbf/in^2 KJ/M^2 Total	Init.	Prop.	Fracture Toughness ksi$\sqrt{in}$ MPa$\sqrt{m}$ K_{ID}	K_{JD}	Stress Intensity Rate ksi$\sqrt{in}$/s MPa$\sqrt{m}$/s
UT30	-80	60.6	536	8	528	-	22.3	0.11E6
	-62	418.2	94	1	92	-	24.5	0.12E6
UT22	-60	>103.5	678	42	636	52.7	-	0.24E6
	-51	>713.5	119	7	111	58.0	-	0.26E6
UT20	-40	> 97.0	1203	37	1166	49.2	-	0.25E6
	-40	>668.7	211	6	204	54.1	-	0.27E6
UT45	-40	> 89.4	970	31	938	45.5	-	0.22E6
	-40	>616.7	170	6	164	50.0	-	0.24E6
UT34	-40	87.2	1283	23	1260	-	37.6	0.22E6
	-40	601.2	225	4	221	-	41.4	0.24E6
UT12	-30	>100.5	1218	40	1179	51.0	-	0.27E6
	-34	>692.9	213	7	206	56.1	-	0.30E6
UT10	-20	105.2	1836	29	1808	-	41.6	0.15E6
	-29	725.1	322	5	317	-	45.7	0.16E6
UT46	-20	86.2	1493	181	1312	-	104.8	0.20E6
	-29	594.5	262	32	230	-	115.2	0.22E6
UT31	-20	94.1	1515	242	1273	-	121.1	0.24E6
	-29	649.0	265	42	223	-	133.0	0.26E6
UT36	-15	101.1	1990	375	1615	-	150.6	0.30E6
	-26	697.4	348	66	283	-	165.5	0.33E6
UT3	-15	98.3	1956	299	1656	-	134.6	0.30E6
	-26	678.1	343	52	290	-	148.0	0.33E6
UT47	-15	108.1	1730	101	1629	-	78.2	0.26E6
	-26	745.2	303	18	285	-	85.9	0.28E6
UT5	0	98.9	2433	468	1966	-	168.0	0.23E6
	-18	682.1	426	82	344	-	184.7	0.25E6
UT6	0	98.1	2243	352	1892	-	145.7	0.30E6
	-18	688.4	393	62	331	-	160.1	0.33E6
UT338	0	108.0	2269	224	2045	-	116.2	0.24E6
	-18	744.7	397	39	358	-	127.7	0.26E6

TABLE D11. CONTINUED

Specimen Code	Test Temp. F / C	Dynamic Yield Stress ksi / MPa	Normalized Energies in-lbf/in² KJ/M² Total	Init.	Prop.	Fracture Toughness ksi√in MPa√m K_{ID}	K_{JD}	Stress Intensity Rate ksi√in/s MPa√m/s
UT9	15	99.8	2519	500	2020	-	173.5	0.27E6
	-9	688.2	441	88	354	-	190.7	0.29E6
UT17	40	98.2	2621	345	2277	-	143.9	0.28E6
	4	663.3	459	60	399	-	158.1	0.31E6
UT7	40	95.7	2589	498	2091	-	173.0	0.26E6
	4	659.6	453	87	366	-	190.1	0.29E6
UT1	90	111.8	2611	588	2022	-	187.2	0.37E6
	32	770.5	457	103	354	-	205.7	0.41E6
UT32	90	112.8	2642	562	2080	-	182.9	0.36E6
	32	777.7	463	98	364	-	201.0	0.40E6
UT16	135	108.3	2563	561	2002	-	182.1	0.36E6
	57	746.8	449	98	351	-	200.1	0.40E6
UT8	135	107.1	2485	509	1976	-	173.5	0.35E6
	57	738.4	435	89	346	-	190.6	0.38E6

Table D12. Young's Modulus and Compliance Values for Plate U, Orientation TL

Specimen	Temp F C	YM ksi x 10^3 MPa x 10^3	C_T in-lbf^{-1} x 10^{-6} mN^{-1} x 10^{-8}	C_S in-lbf^{-1} x 10^{-6} mN^{-1} x 10^{-8}	C_M in-lbf^{-1} x 10^{-6} mN^{-1} x 10^{-8}
UT30	-80	31	12.0	4.6	7.9
	-62	214	6.8	2.6	4.5
UT22	-60	33	8.7	4.1	4.6
	-51	228	5.0	2.3	2.6
UT20	-40	33	8.6	4.2	4.4
	-40	228	4.9	2.4	2.5
UT45	-40	33	11.0	4.2	6.5
	-40	228	6.3	2.4	3.7
UT34	-40	30	9.5	4.7	4.8
	-40	207	5.4	2.7	2.7
UT12	-30	33	7.9	4.2	3.7
	-34	228	4.5	2.4	2.1
UT10	-20	30	9.9	4.4	5.5
	-29	207	5.6	2.5	3.1
UT46	-20	30	11.0	4.4	6.6
	-29	207	6.3	2.5	3.8
UT31	-20	30	9.2	5.1	4.2
	-29	207	5.2	2.9	2.4
UT36	-15	30	9.1	4.7	4.5
	-26	207	5.2	2.7	2.6
UT3	-15	30	9.5	4.4	5.0
	-26	207	5.7	2.5	2.9
UT47	-15	30	10.0	4.4	6.0
	-26	207	5.7	2.5	3.4
UT5	0	30	9.8	4.9	4.9
	-17	207	5.6	2.8	2.8
UT6	0	30	9.4	4.4	5.0
	-17	207	5.4	2.5	2.9
UT338	0	30	16.0	4.8	11.0
	-17	207	9.1	2.7	6.3

Table D12. Continued.

Specimen	Temp F C	YM ksi x 10^3 MPa x 10^3	C_T in-lbf^{-1} x 10^{-6} mN^{-1} x 10^{-8}	C_S in-lbf^{-1} x 10^{-6} mN^{-1} x 10^{-8}	C_M in-lbf^{-1} x 10^{-6} mN^{-1} x 10^{-8}
UT9	15	30	10.0	5.1	5.0
	-9	207	5.7	2.9	2.9
UT17	40	30	10.0	4.6	5.7
	4	207	5.7	2.6	3.2
UT7	40	30	10.0	4.7	5.5
	4	207	5.7	2.7	3.1
UT1	90	30	9.7	4.3	5.4
	32	207	5.5	2.5	3.1
UT32	90	30	10.0	4.9	5.4
	32	207	5.7	2.8	3.1
UT16	135	30	10.0	4.6	5.6
	57	207	5.7	2.6	3.2
UT8	135	30	11.0	5.2	5.6
	57	207	6.3	3.0	3.2

Table D13. Raw Data for Instrumented Impact Evaluation of Precracked Charpy Specimens, Plate S, Orientation LT

Specimen Code	Test Temperature F C	Dial Energy ft-lbf J	Loads P_{GY} lbf N	Loads P_M lbf N	Times t_{GY} ms	Times t_M ms	Initiation Energy ft-lbf J	a/W
SL8	110	12.9	884	884	-	.130	.4	.49
	43	17.5	3932	3932			.5	
SL9	135	21.3	1012	1104	.130	.990	4.5	.46
	57	28.6	4502	4912			6.0	
SL3	135	15.7	761	861	.160	.190	.4	.50
	57	21.3	3383	3828			.5	
SL12	160	21.2	842	1046	.150	.980	3.9	.49
	71	28.7	3744	4652			5.3	
SL1	160	18.7	952	952	-	.490	2.0	.52
	71	25.4	4235	4235			2.7	
SL5	200	25.1	1191	1191	-	1.250	6.1	.48
	93	34.0	5300	5300			8.2	
SL2	200	22.1	488	488	-	1.030	4.3	.51
	93	30.0	4393	4393			5.9	

Table D14. Results of Instrumented Impact Evaluation of Precracked Charpy Specimens, Plate S, Orientation LT

Specimen Code	Test Temp. F / C	Dynamic Yield Stress ksi / MPa	Normalized Energies in-lbf/in^2 KJ/M^2 Total	Init.	Prop.	Fracture Toughness ksi$\sqrt{in}$ MPa$\sqrt{m}$ K_{ID}	K_{JD}	Stress Intensity Rate ksi$\sqrt{in}$/s MPa$\sqrt{m}$/s
SL8	110	71.5	1945	28	1917	-	40.6	0.31E6
	42	492.9	341	5	336	-	44.7	0.34E6
SL9	135	74.3	3060	613	2447	-	190.5	0.19E6
	57	512.4	536	107	428	-	209.3	0.21E6
SL3	135	65.3	2440	17	2422	-	32.1	0.17E6
	57	450.5	427	3	424	-	35.3	0.19E6
SL12	160	68.8	3212	555	2657	-	180.9	0.18E6
	71	474.1	563	97	465	-	198.7	0.20E6
SL1	160	88.9	3029	292	2738	-	131.1	0.27E6
	71	612.9	531	51	479	-	144.0	0.29E6
SL5	200	93.6	3729	846	2883	-	222.6	0.18E6
	93	645.0	653	148	505	-	244.6	0.19E6
SL2	200	88.4	3506	647	2859	-	194.6	0.19E6
	93	609.6	614	113	501	-	213.9	0.21E6

Table D15. Young's Modulus and Compliance Values for Plate S, Orientation LT

Specimen	Temp F C	YM ksi x 10^3 MPa x 10^3	C_T in-lbf^{-1} x 10^{-6} mN^{-1} x 10^{-8}	C_S in-lbf^{-1} x 10^{-6} mN^{-1} x 10^{-8}	C_M in-lbf^{-1} x 10^{-6} mN^{-1} x 10^{-8}
SL8	110	30	10.0	4.6	5.4
	43	207	5.7	2.6	3.1
SL9	135	30	7.8	4.2	3.6
	57	207	4.4	2.4	2.1
SL3	135	30	14.0	4.9	8.8
	57	207	8.0	2.8	5.0
SL12	160	29	11.0	4.7	6.1
	71	200	6.3	2.7	3.5
SL1	160	29	11.0	5.4	5.8
	71	200	6.3	3.1	3.3
SL5	200	29	11.0	4.6	6.0
	93	200	6.3	2.6	3.4
SL2	200	29	11.0	5.2	6.0
	93	200	6.3	3.0	3.4

Table D16. Raw Data for Instrumented Impact Evaluation of Precracked Charpy Specimens, Plate S, Orientation TL

Specimen Code	Test Temperature F / C	Dial Energy ft-lbf / J	Loads P_{GY} lbf / N	Loads P_M lbf / N	Times t_{GY} ms	Times t_M ms	Initiation Energy ft-lbf / J	a/W
ST9	40	6.6	-	826	-	.140	.3	.49
	4	8.9	-	3674			.4	
ST21	70	9.5	-	840	-	.150	.3	.48
	21	12.9	-	3738			.4	
ST2	100	11.2	954	954	.180	.180	.4	.48
	38	15.9	4245	4245			.5	
ST17	100	11.7	952	952	.130	.130	.3	.48
	38	15.9	4234	4234			.5	
ST16	110	13.3	1009	1079	.150	.180	.5	.46
	43	18.0	4490	4801			.6	
ST10	110	14.0	-	1041	-	.140	.4	.48
	43	19.0	-	4630			.5	
ST13	120	14.8	-	968	-	.140	.4	.48
	49	20.1	-	4304			.5	
ST14	120	14.4	-	966	-	.150	.4	.48
	49	19.5	-	4298			.6	
ST30	125	14.9	-	958	-	.170	.4	.48
	52	20.2	-	4262			.5	
ST5	125	14.7	939	1057	.130	.720	2.8	.47
	52	19.9	4179	4704			3.8	
ST3	135	15.9	1055	1055	.785	.785	3.5	.48
	57	21.6	4695	4695			4.8	
ST4	135	15.0	791	1043	.130	.730	3.2	.48
	57	20.3	3517	4638			4.4	
ST8	160	15.6	981	981	.580	.580	2.5	.49
	71	21.2	4363	4363			3.4	
ST20	160	16.4	1049	1049	.810	.810	3.7	.48
	71	22.2	4666	4666			5.0	
ST29	200	16.7	748	1000	.130	.720	3.0	.49
	43	22.6	3329	4450			4.0	
ST24	200	17.0	913	1059	.176	.640	4.0	.48
	93	23.0	4061	4711			5.5	

Table D17. Results of Instrumented Impact Evaluation of Precracked Charpy Specimens, Plate S, Orientation TL

Specimen Code	Test Temp. F C	Dynamic Yield Stress ksi MPa	Normalized Energies in-lbf/in^2 KJ/M^2 Total	Init.	Prop.	Fracture Toughness ksi$\sqrt{in}$ MPa$\sqrt{m}$ K_{ID}	K_{JD}	Stress Intensity Rate ksi$\sqrt{in}$/s MPa$\sqrt{m}$/s
ST9	40	> 66.8	995	18	977	34.0	-	0.24E6
	4	>460.6	174	3	171	37.4	-	0.27E6
ST21	70	> 66.0	1411	18	1394	33.8	-	0.23E6
	21	>455.0	247	3	244	37.2	-	0.25E6
ST2	100	75.7	1672	36	1636	-	46.4	0.26E6
	38	521.8	293	6	287	-	51.0	0.28E6
ST17	100	74.7	1738	21	1717	-	35.7	0.27E6
	38	515.3	304	4	301	-	39.3	0.30E6
ST16	110	74.1	1911	37	1874	-	47.0	0.26E6
	43	511.0	335	7	328	-	51.6	0.28E6
ST10	110	> 80.9	2070	27	2043	41.6	-	0.30E6
	43	>558.0	362	5	358	45.7	-	0.33E6
ST13	120	> 75.3	2188	23	2165	38.6	-	0.28E6
	49	>518.9	383	4	379	42.5	-	0.30E6
ST14	120	> 76.6	2150	24	2126	39.2	-	0.26E6
	49	>528.3	377	4	372	43.1	-	0.29E6
ST30	125	> 76.0	2225	24	2201	38.9	-	0.23E6
	52	>523.9	390	4	385	42.7	-	0.25E6
ST5	125	72.3	2163	387	1776	-	151.4	0.21E6
	52	498.8	379	68	311	-	166.3	0.23E6
ST3	135	81.3	2339	482	1857	-	168.9	0.21E6
	57	560.4	410	84	325	-	185.6	0.24E6
ST4	135	62.1	2229	439	1789	-	161.2	0.22E6
	57	428.0	390	77	313	-	177.2	0.24E6
ST8	160	79.3	2352	338	2014	-	141.1	0.24E6
	71	546.9	412	59	353	-	155.0	0.27E6
ST20	160	83.2	2448	514	1935	-	174.0	0.21E6
	71	573.5	429	90	339	-	191.2	0.24E6
ST29	200	61.1	2530	410	2120	-	155.0	0.21E6
	93	421.5	443	72	371	-	170.3	0.24E6
ST24	200	71.7	2526	503	2022	-	171.7	0.27E6
	93	494.3	442	88	354	-	188.6	0.29E6

Table D18. Young's Modulus and Compliance Values for Plate S, Orientation TL

Specimen	Temp F C	YM ksi x 10^3 MPa x 10^3	C_T in-lbf^{-1} x 10^{-6} mN^{-1} x 10^{-8}	C_S in-lbf^{-1} x 10^{-6} mN^{-1} x 10^{-8}	C_M in-lbf^{-1} x 10^{-6} mN^{-1} x 10^{-8}
ST9	40	33	11.0	4.2	6.9
	4	228	6.3	2.4	3.9
ST21	70	33	9.0	4.1	5.0
	21	228	5.1	2.3	2.9
ST2	100	30	9.9	4.5	5.4
	38	207	5.6	2.6	3.1
ST17	100	30	9.9	4.5	5.4
	38	207	5.6	2.6	3.1
ST16	110	30	8.3	4.2	4.1
	43	207	4.7	2.4	2.3
ST10	110	33	8.8	4.0	4.7
	43	228	5.0	2.3	2.7
ST13	120	33	9.4	4.1	5.4
	49	228	5.4	2.3	3.1
ST14	120	33	10.0	4.1	6.0
	49	228	5.7	2.3	3.4
ST30	125	23	9.9	4.1	5.7
	52	228	5.6	2.3	3.2
ST5	125	30	7.7	4.4	3.3
	52	207	4.4	2.5	1.9
ST3	135	30	10.0	4.4	5.6
	57	207	5.7	2.5	3.2
ST4	135	30	11.0	4.5	6.2
	57	207	6.3	2.5	3.2
ST8	160	29	10.0	4.7	5.8
	71	200	5.7	2.7	3.3
ST20	160	29	10.0	4.6	5.8
	71	200	5.7	2.6	3.3
ST29	200	29	11.0	4.7	6.6
	93	200	6.3	2.7	3.8
ST24	200	29	18.0	4.6	14.0
	93	200	10.0	2.6	8.0

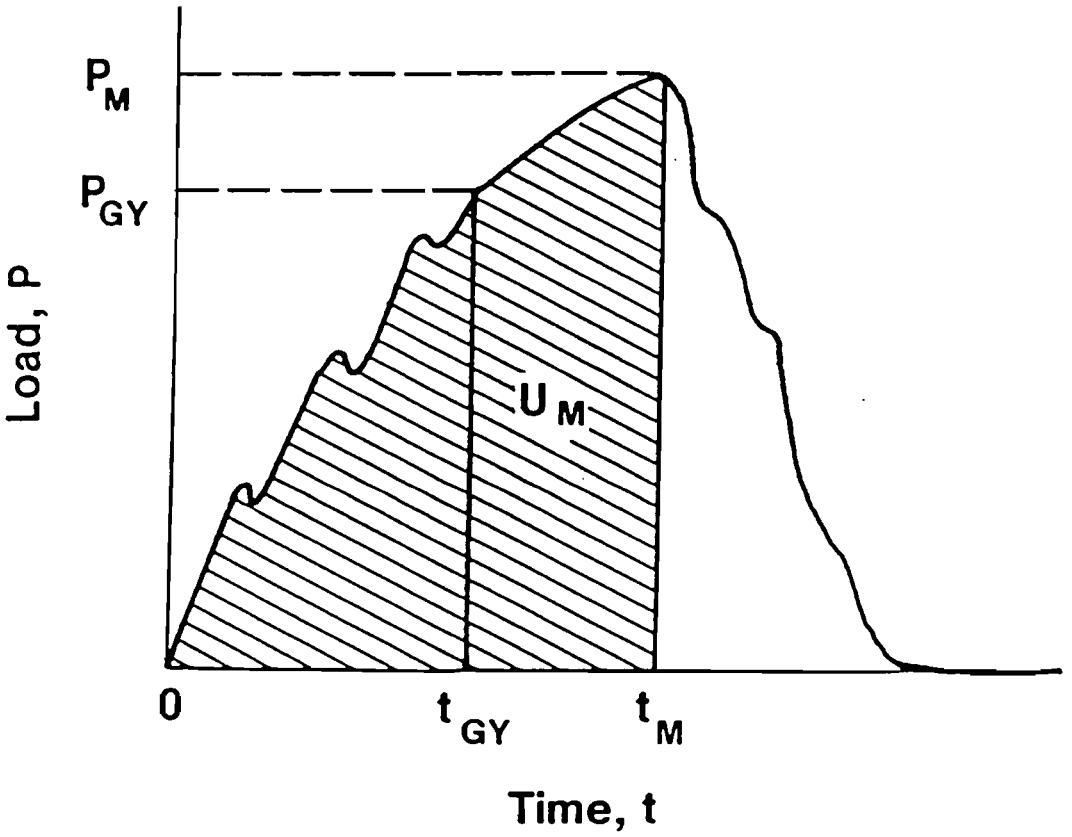

Figure 1. Idealized Load-Time Record for a Three Point Bend Specimen.

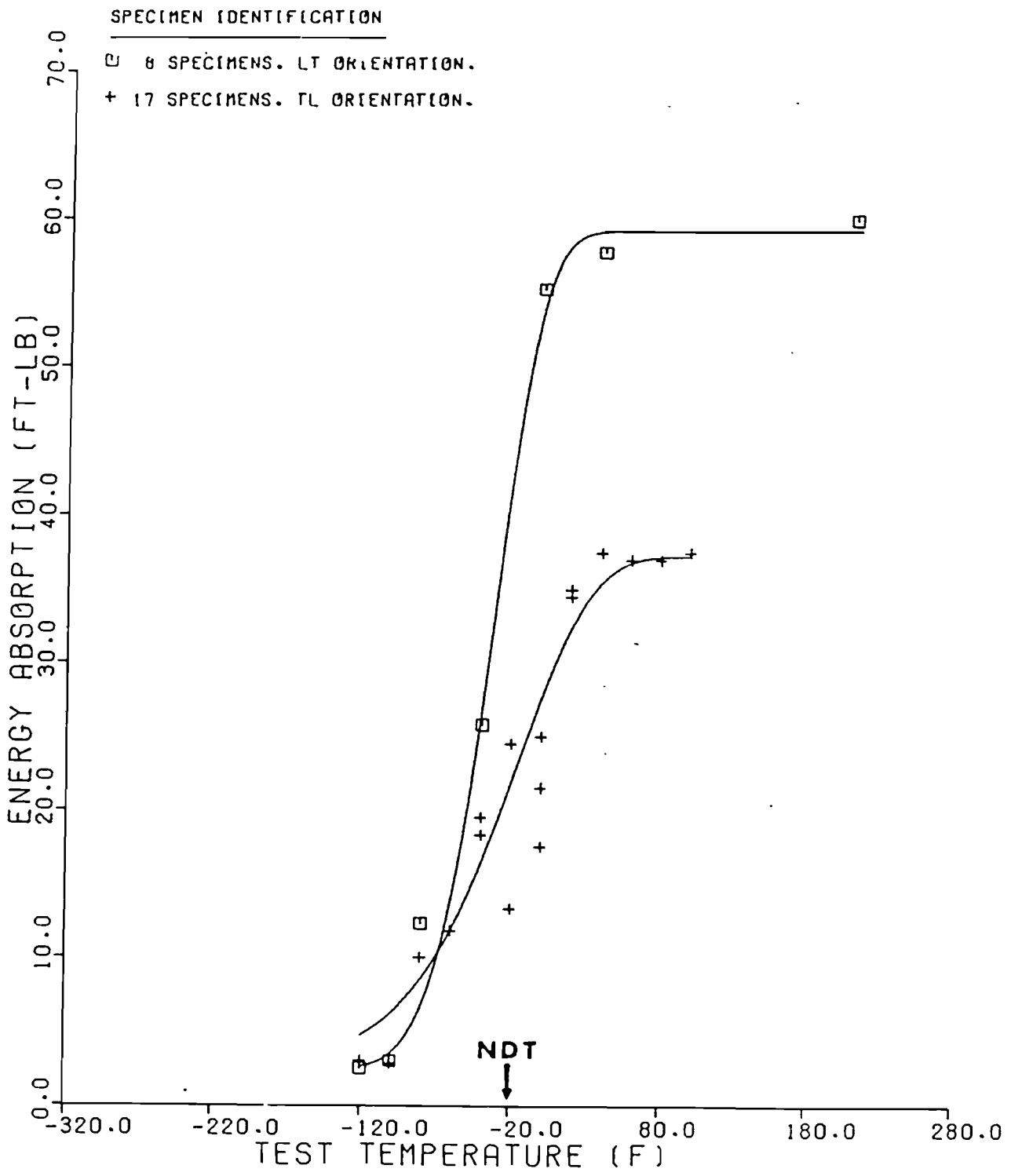

Figure 2. Charpy V-notch-Energy Absorption Results for Plate G.

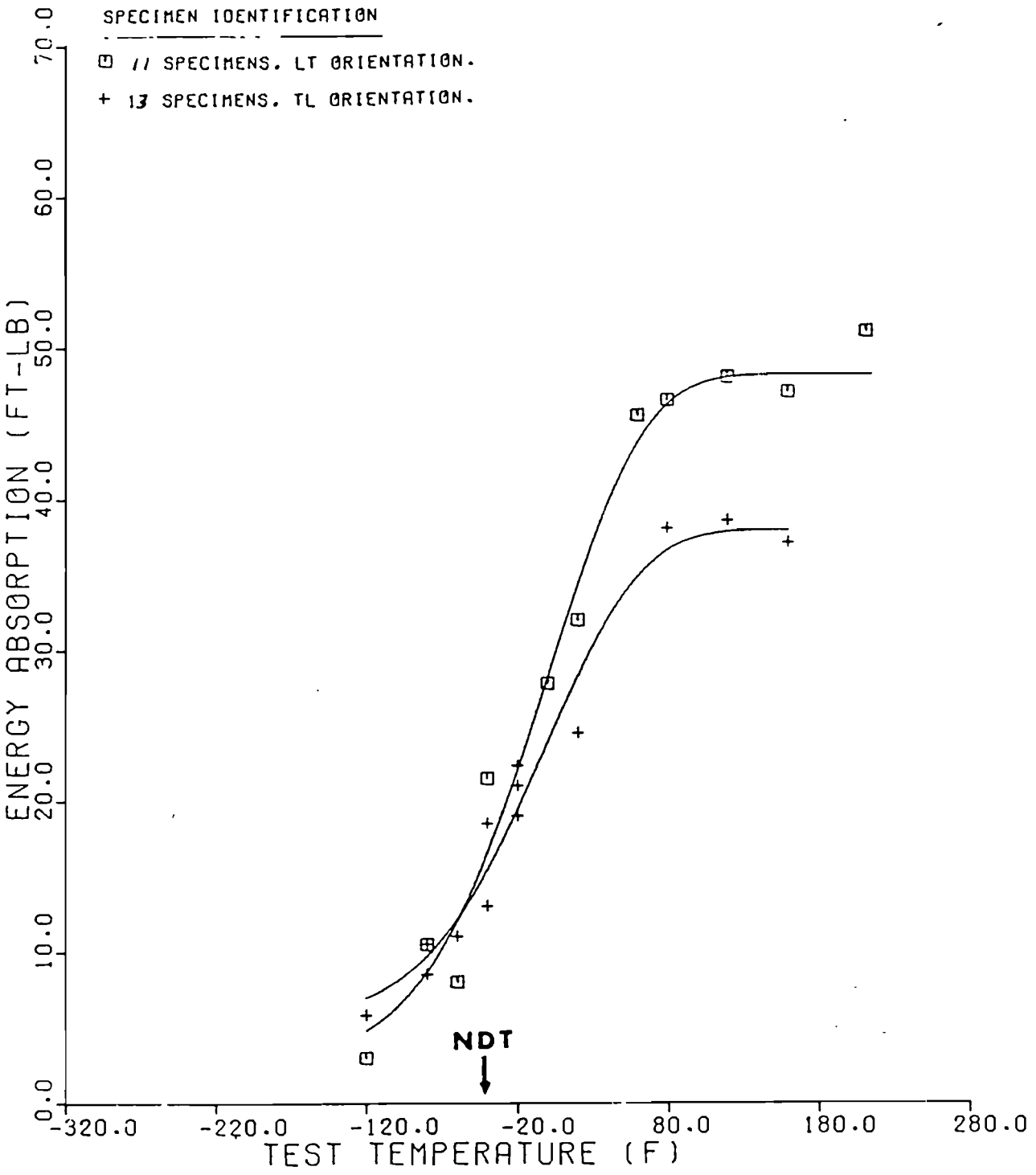

Figure 3. Charpy V-notch-Energy Absorption Results for Plate U.

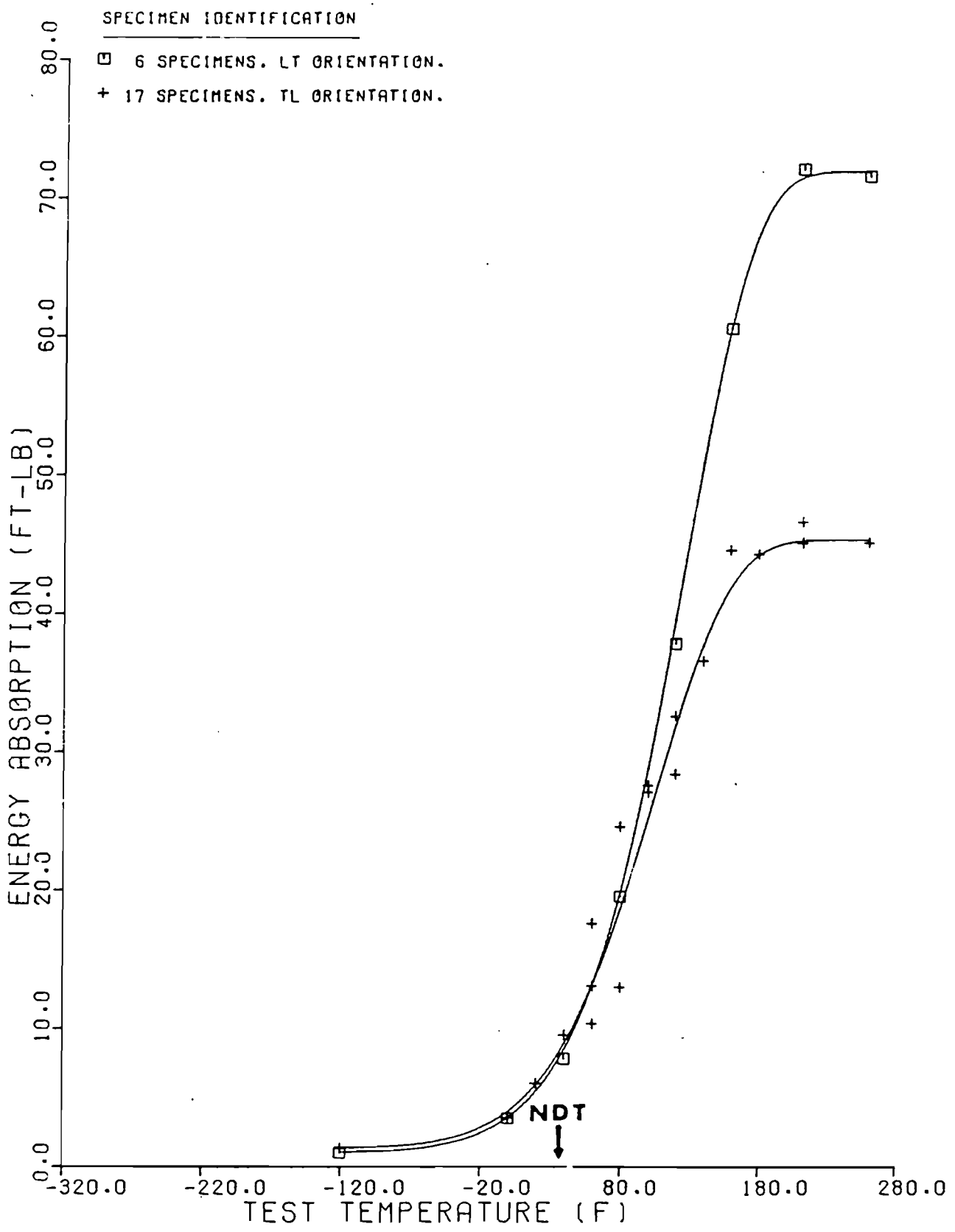

Figure 4. Charpy V-notch-Energy Absorption Results for Plate S.

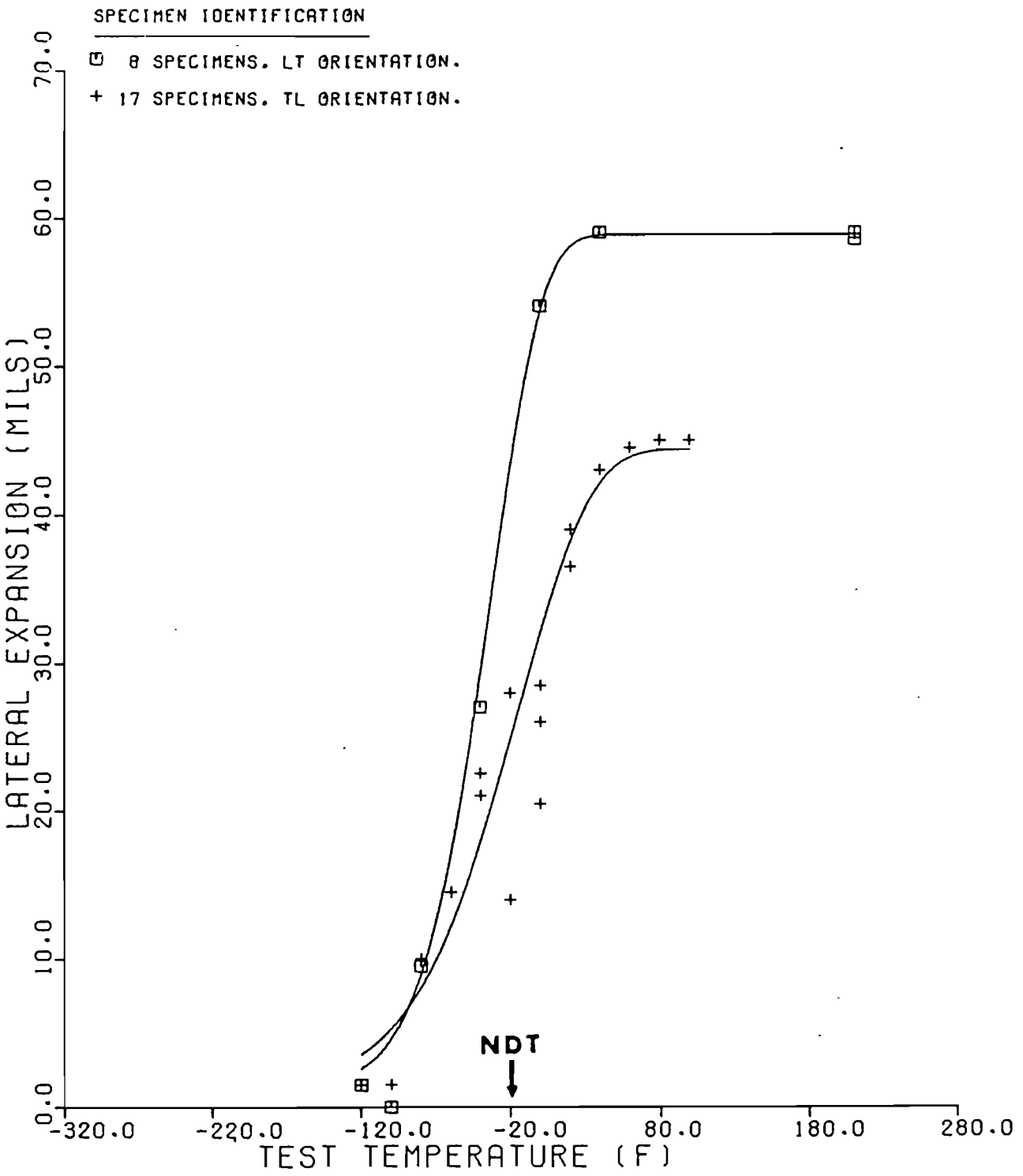

Figure 5. Charpy V-notch-Lateral Expansion Results for Plate G.

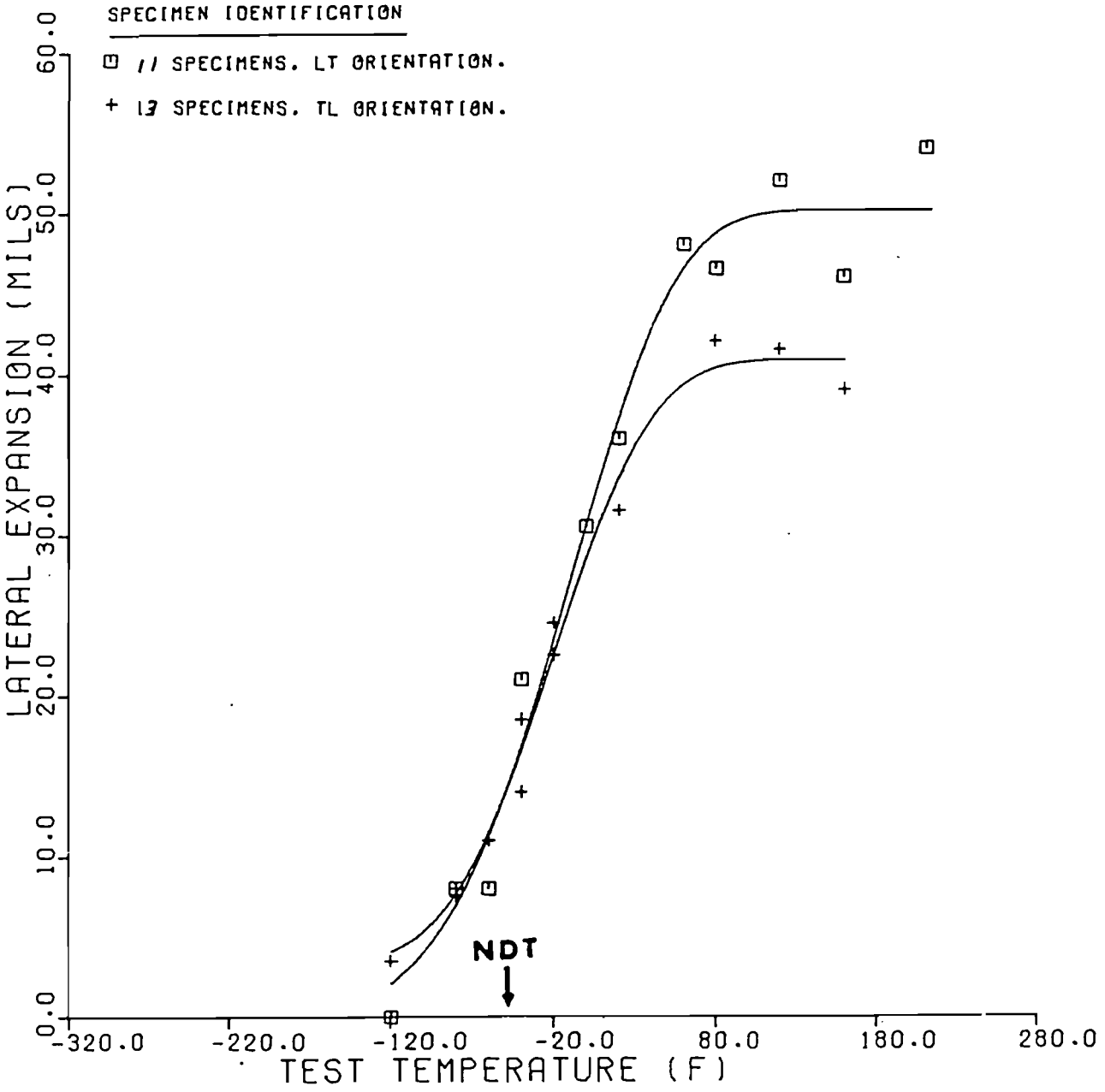

Figure 6. Charpy V-notch-Lateral Expansion Results for Plate U.

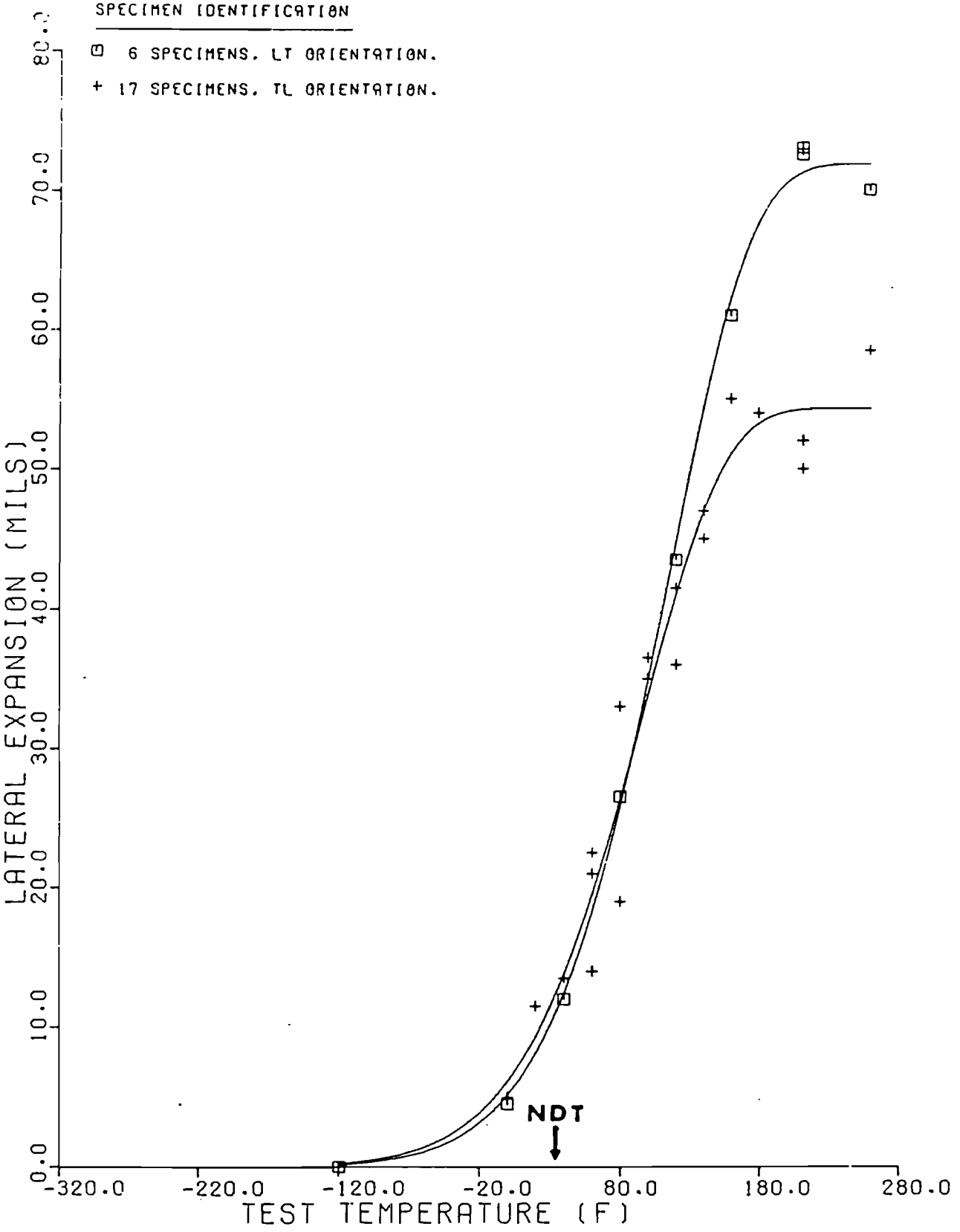

Figure 7. Charpy V-notch-Lateral Expansion Results for Plate S.

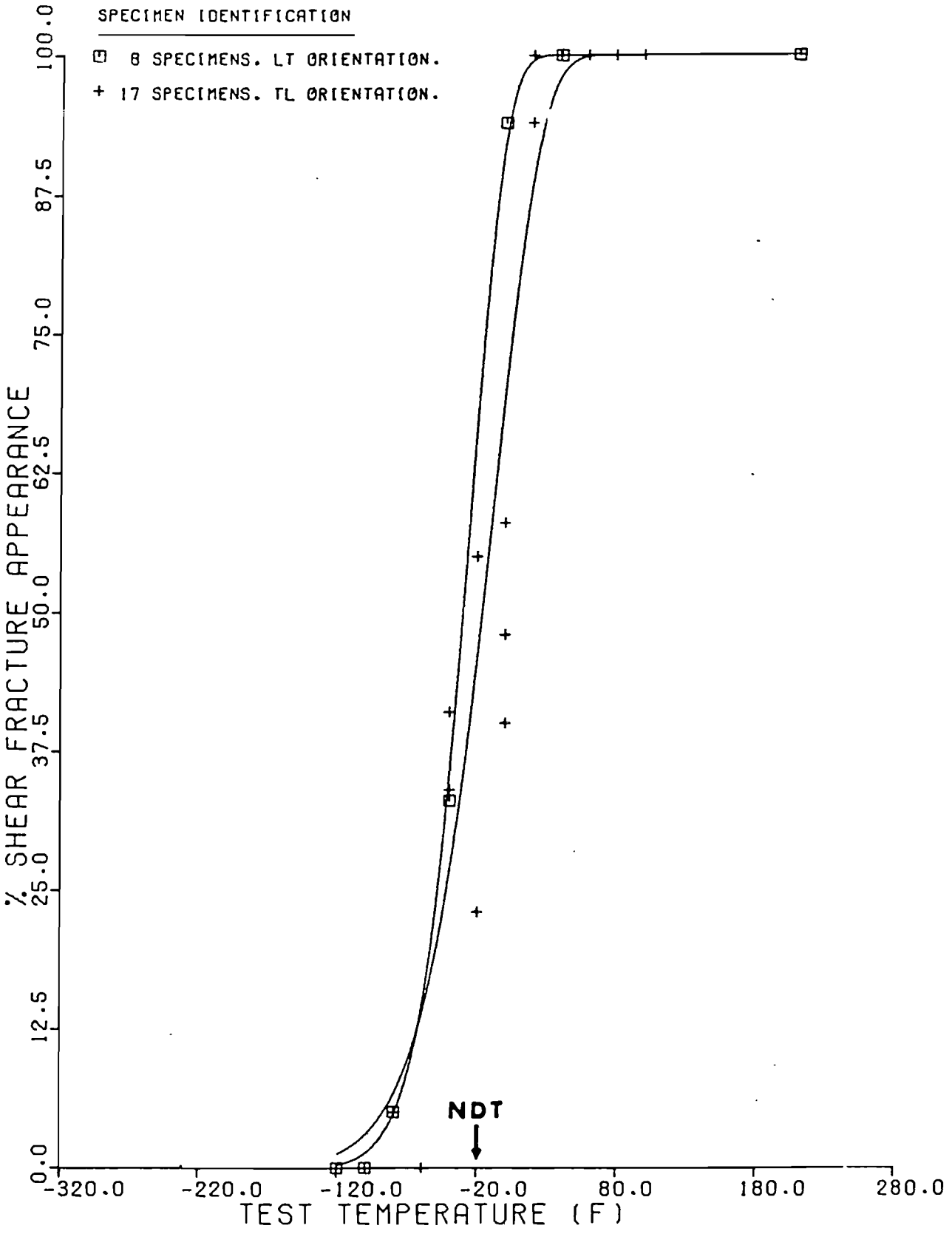

Figure 8. Charpy V-notch-Shear Fracture Appearance Results for Plate G.

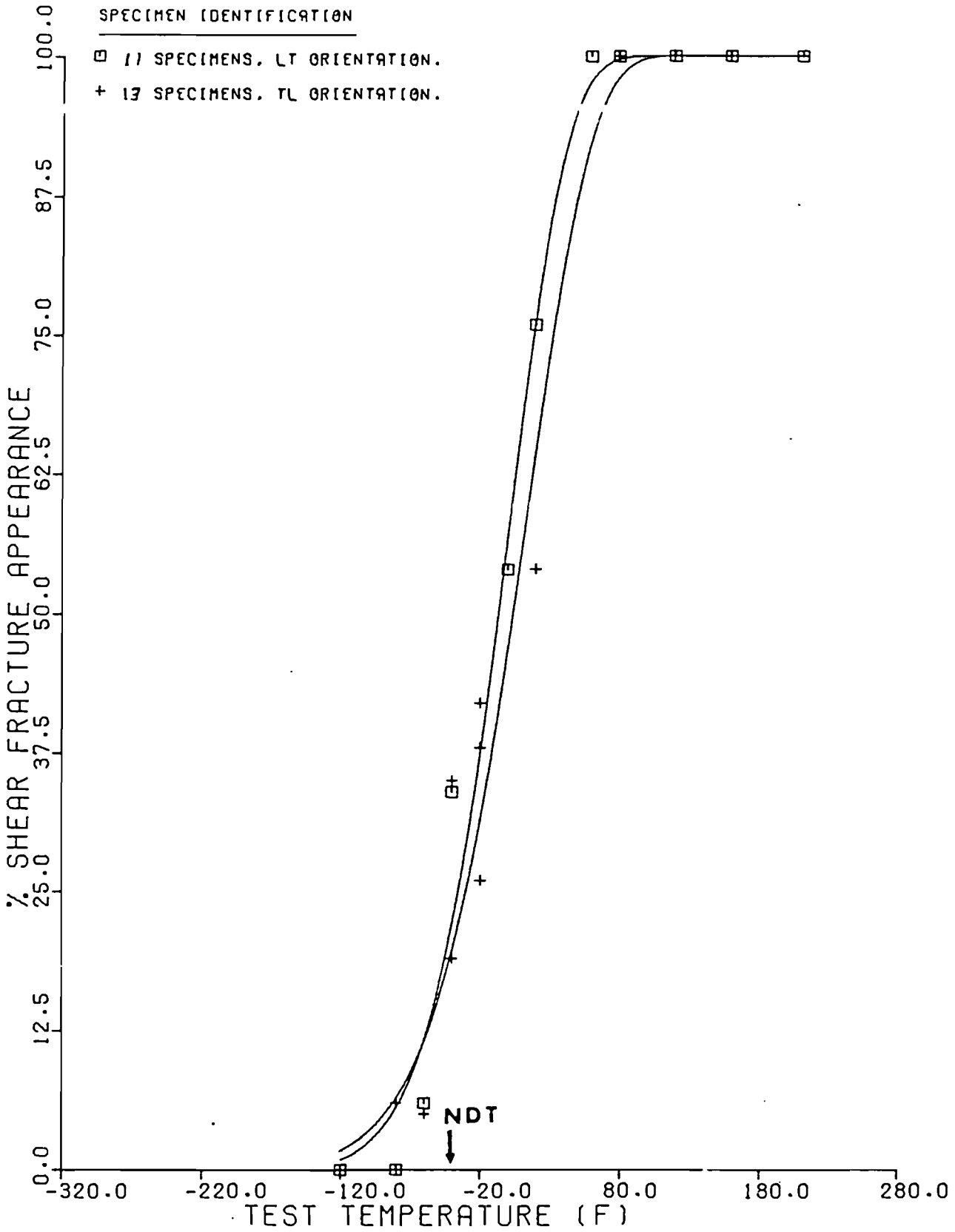

Figure 9. Charpy V-notch-Shear Fracture Appearance Results for Plate U.

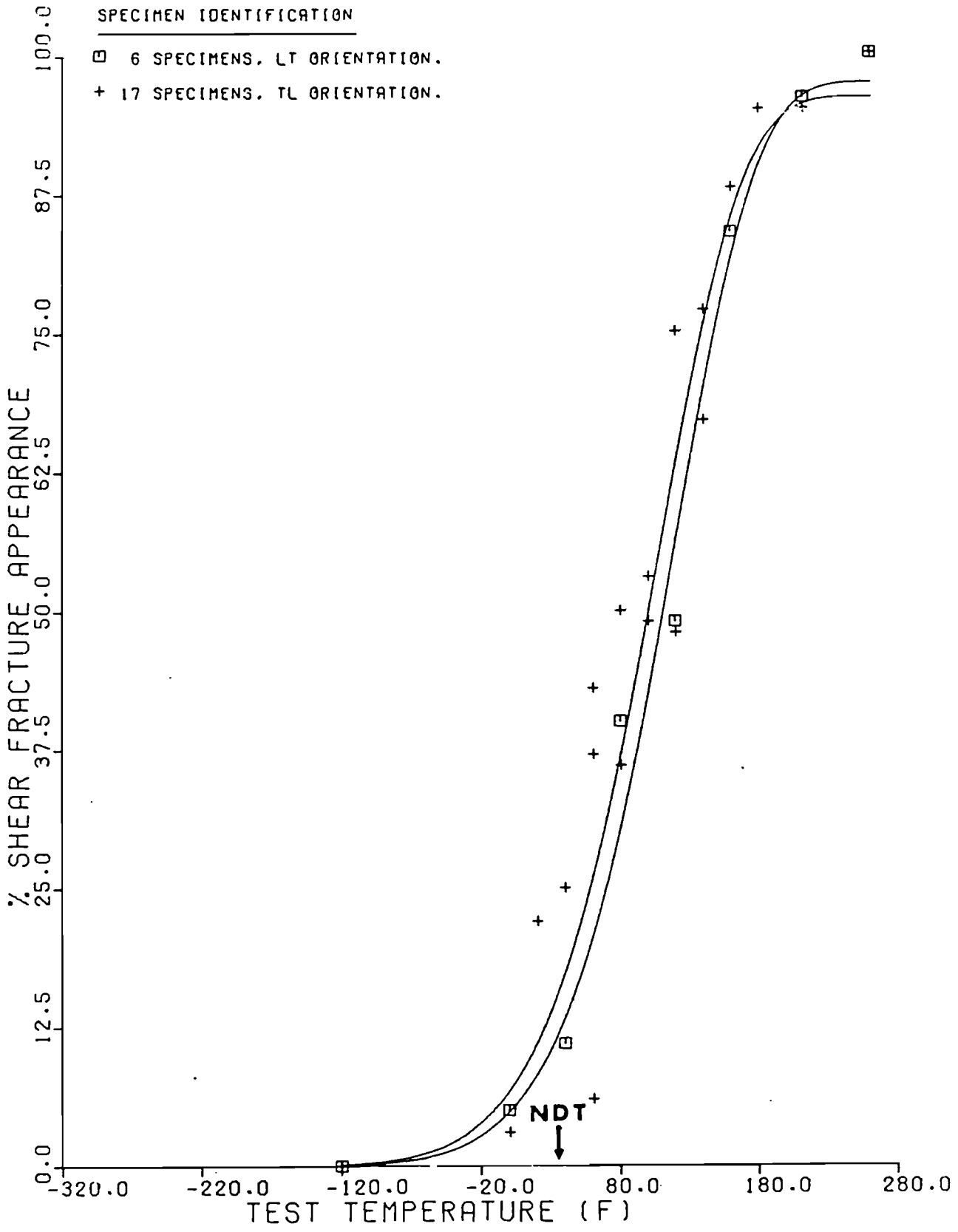

Figure 10. Charpy V-notch-Shear Fracture Appearance Results for Plate S.

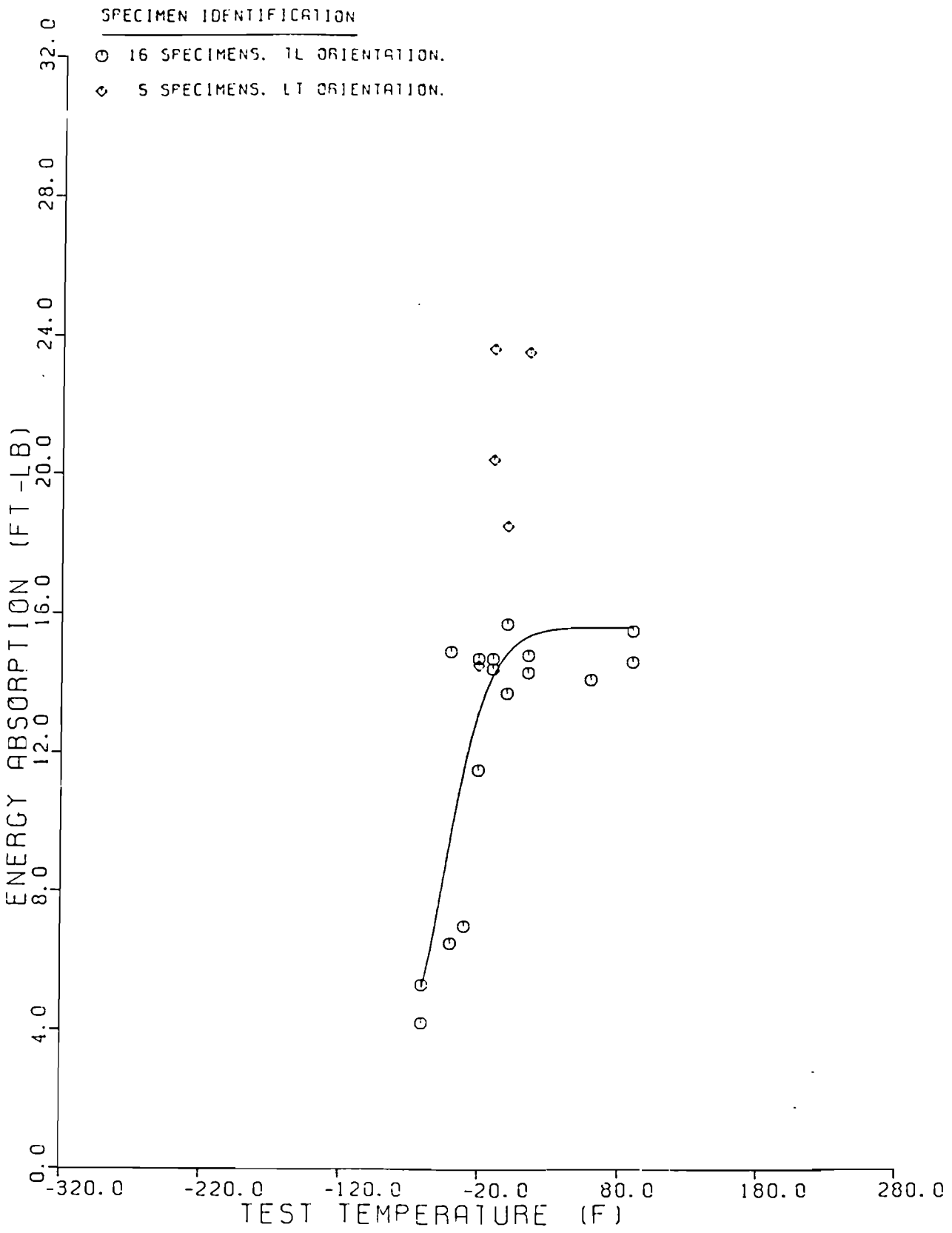

Figure 11. Precracked Charpy-Total Energy Absorption Results for Plate G.

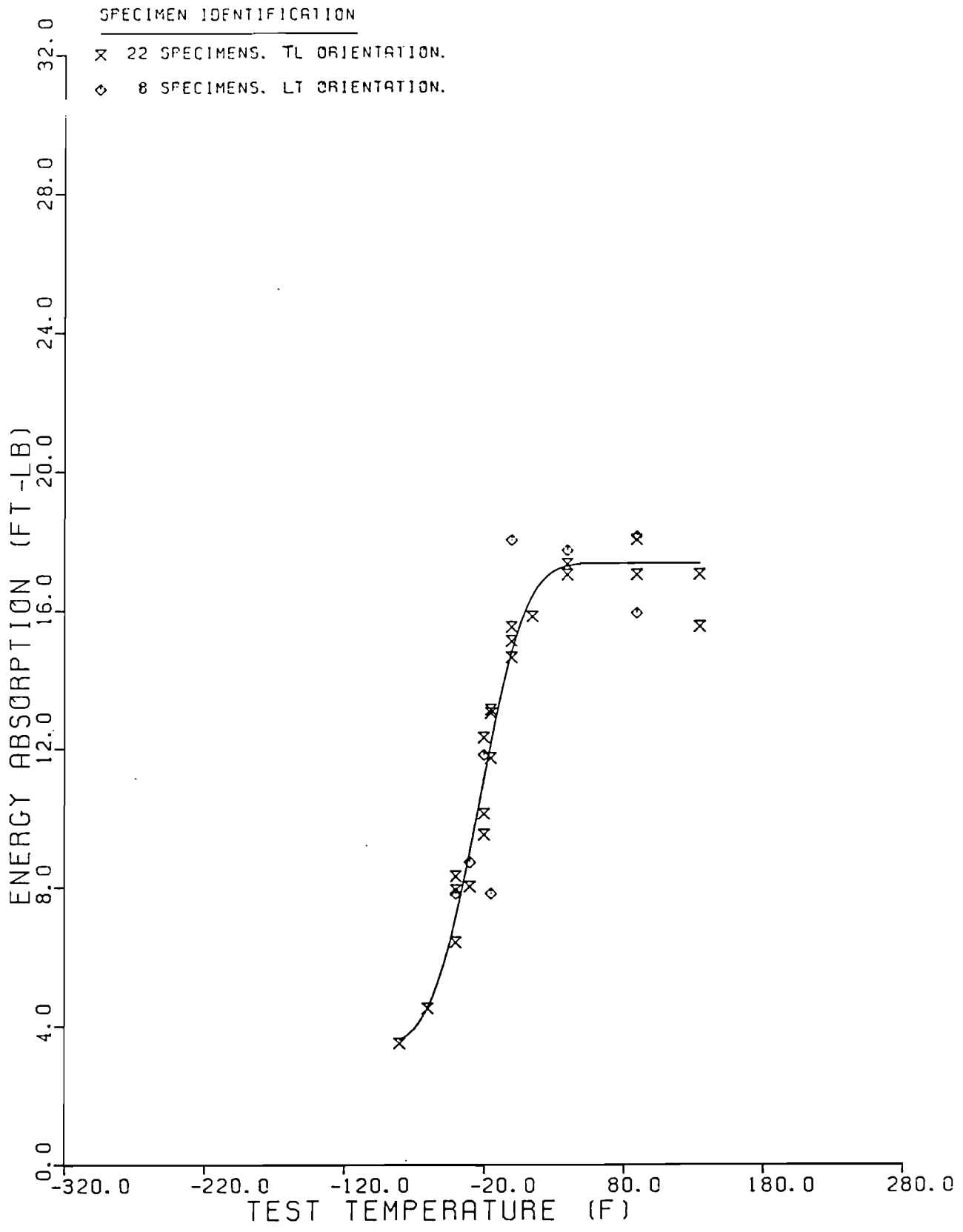

Figure 12. Precracked Charpy-Total Energy Absorption Results for Plate U.

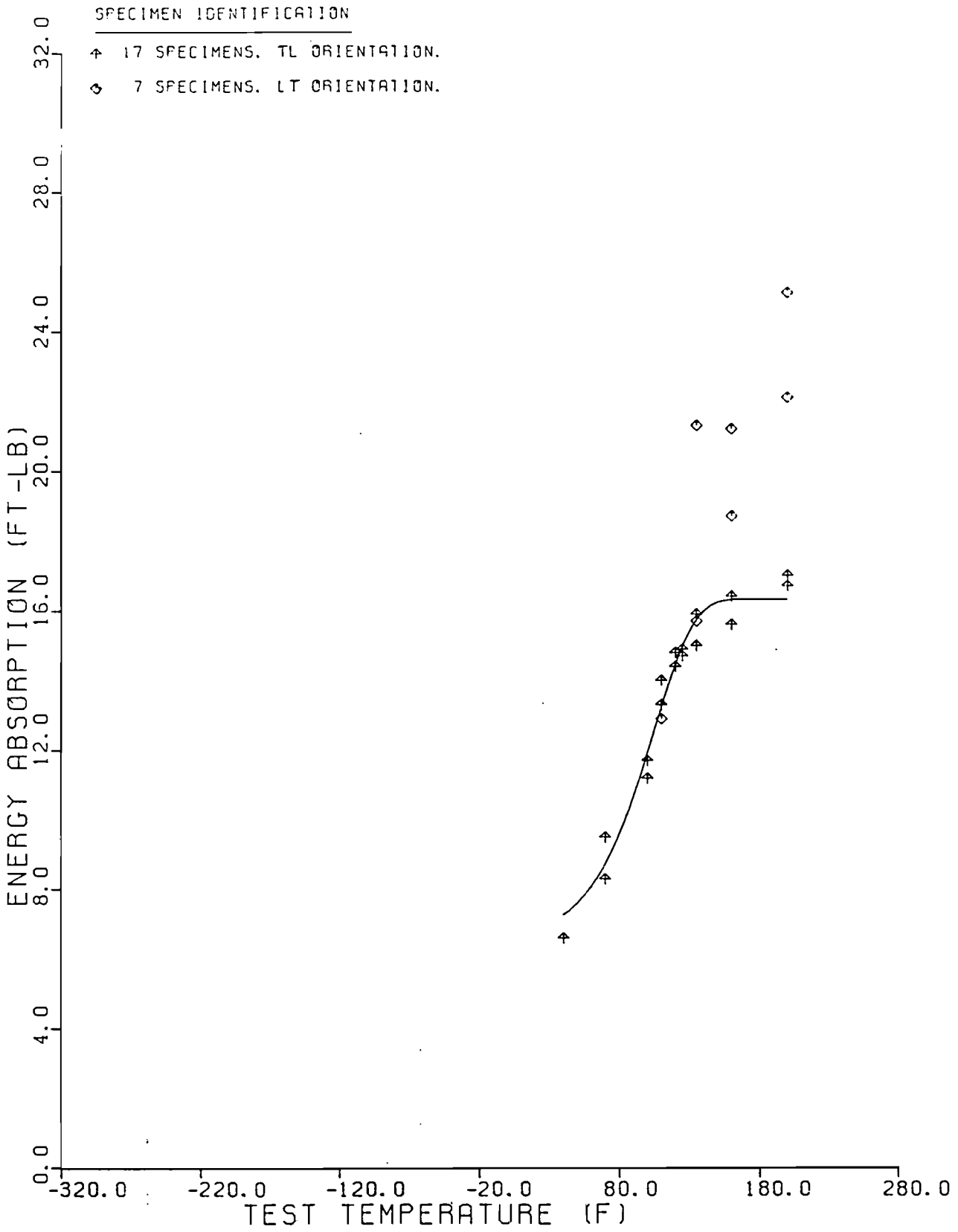

Figure 13. Precracked Charpy-Total Energy Absorption Results for Plate S.

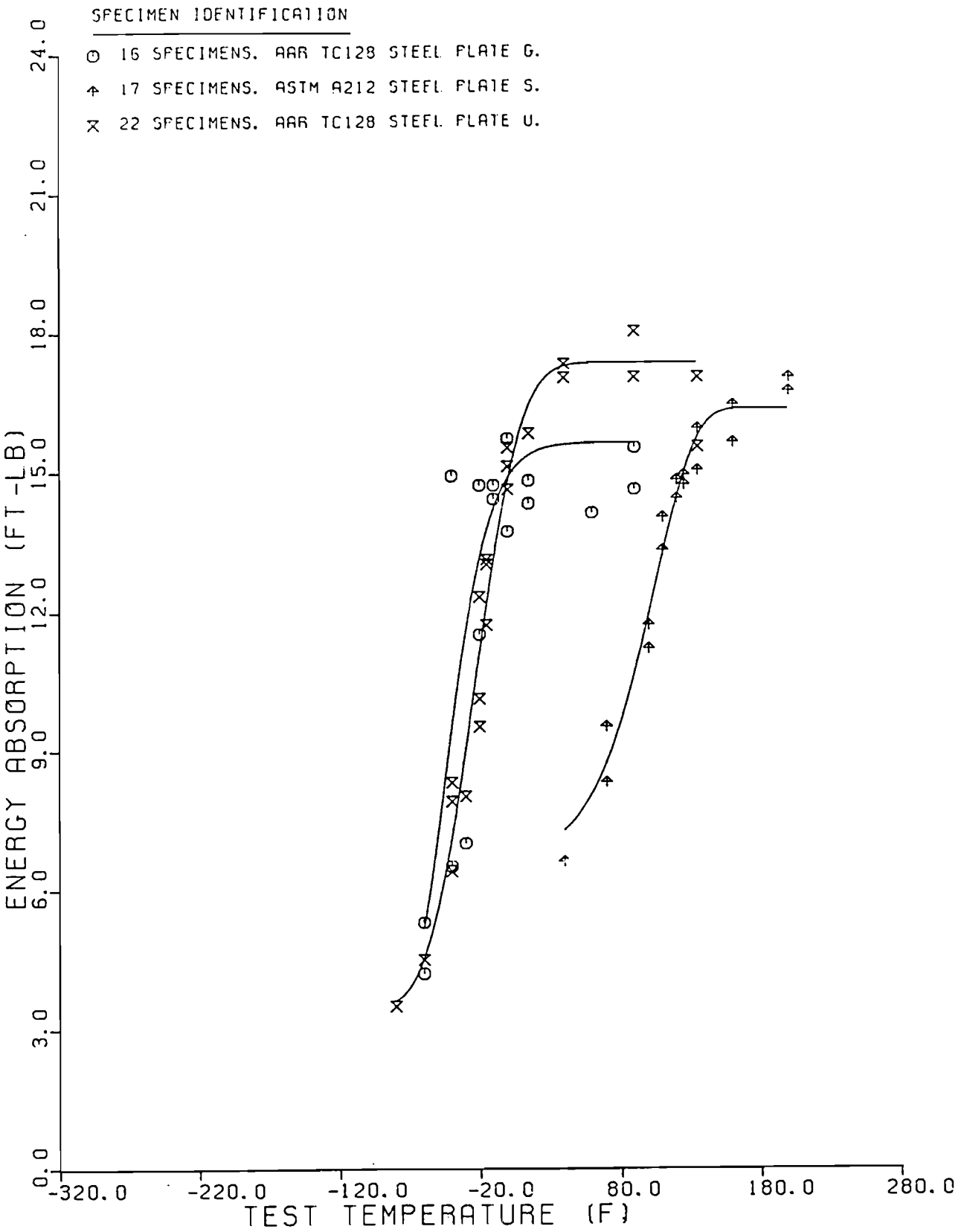

Figure 14. Comparison of Total Energy Absorbed for Plates G, U, and S.

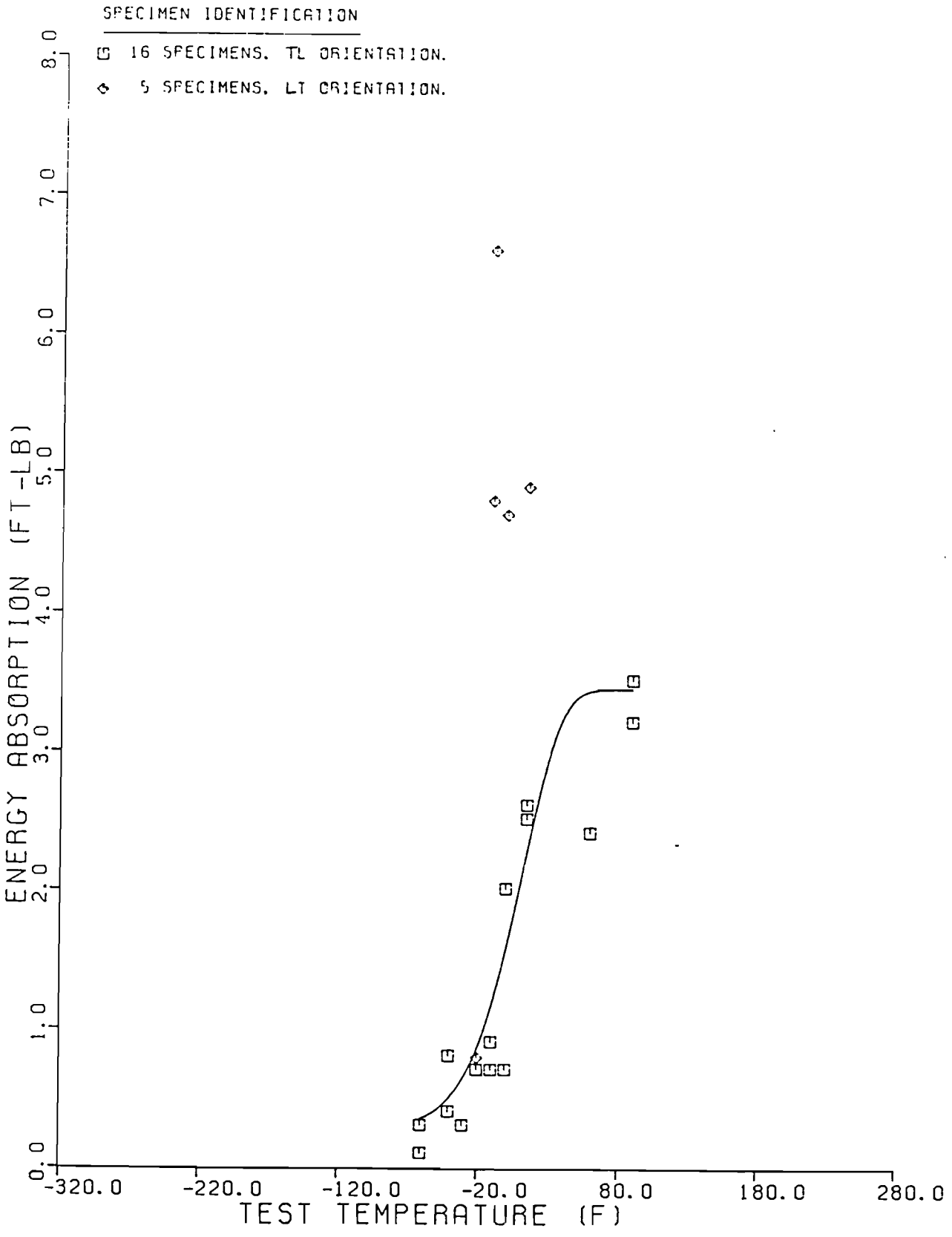

Figure 15. Precracked Charpy-Energy Absorbed to Maximum Load for Plate G.

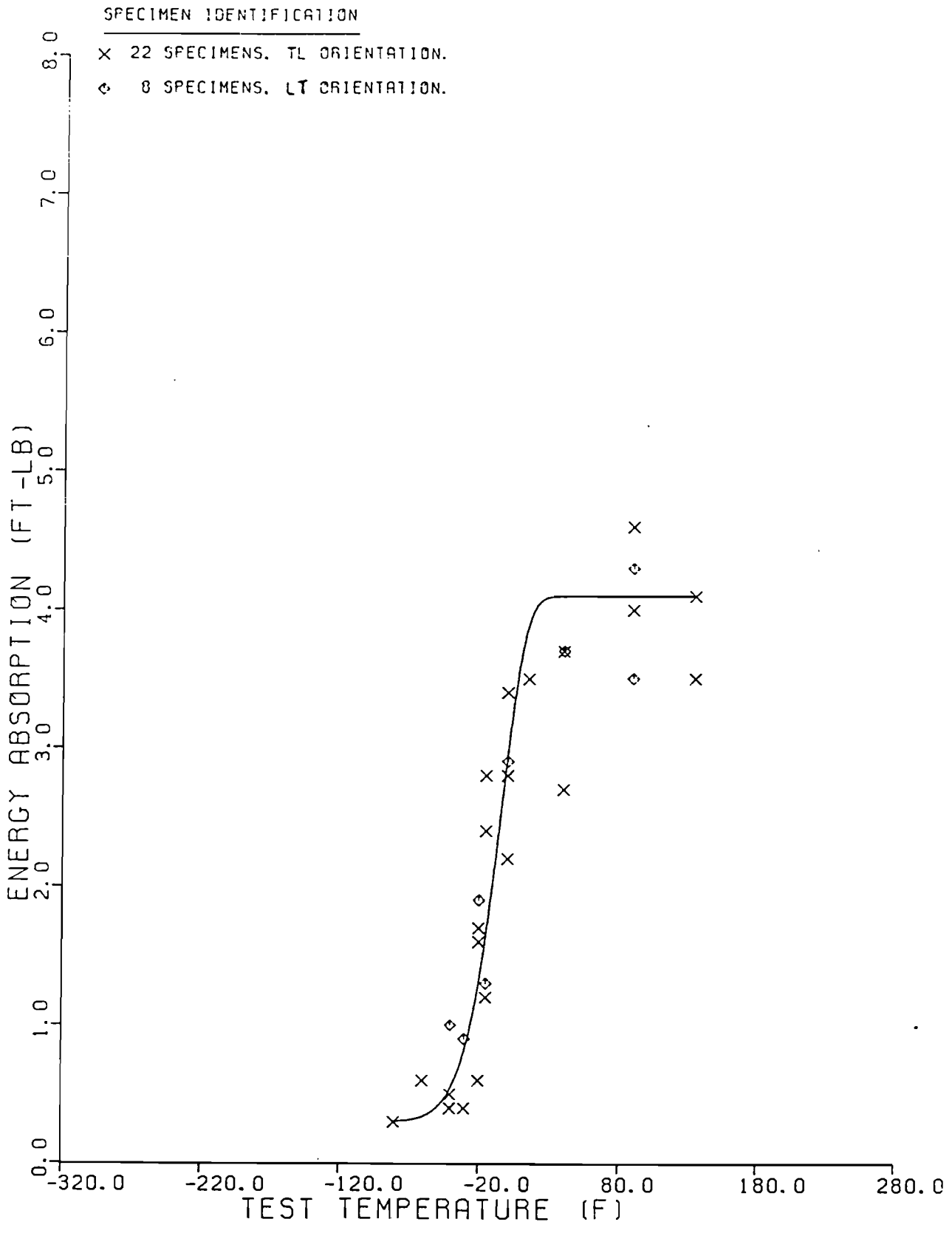

Figure 16. Precracked Charpy-Energy Absorbed to Maximum Load for Plate U.

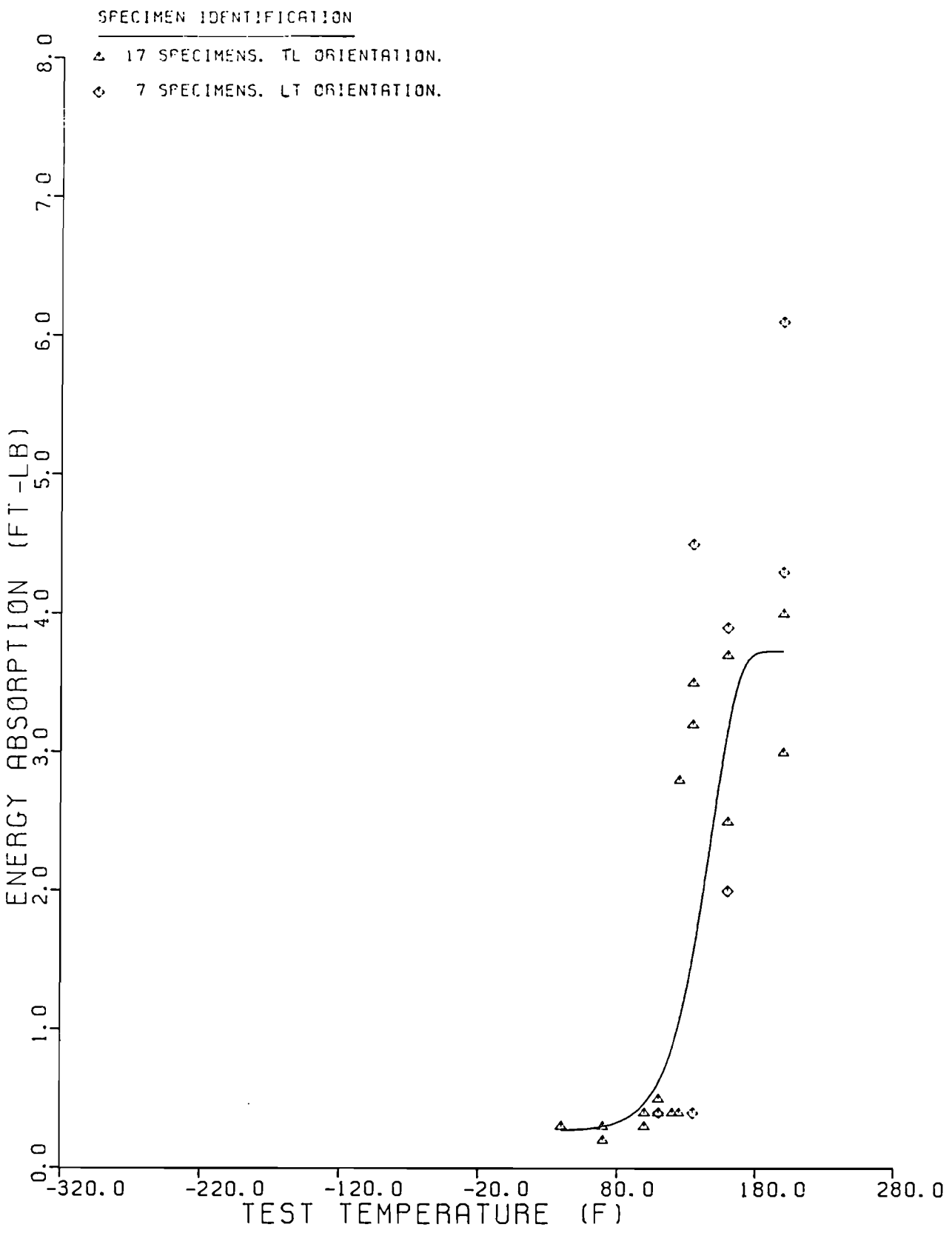

Figure 17. Precracked Charpy-Energy Absorbed to Maximum Load for Plate S.

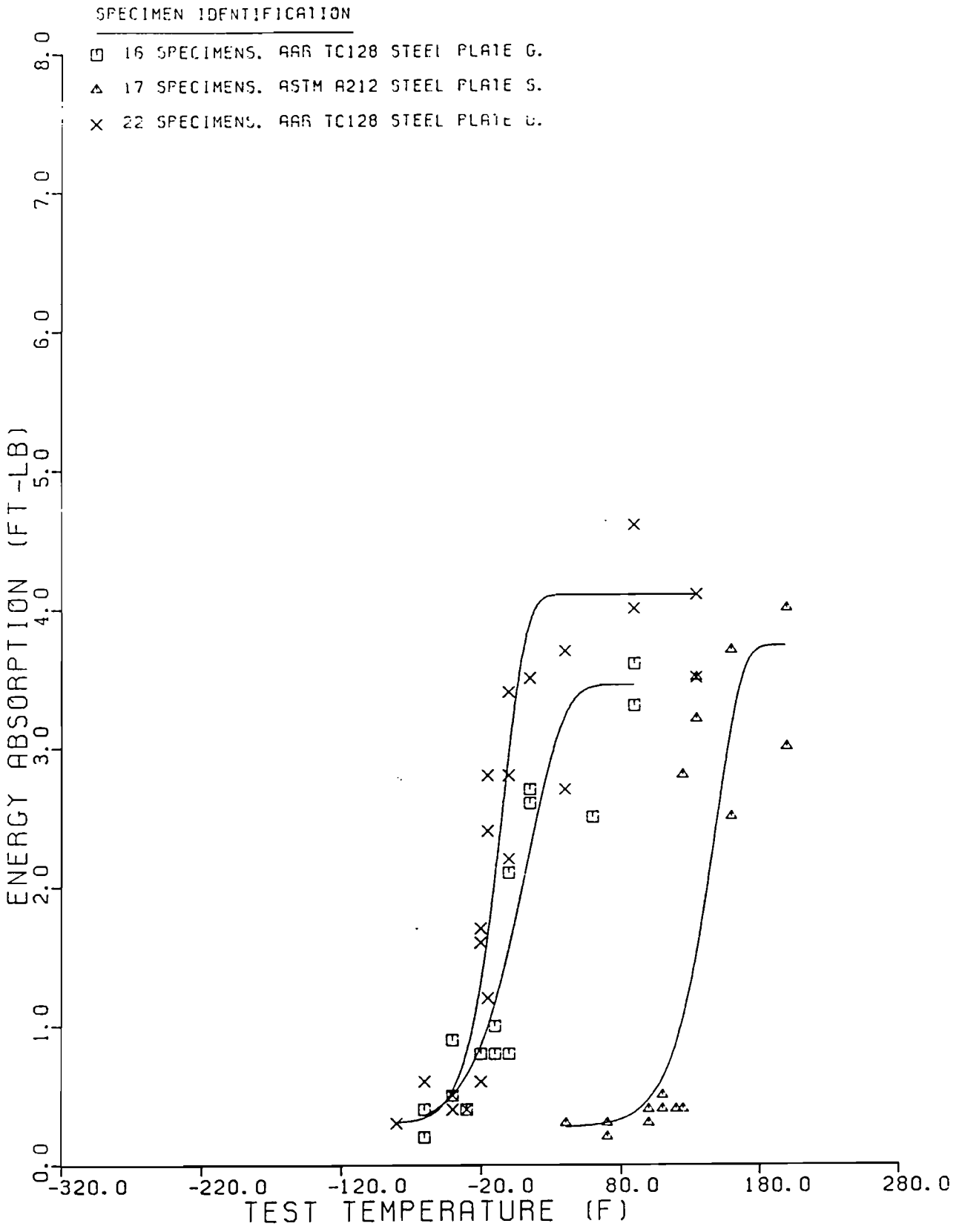

Figure 18. Comparison of Energy Absorbed to Maximum Load for Plates G, U, and S.

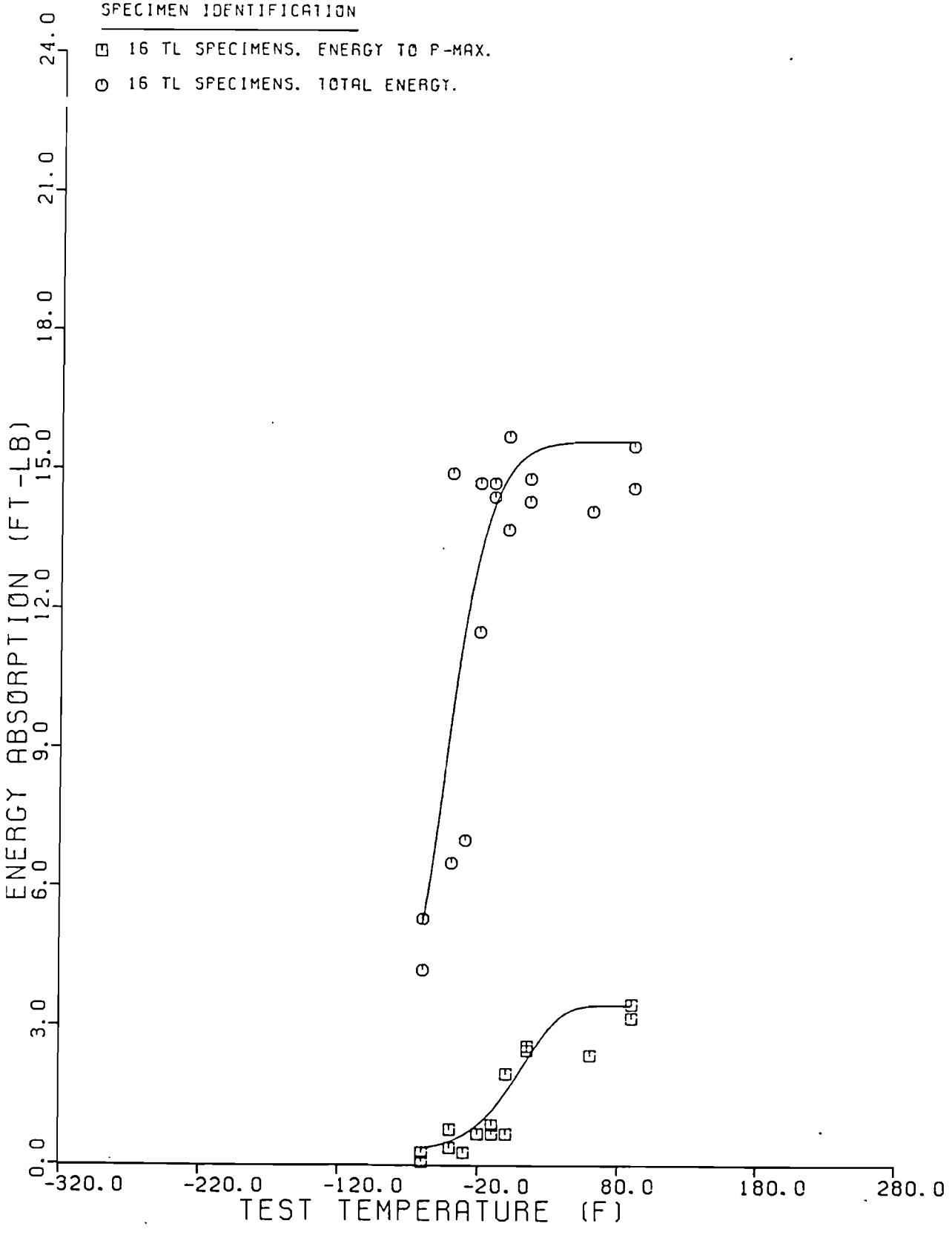

Figure 19. Comparison of Total Energy and Energy Absorbed to Maximum Load for Plate G.

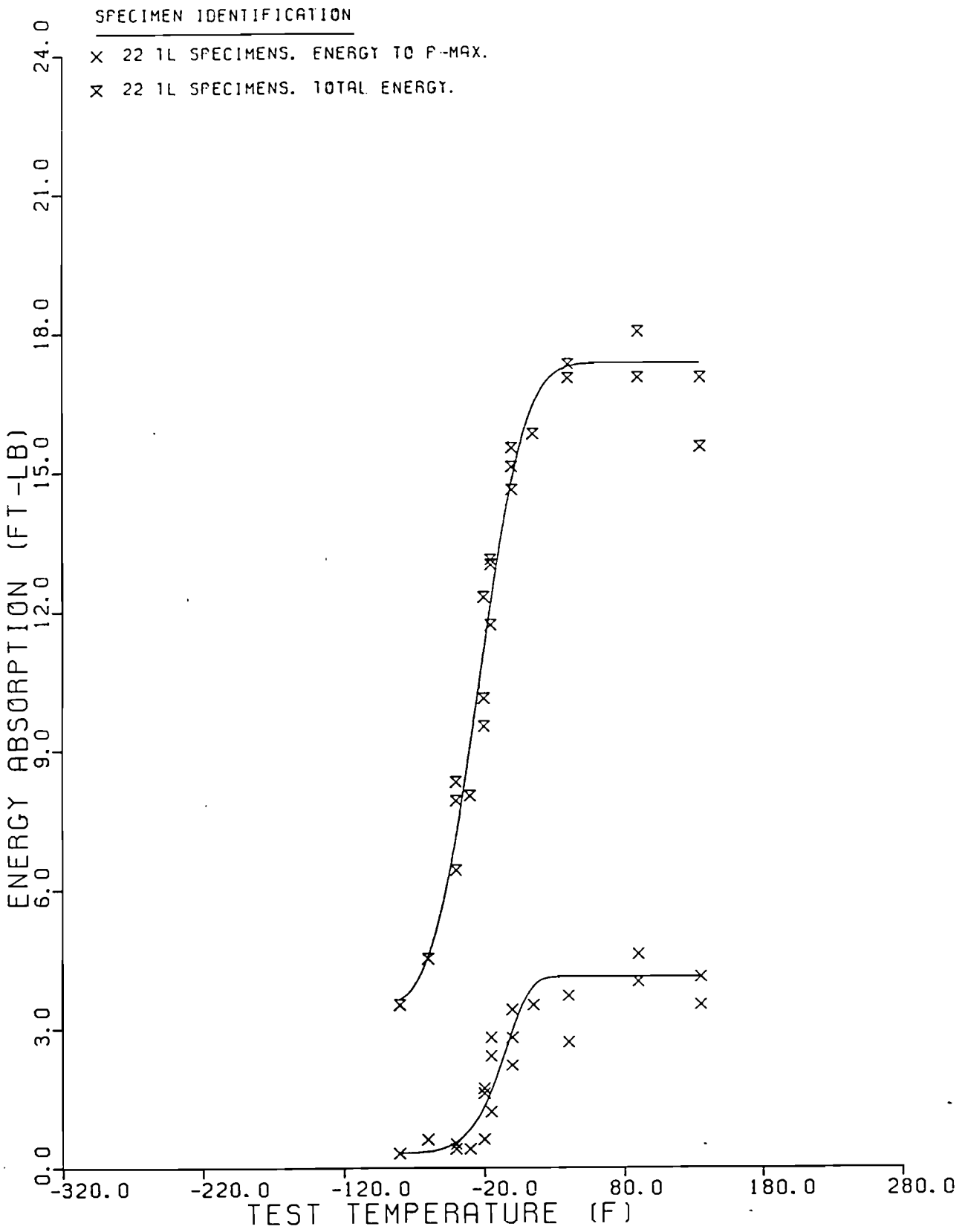

Figure 20. Comparison of Total Energy and Energy Absorbed to Maximum Load for Plate U.

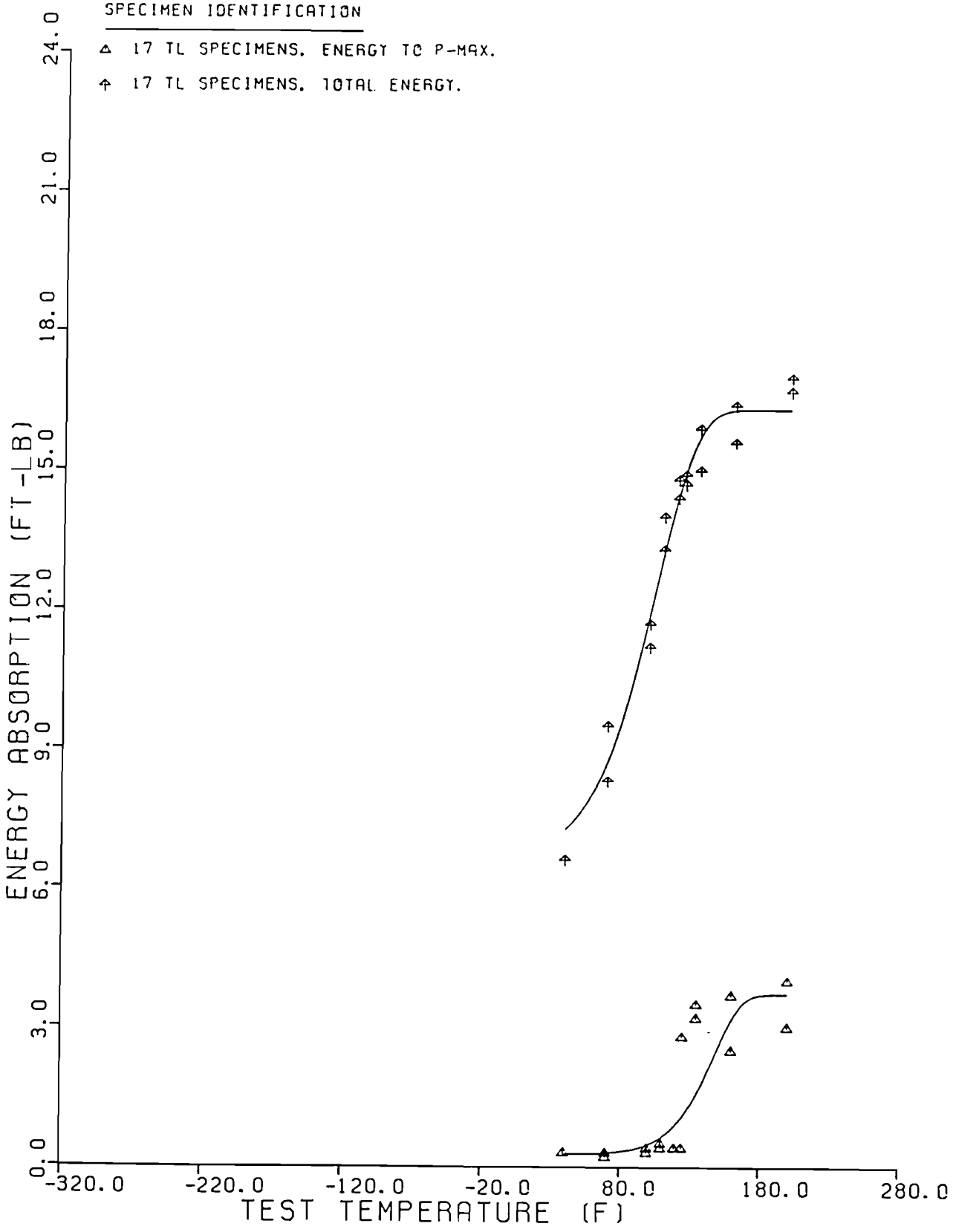

Figure 21. Comparison of Total Energy and Energy Absorbed to Maximum Load for Plate S.

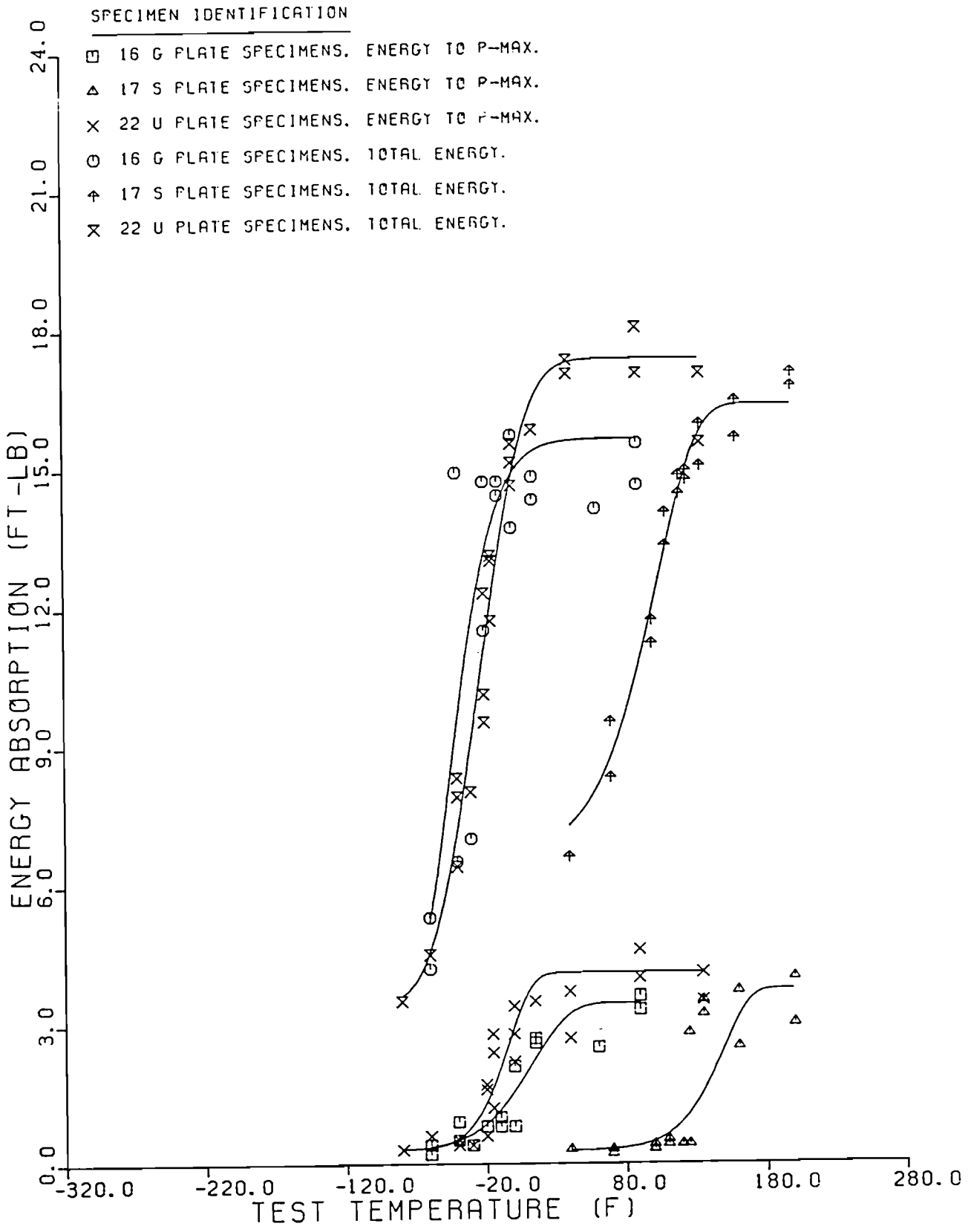

Figure 22. Comparison of Total Energy and Energy Absorbed to Maximum Load for Plates G, U, and S.

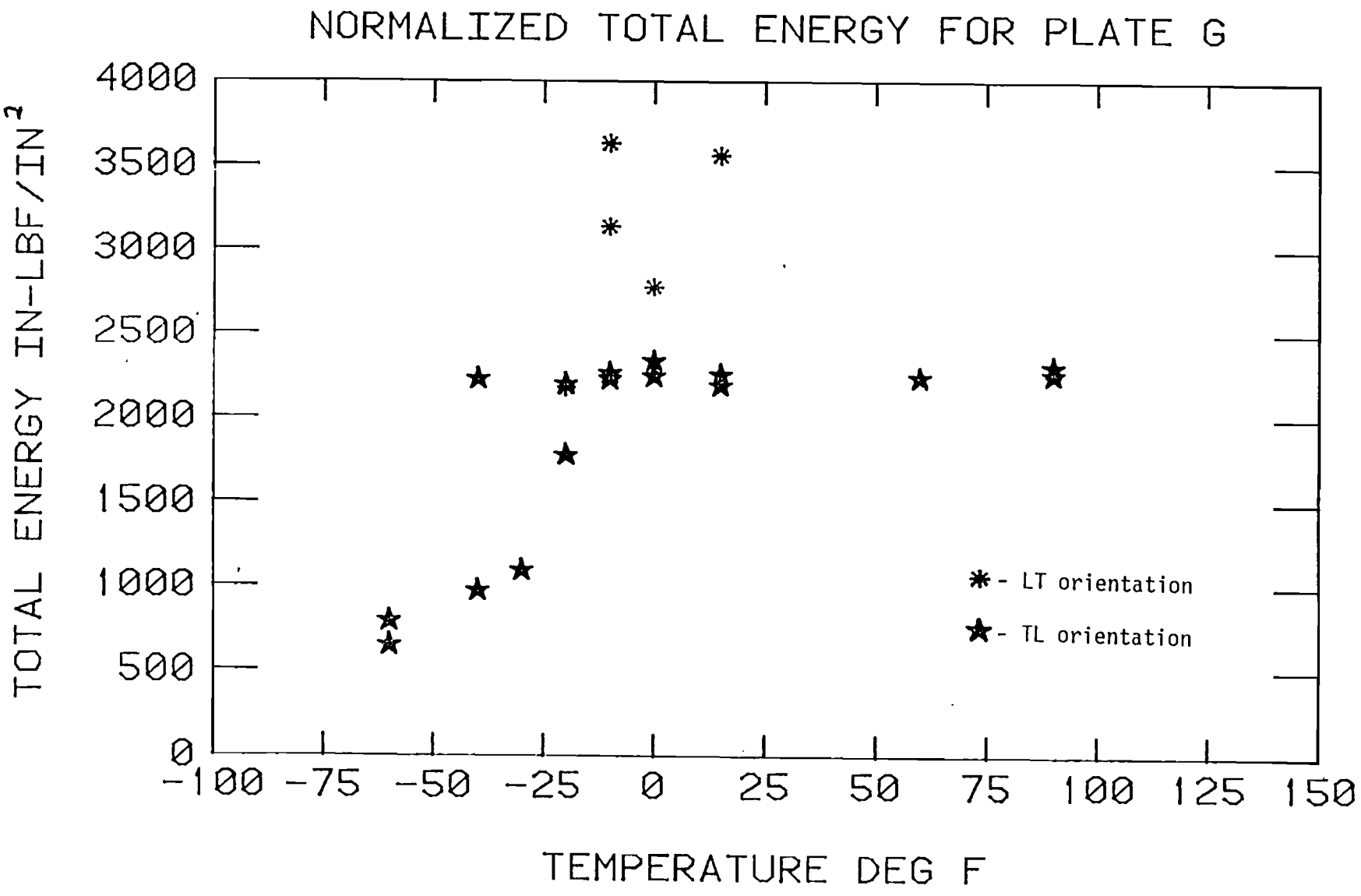

Figure 23. Precracked Charpy-Normalized Total Energies for Plate G.

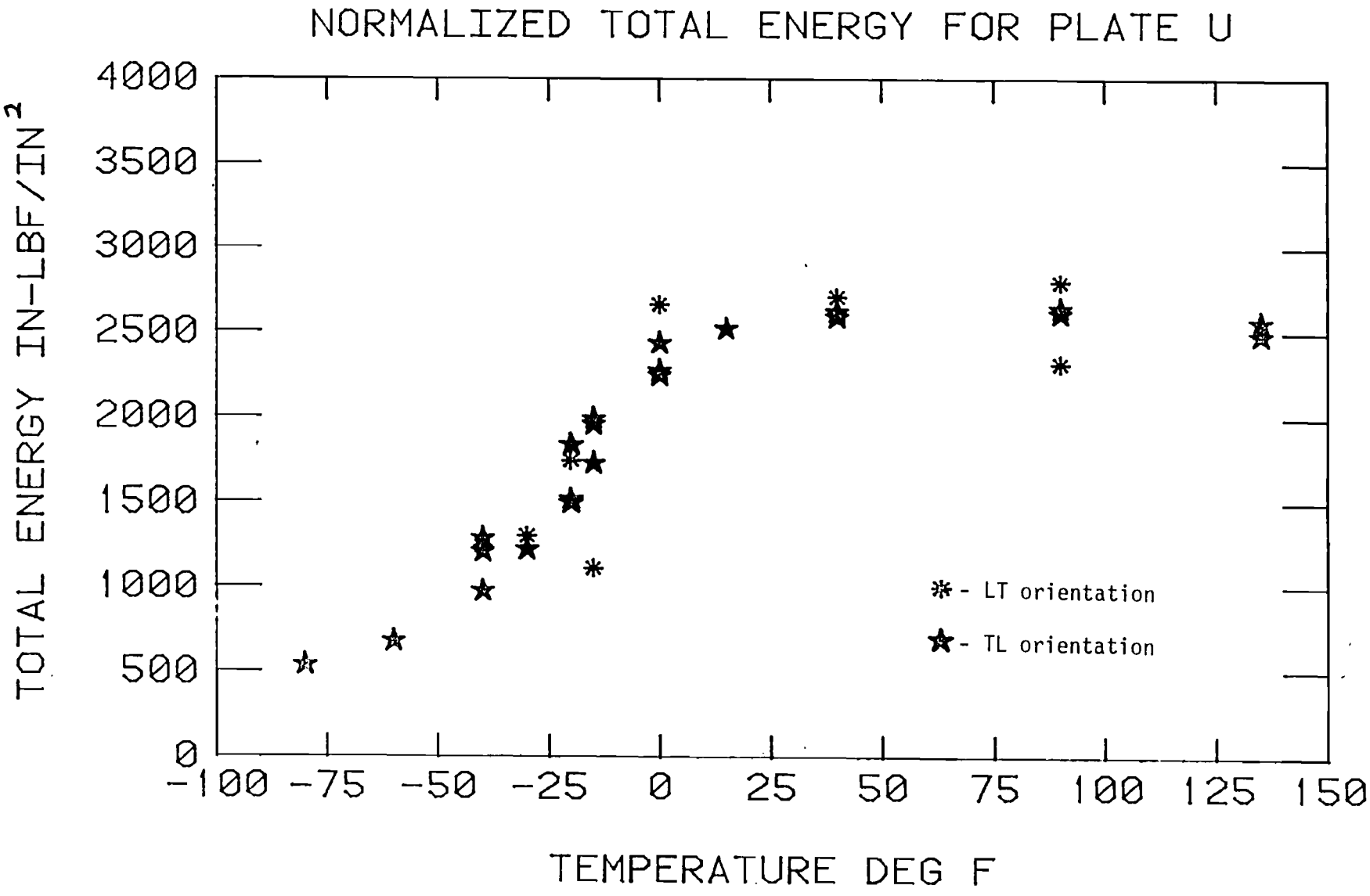

Figure 24. Precracked Charpy-Normalized Total Energies for Plate U.

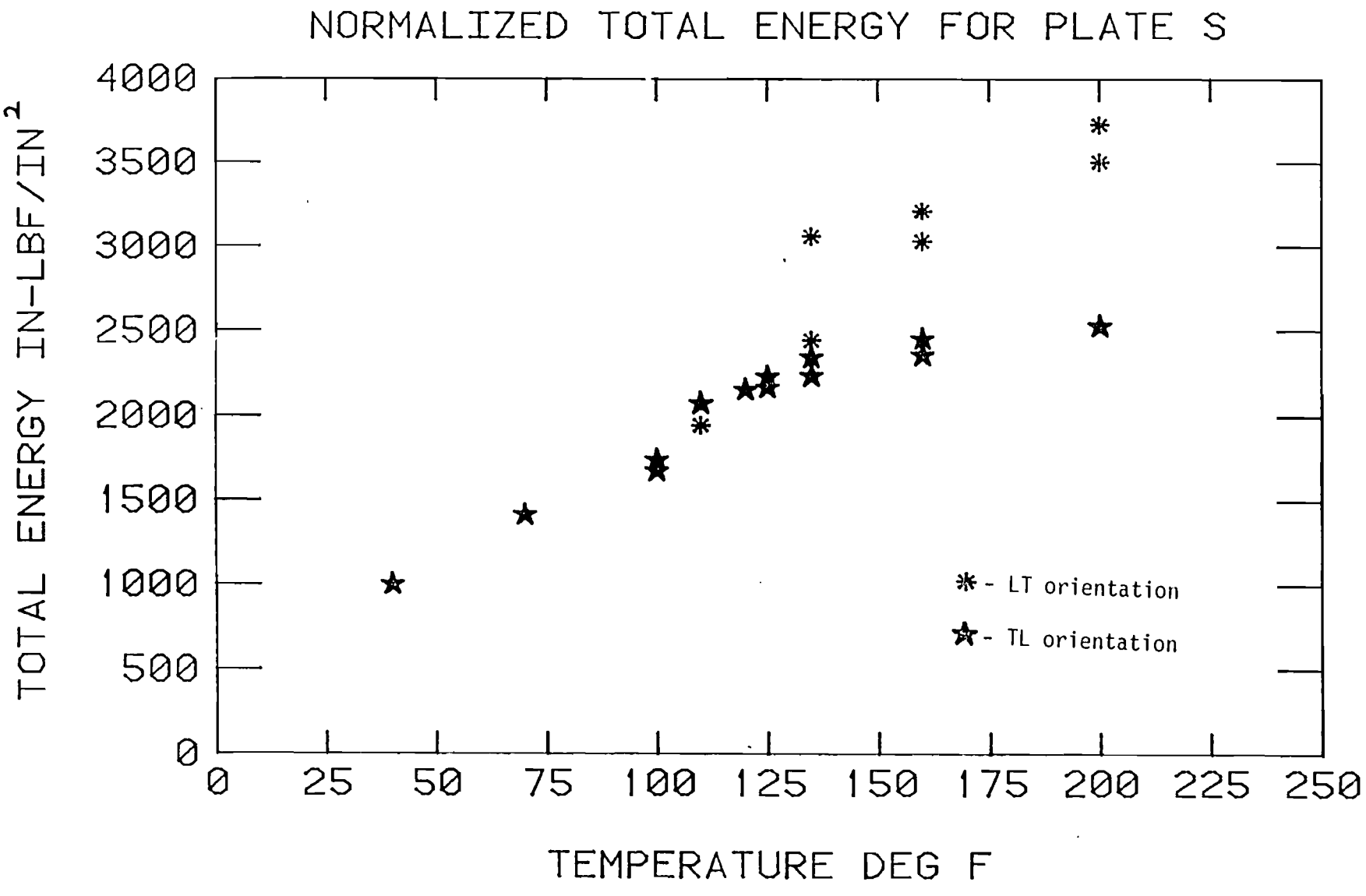

Figure 25. Precracked Charpy-Normalized Total Energies for Plate S.

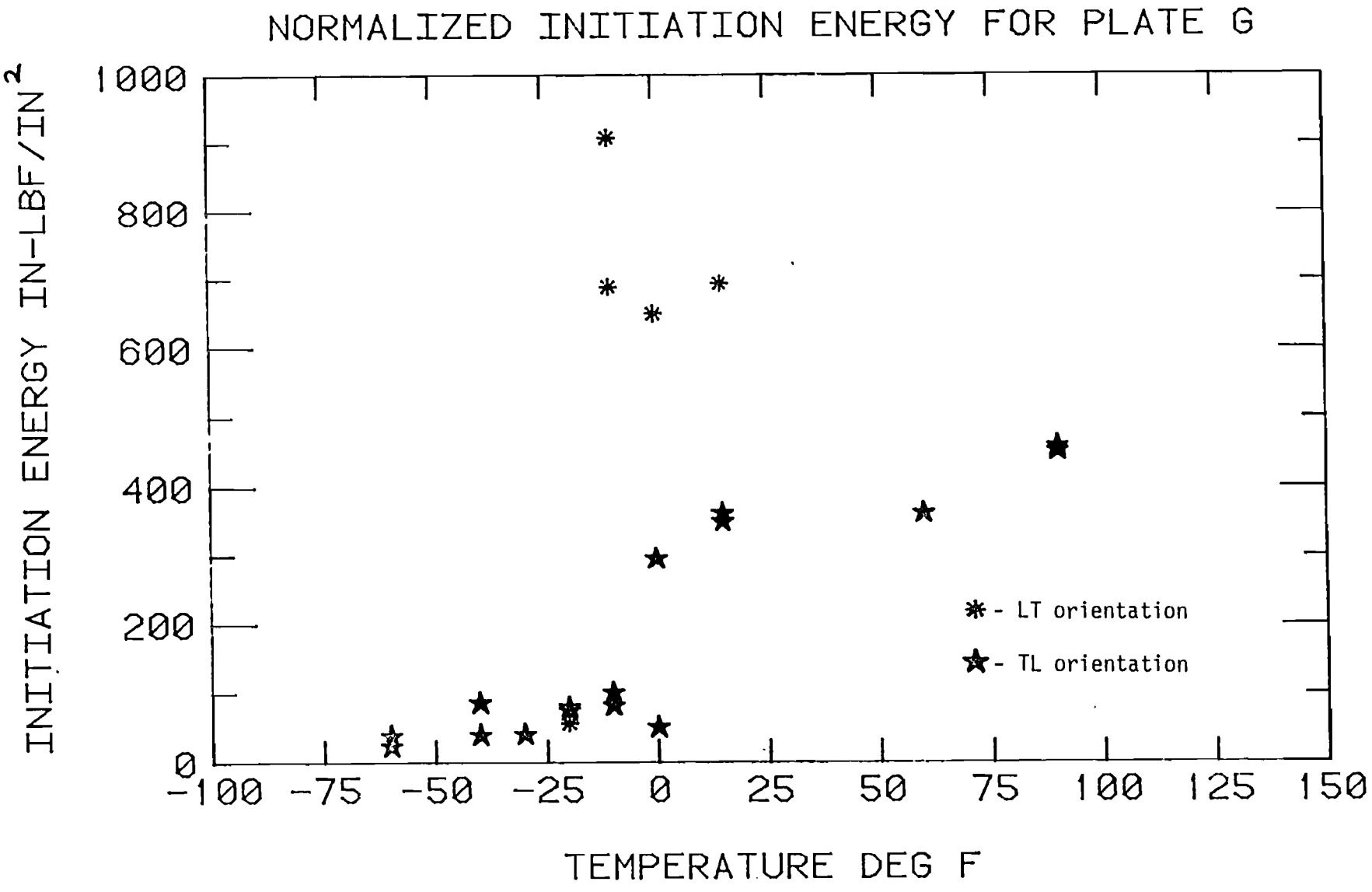

Figure 26. Precracked Charpy-Normalized Initiation Energies for Plate G.

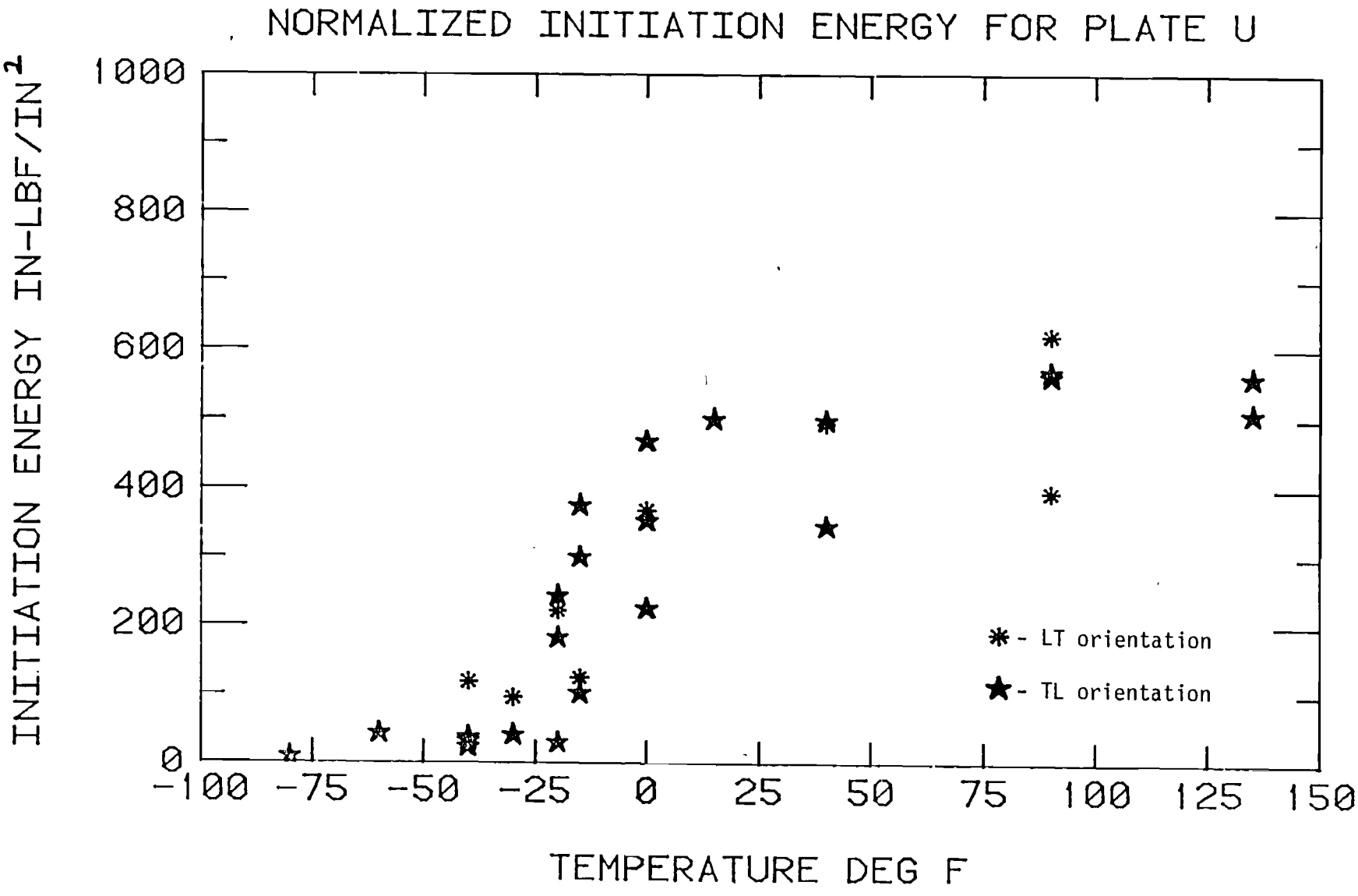

Figure 27. Precracked Charpy-Normalized Initiation Energies for Plate U.

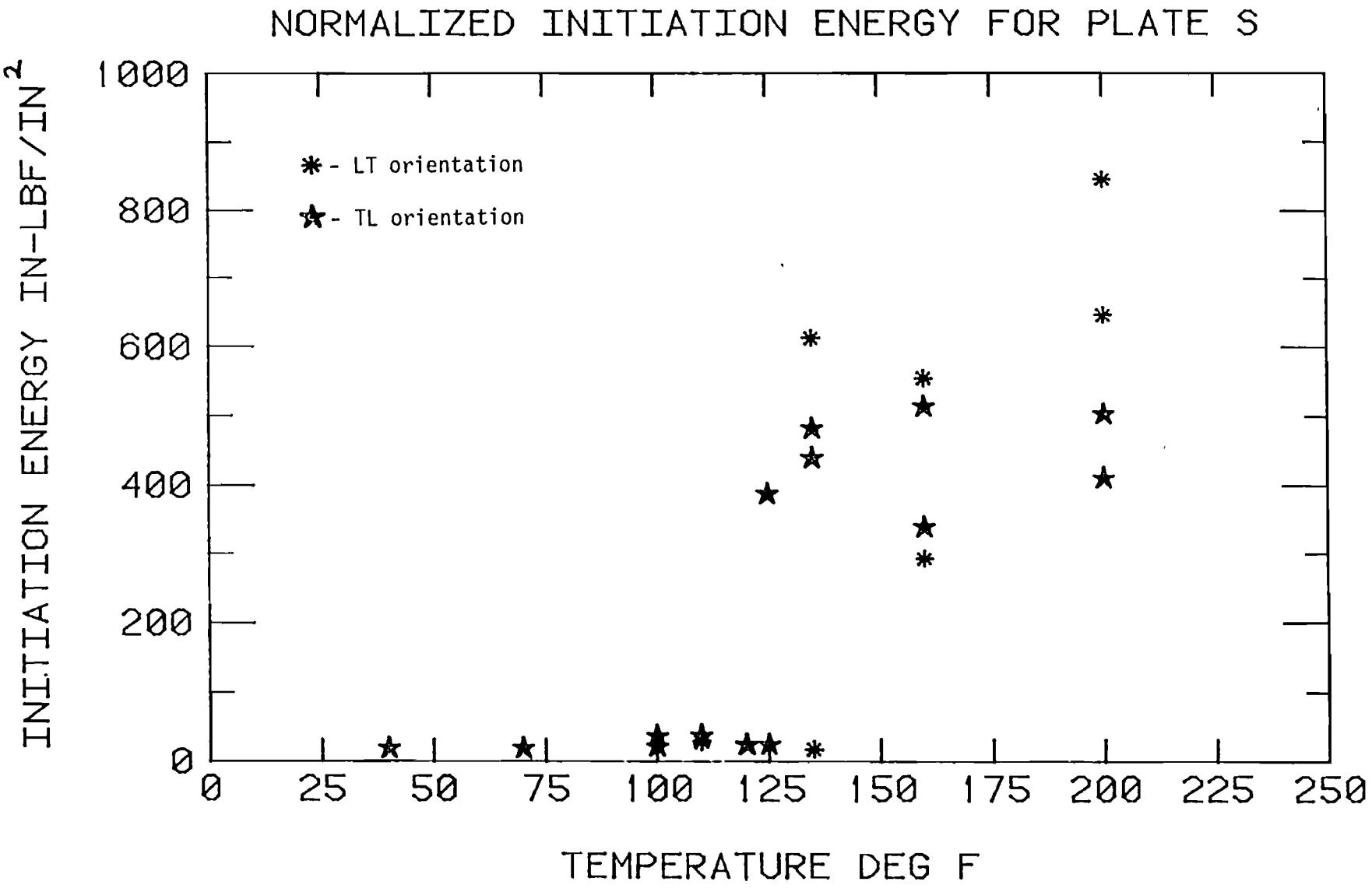

Figure 28. Precracked Charpy-Normalized Initiation Energies for Plate S.

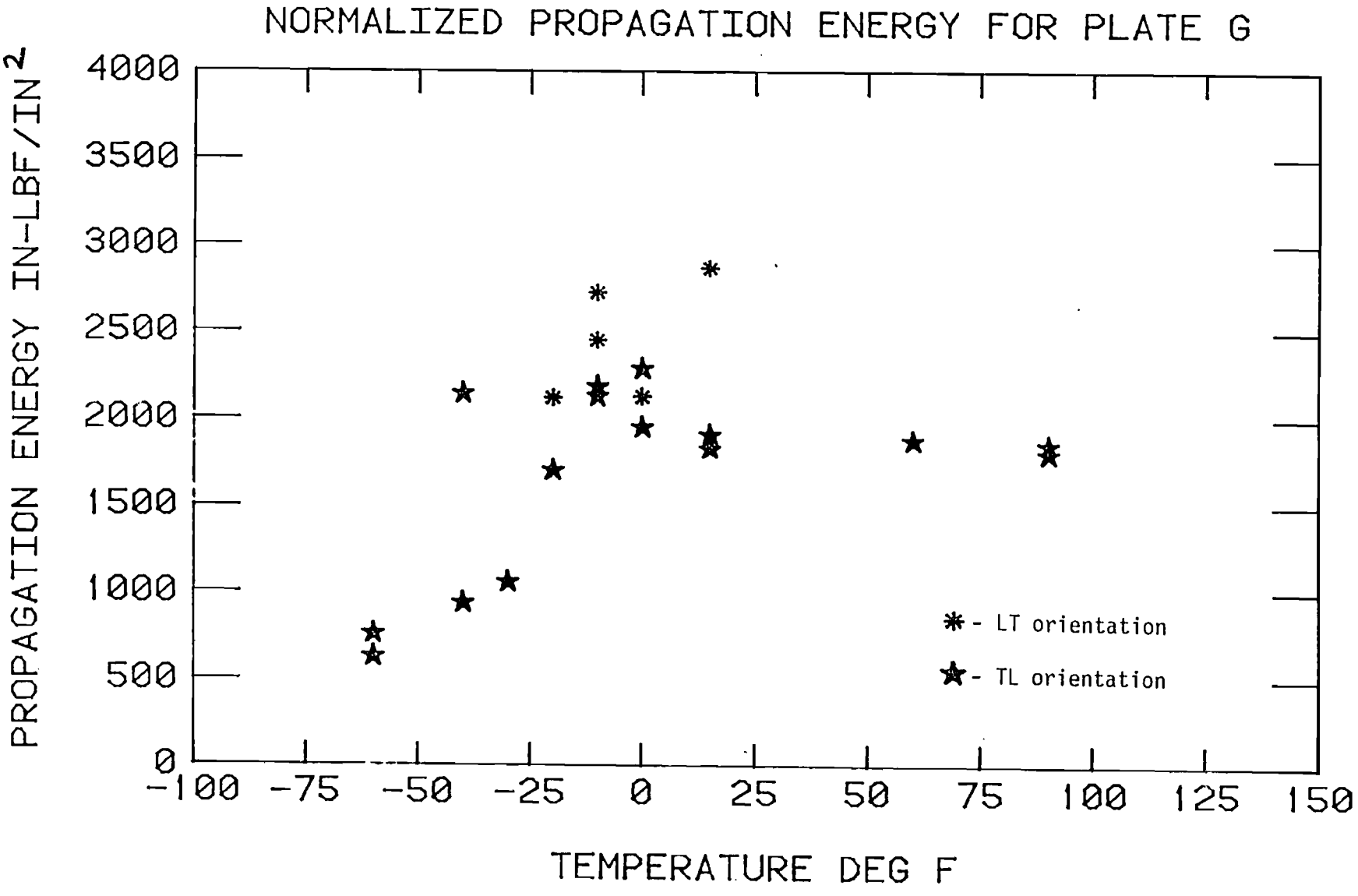

Figure 29. Precracked Charpy-Normalized Propagation Energies for Plate G.

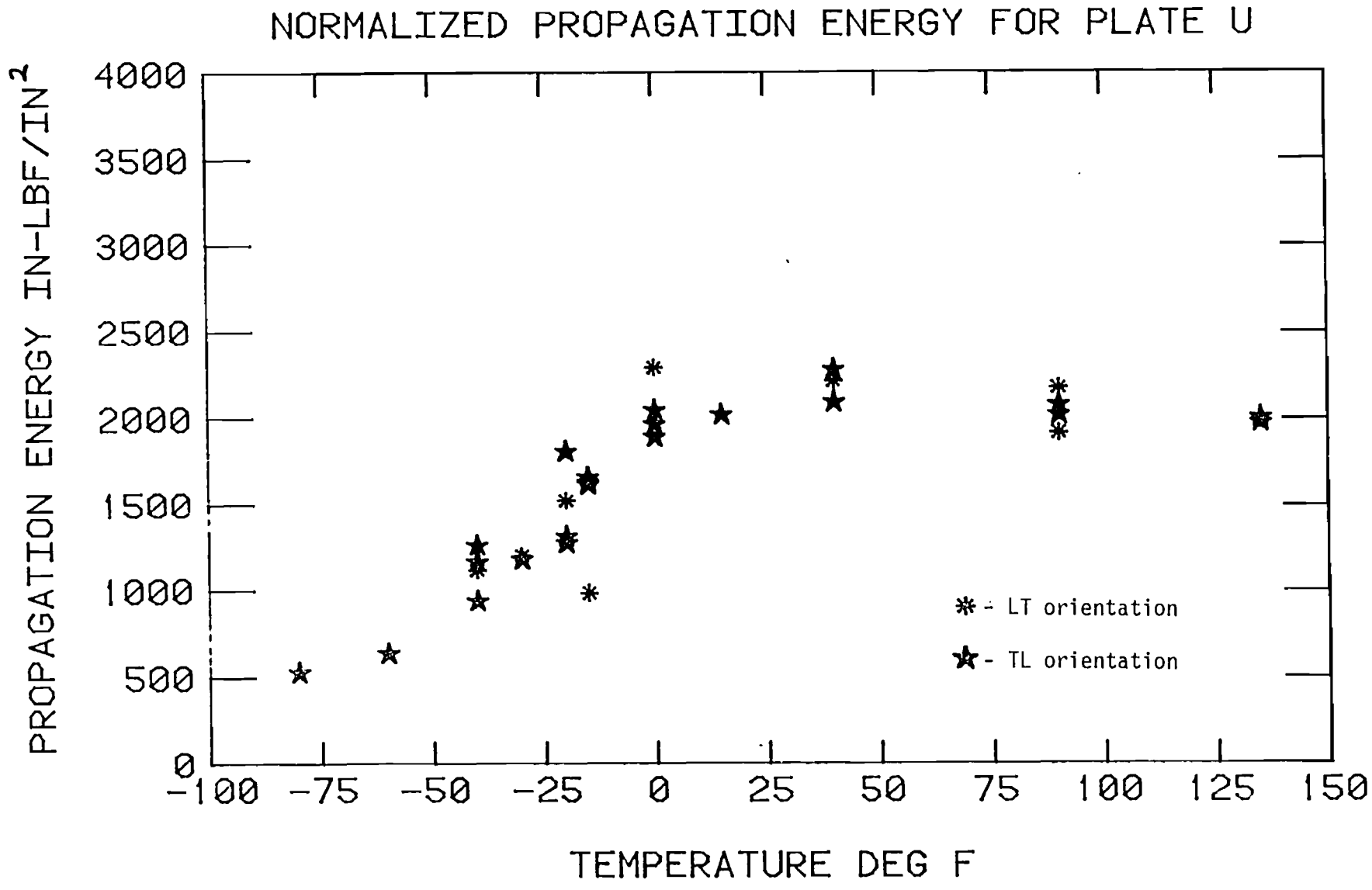

Figure 30. Precracked Charpy-Normalized Propagation Energies for Plate U.

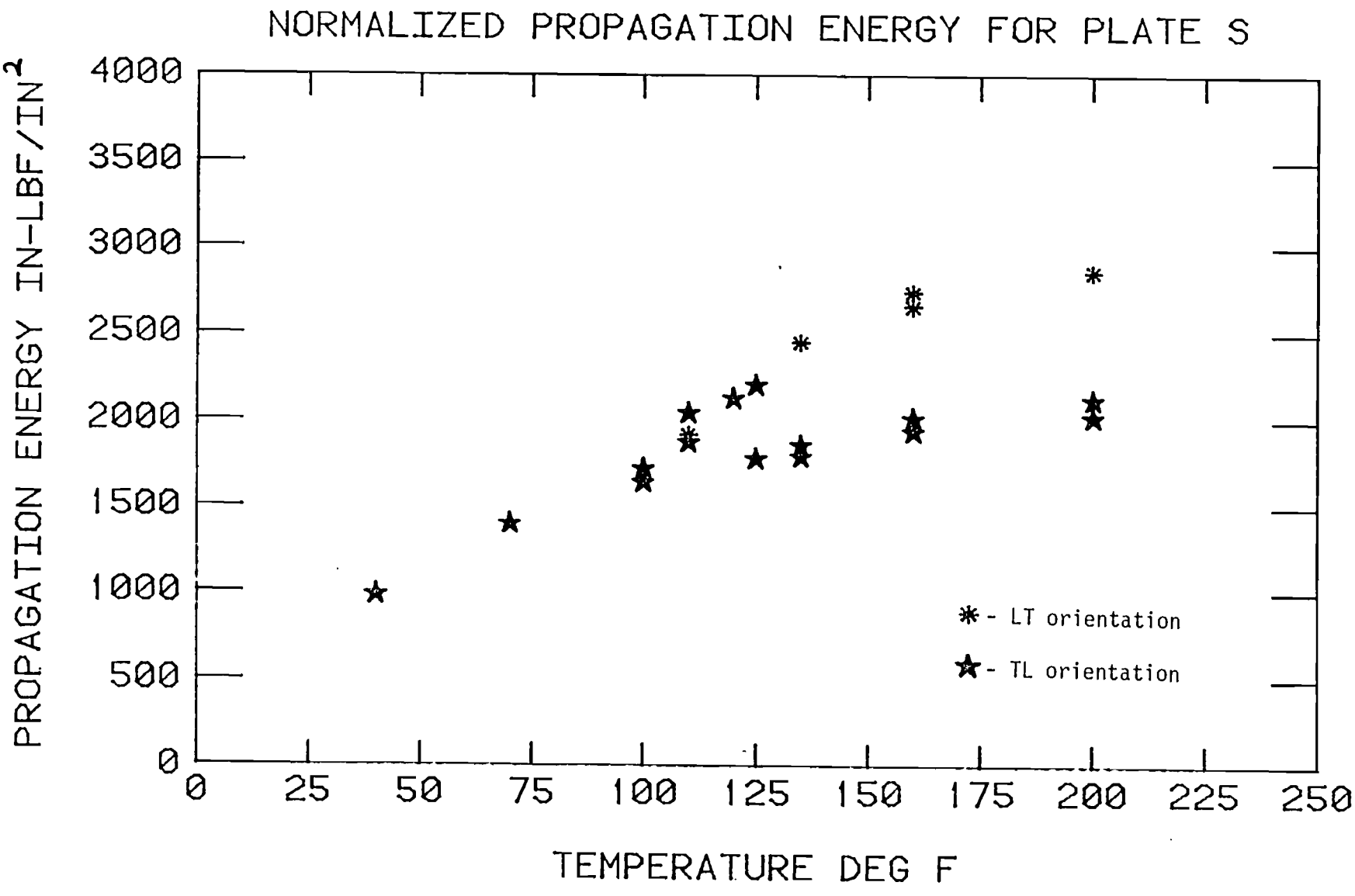

Figure 31. Precracked Charpy-Normalized Propagation Energies for Plate S.

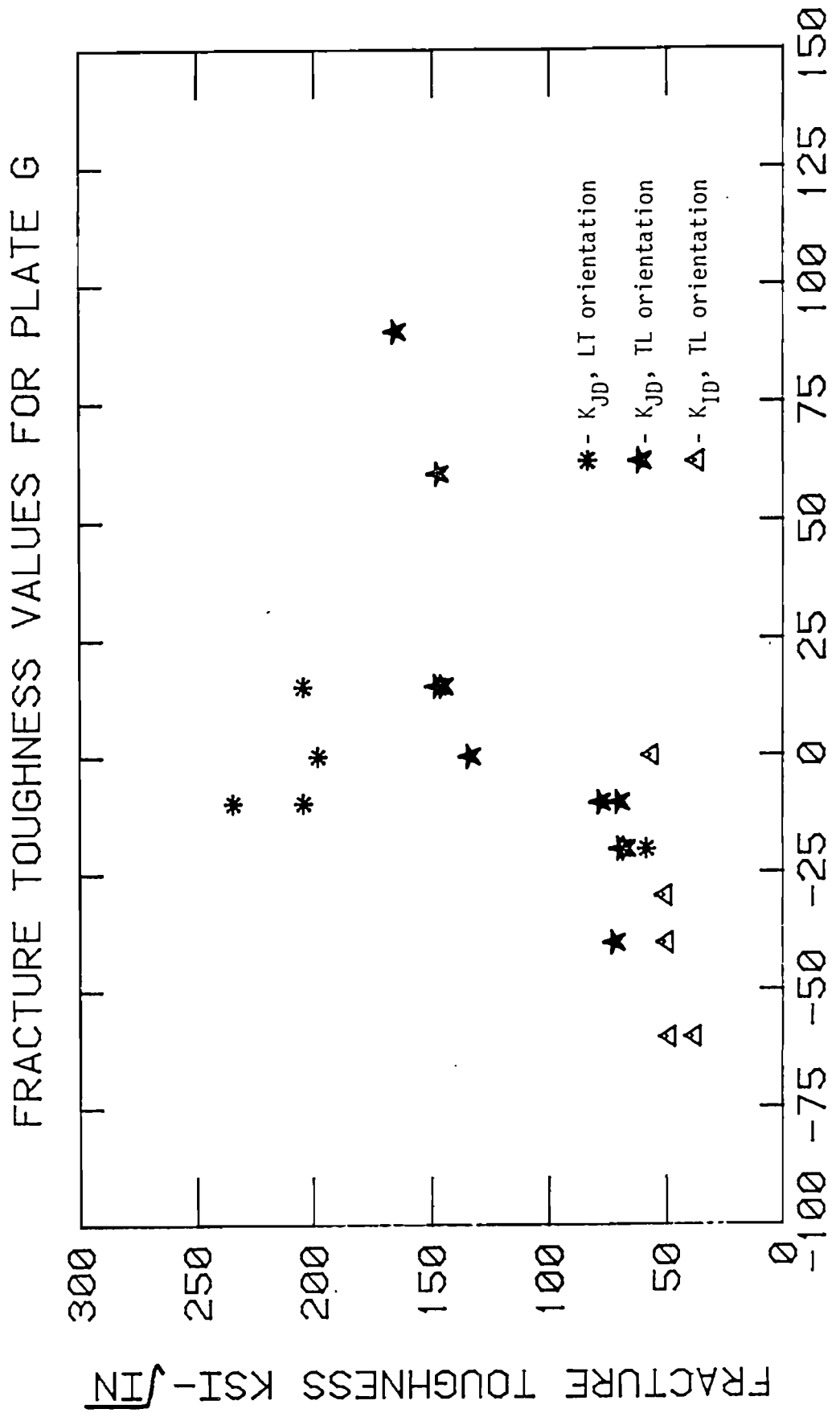

Figure 32. Fracture Toughness Values for Plate G.

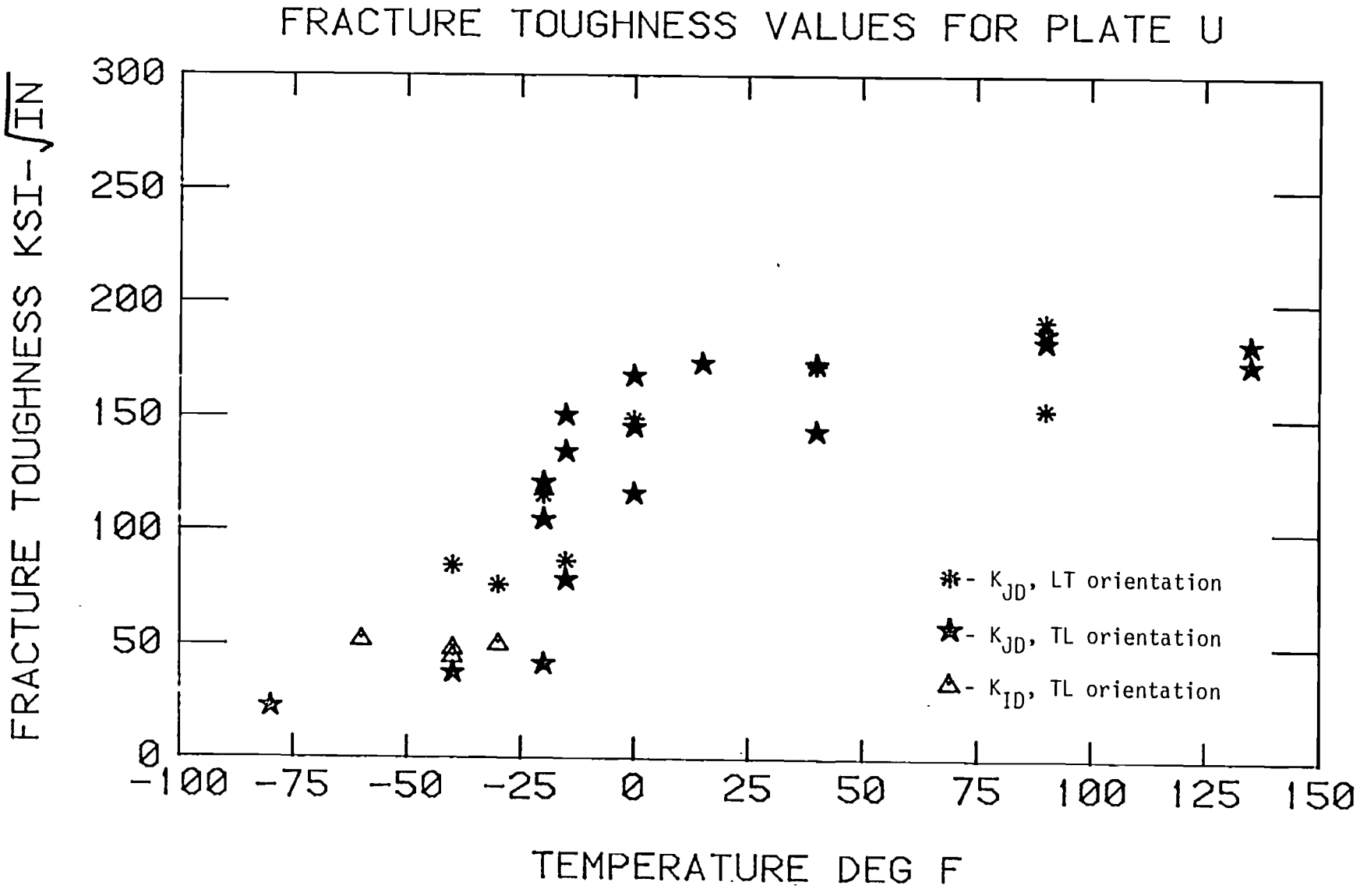

Figure 33. Fracture Toughness Values for Plate U.

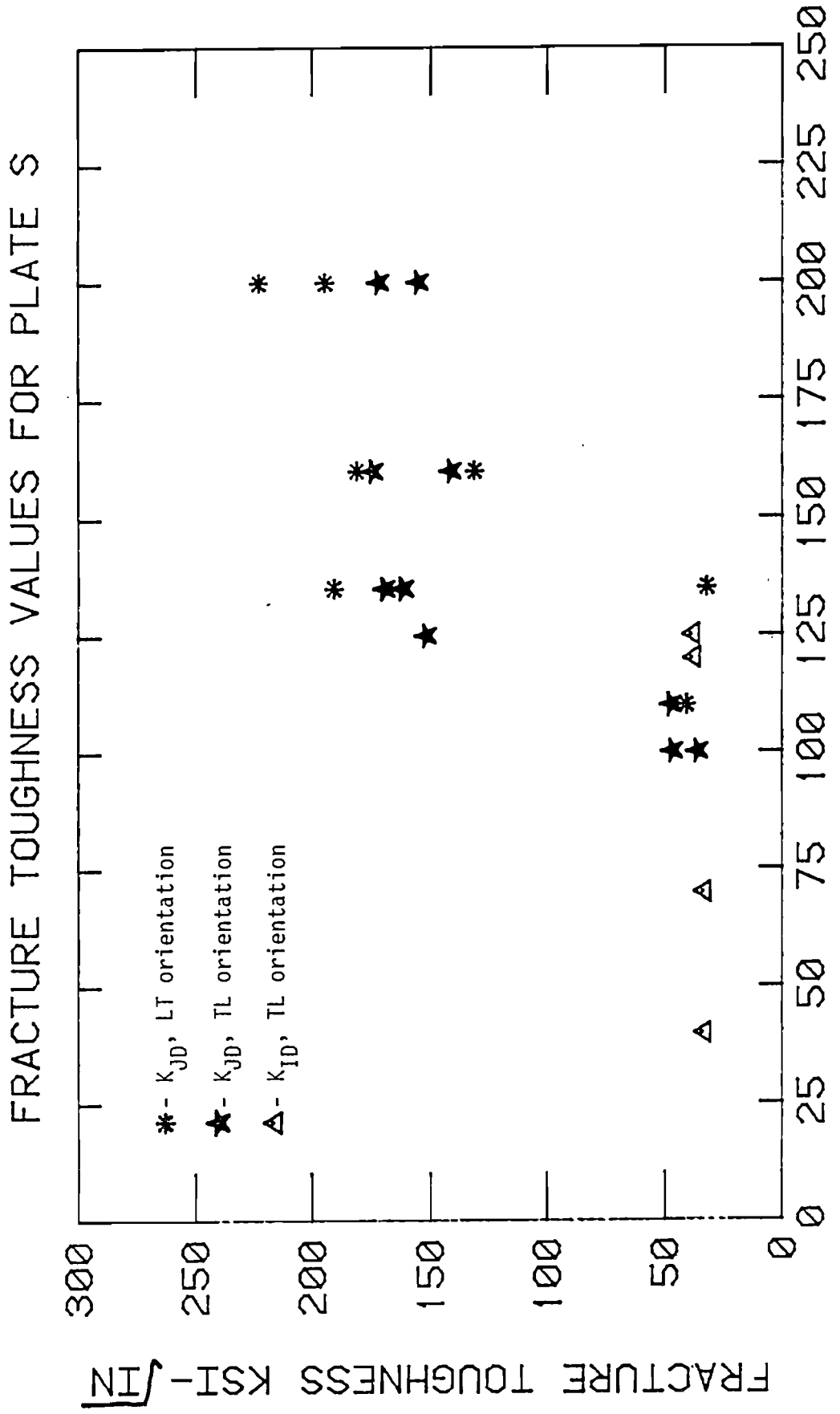

Figure 34. Fracture Toughness Values for Plate S.

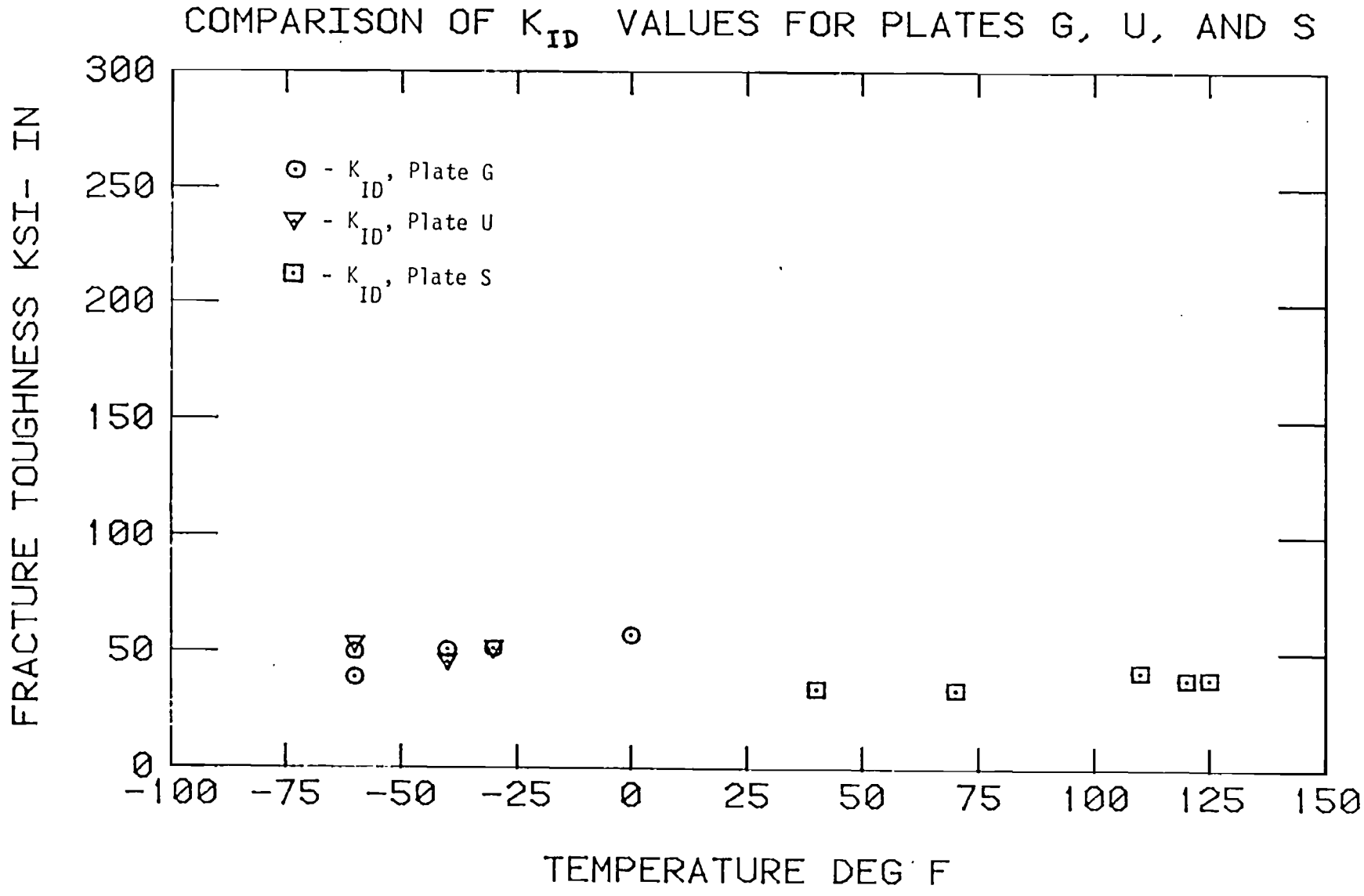

Figure 35. Comparison of K_{ID} Values for Plates G, U, and S.

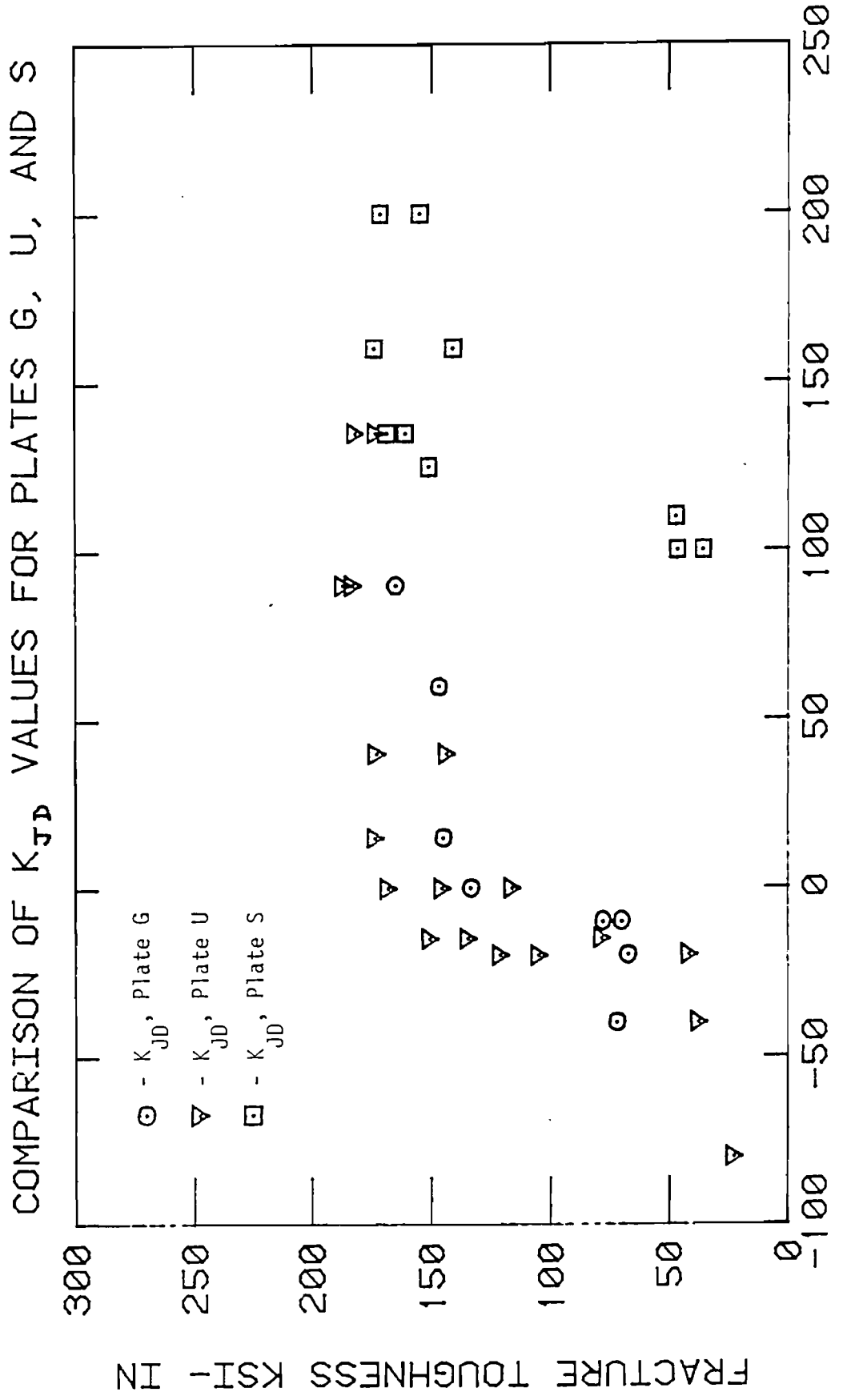

Figure 36. Comparison of K_{JD} Values for Plates G, U, and S.

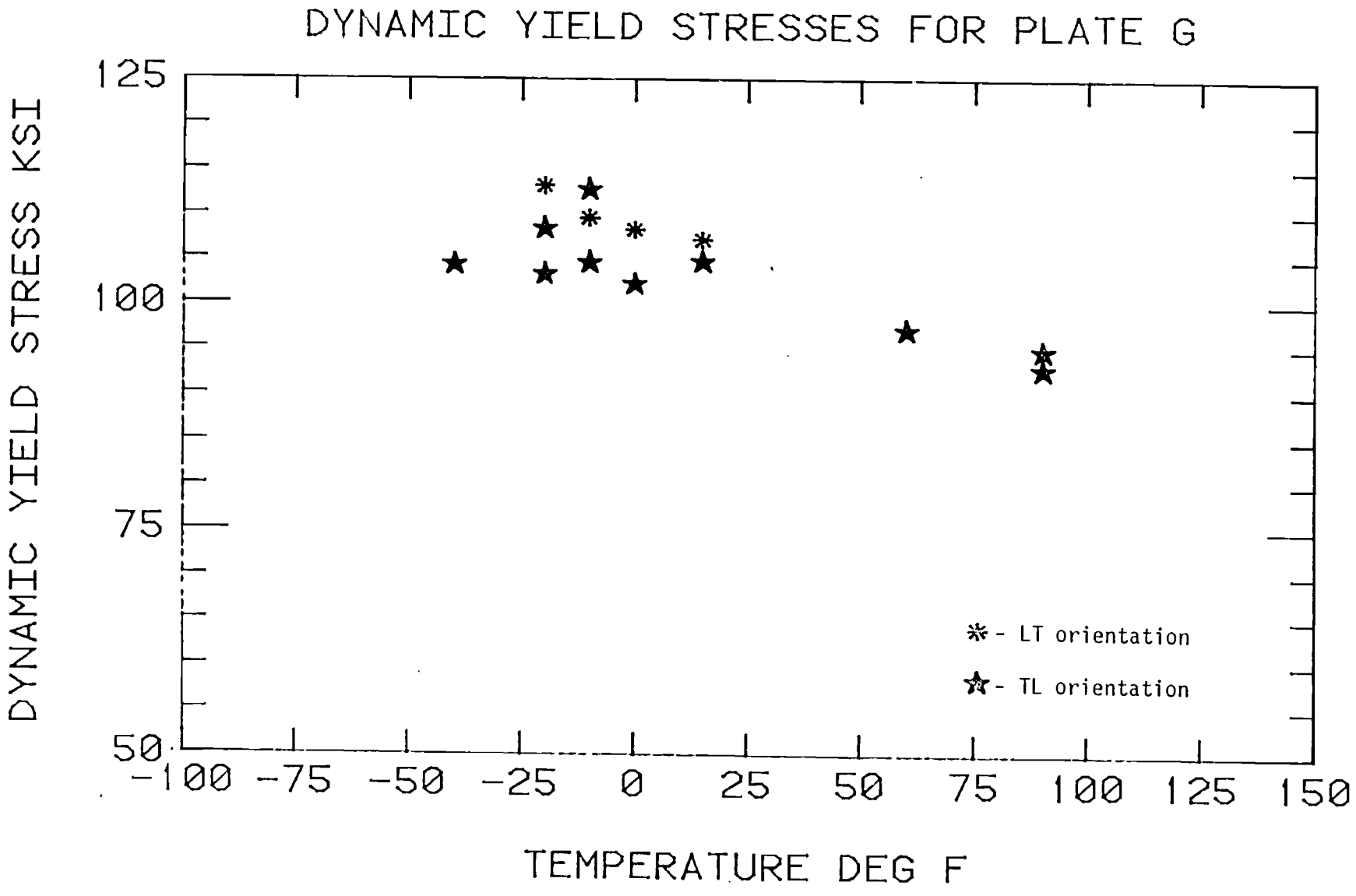

Figure 37. Dynamic Yield Stresses for Plate G.

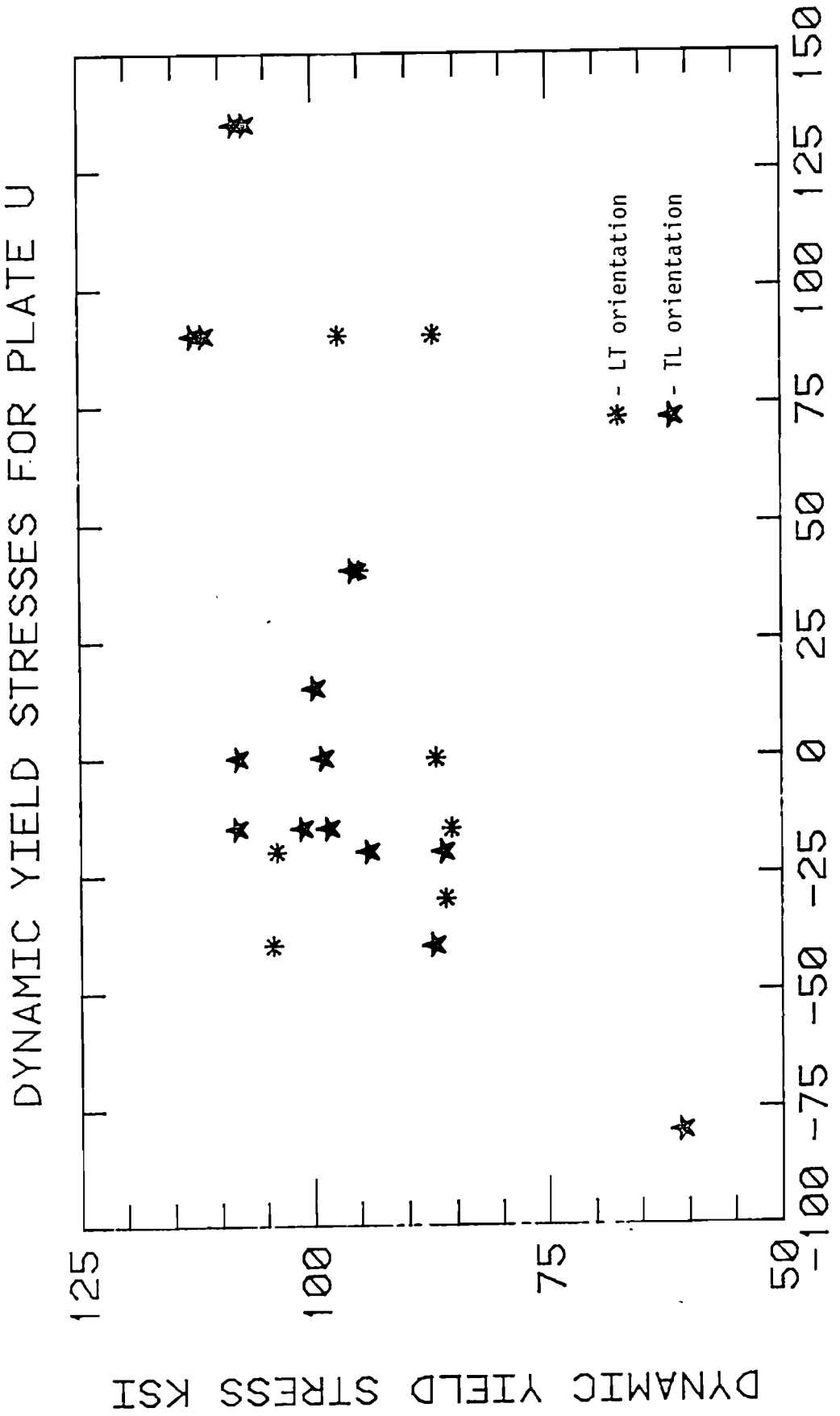

Figure 38. Dynamic Yield Stresses for Plate U.

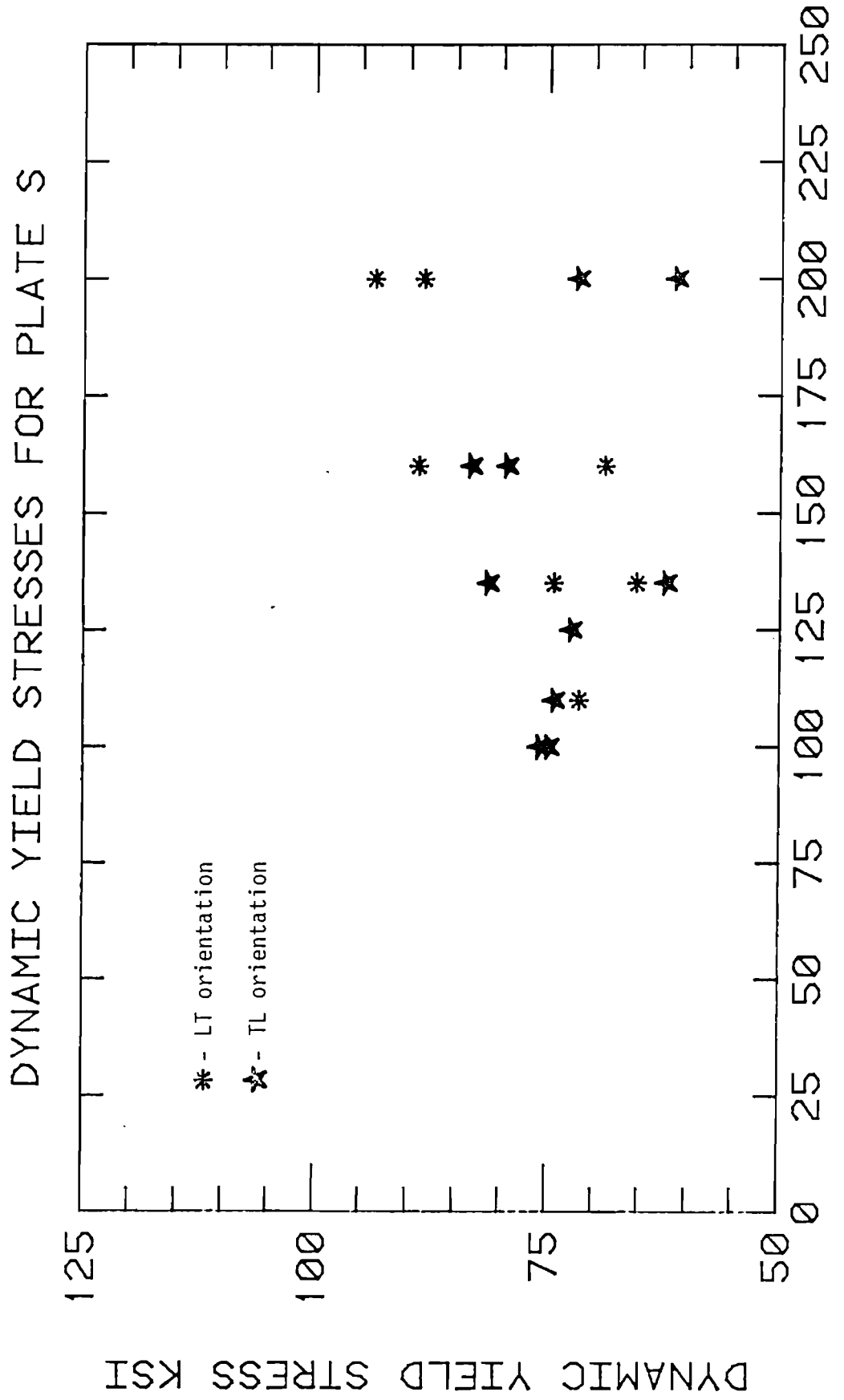

Figure 39. Dynamic Yield Stresses for Plate S.

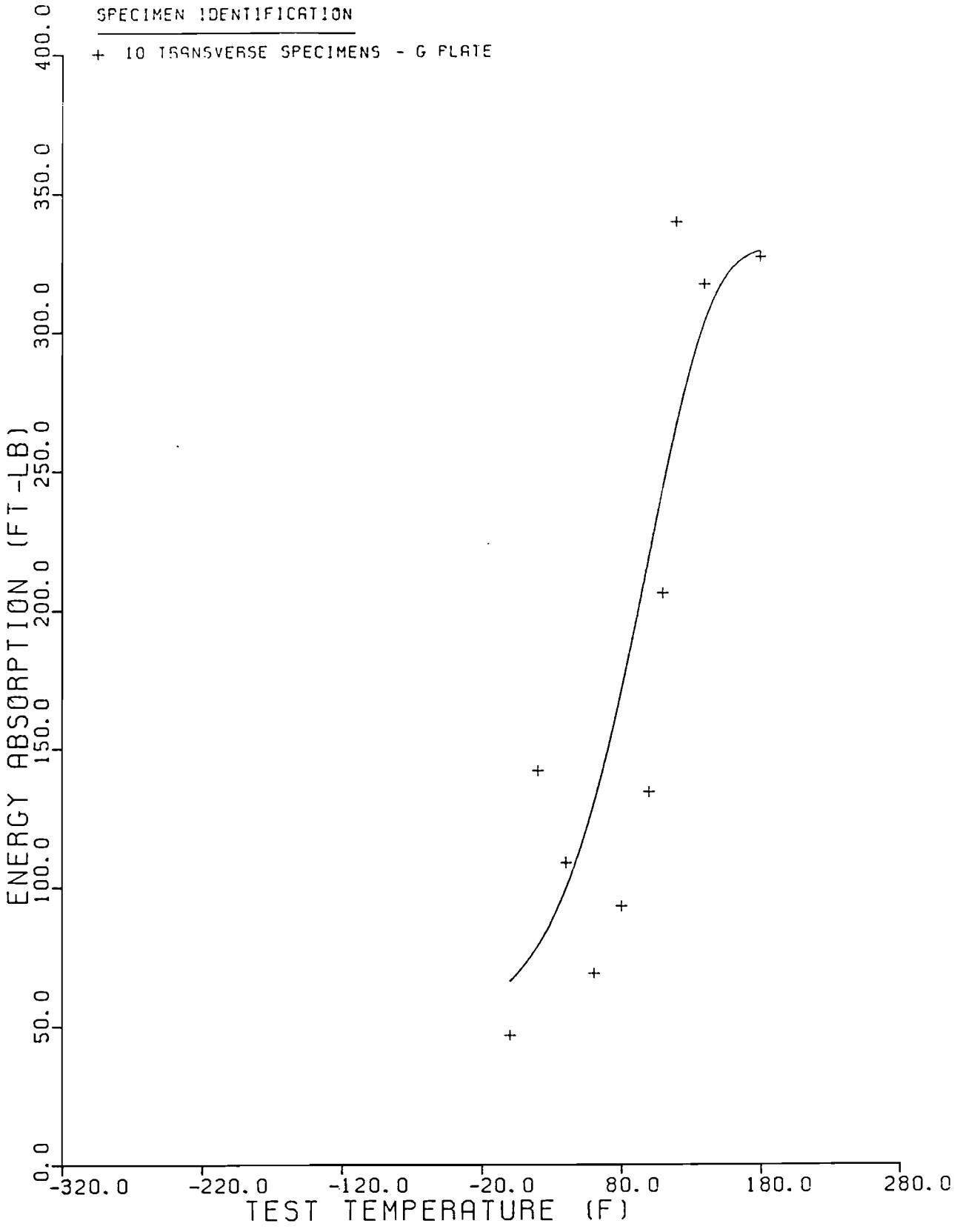

Figure 40. Dynamic Tear-Energy Absorption Values for Plate G.

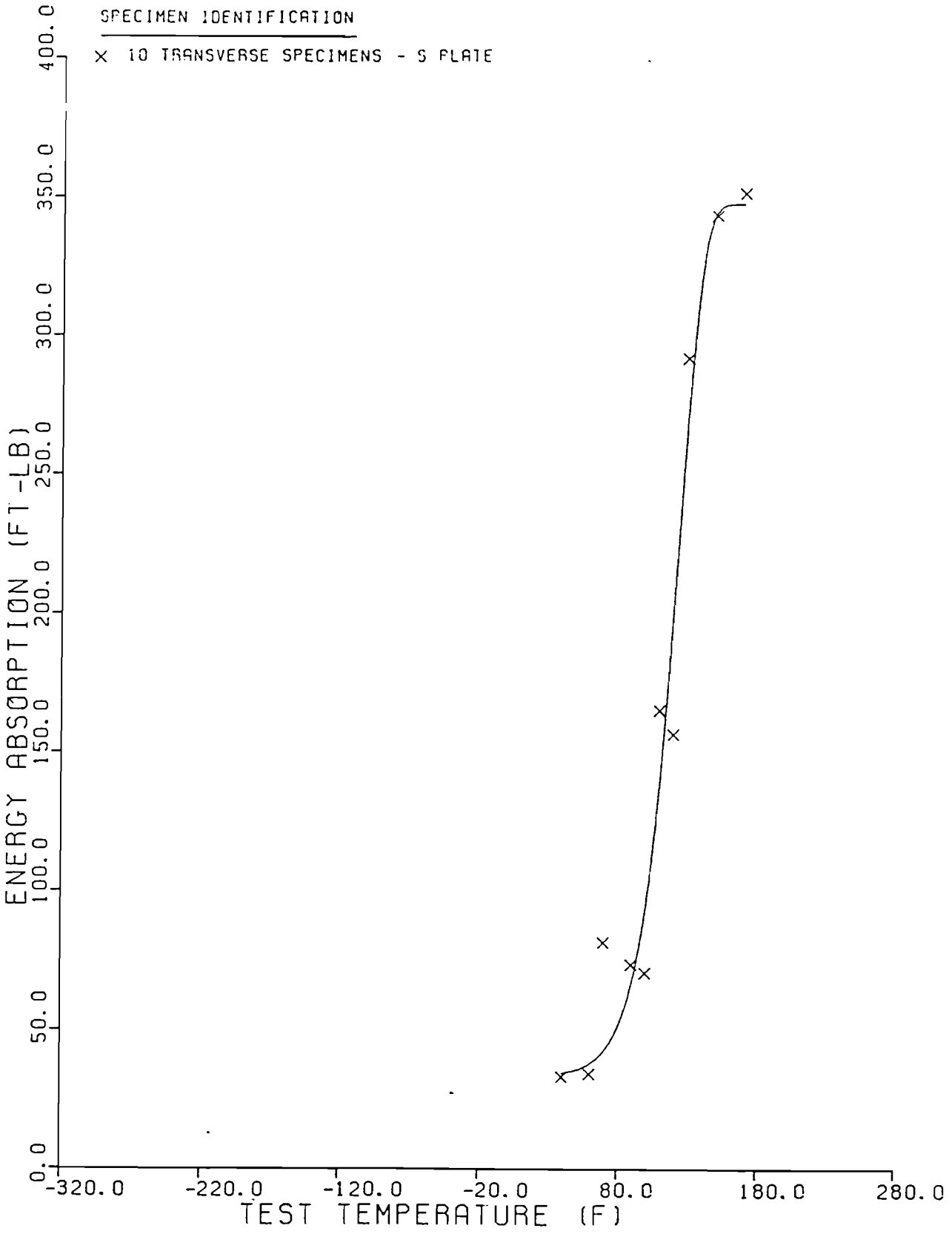

Figure 41. Dynamic Tear-Energy Absorption Values for Plate S.

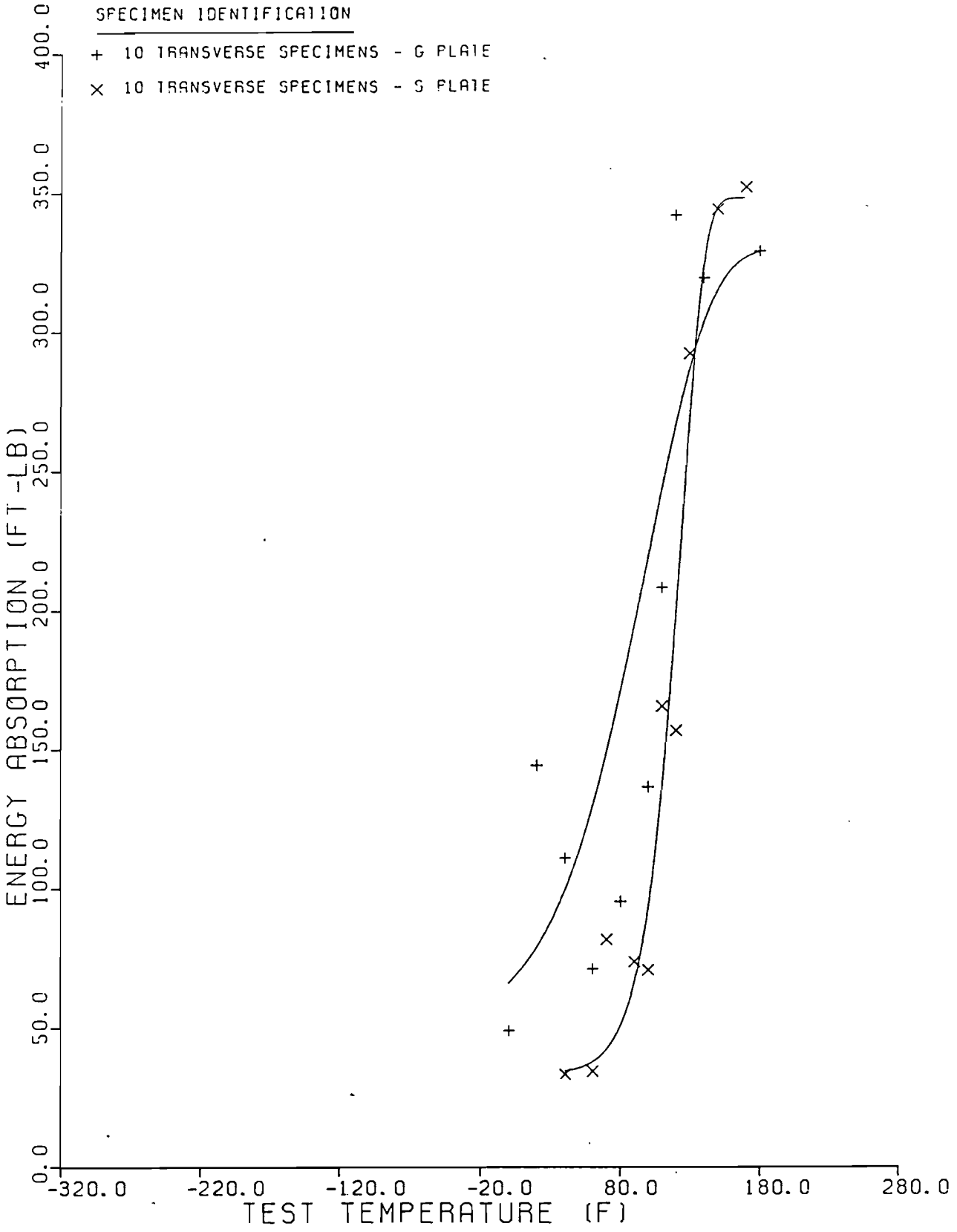

Figure 42. Comparison of Dynamic Tear Results for Plates G and S.

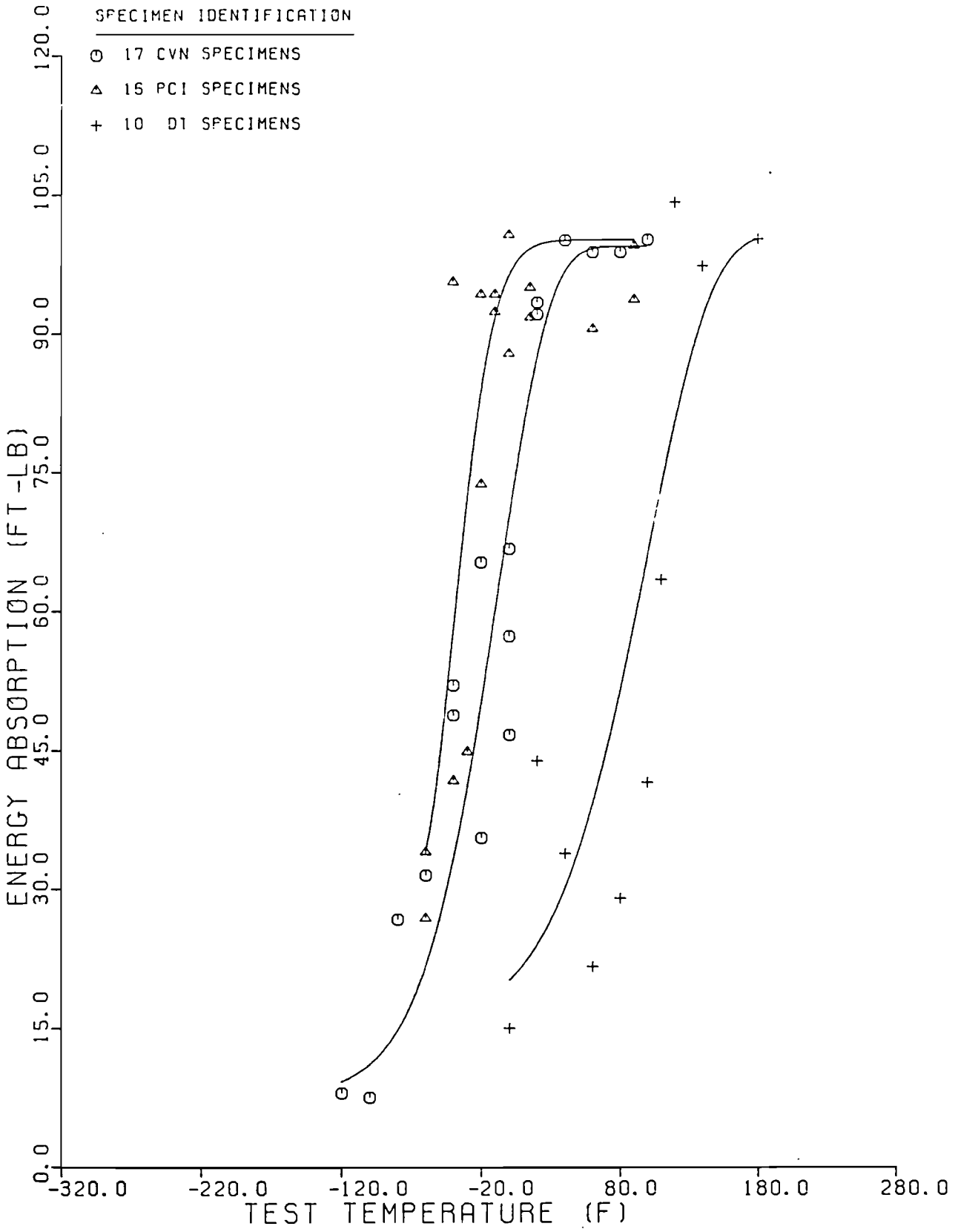

Figure 43. Comparison of Results for CVN, PCI, and DT Tests for Plate G.

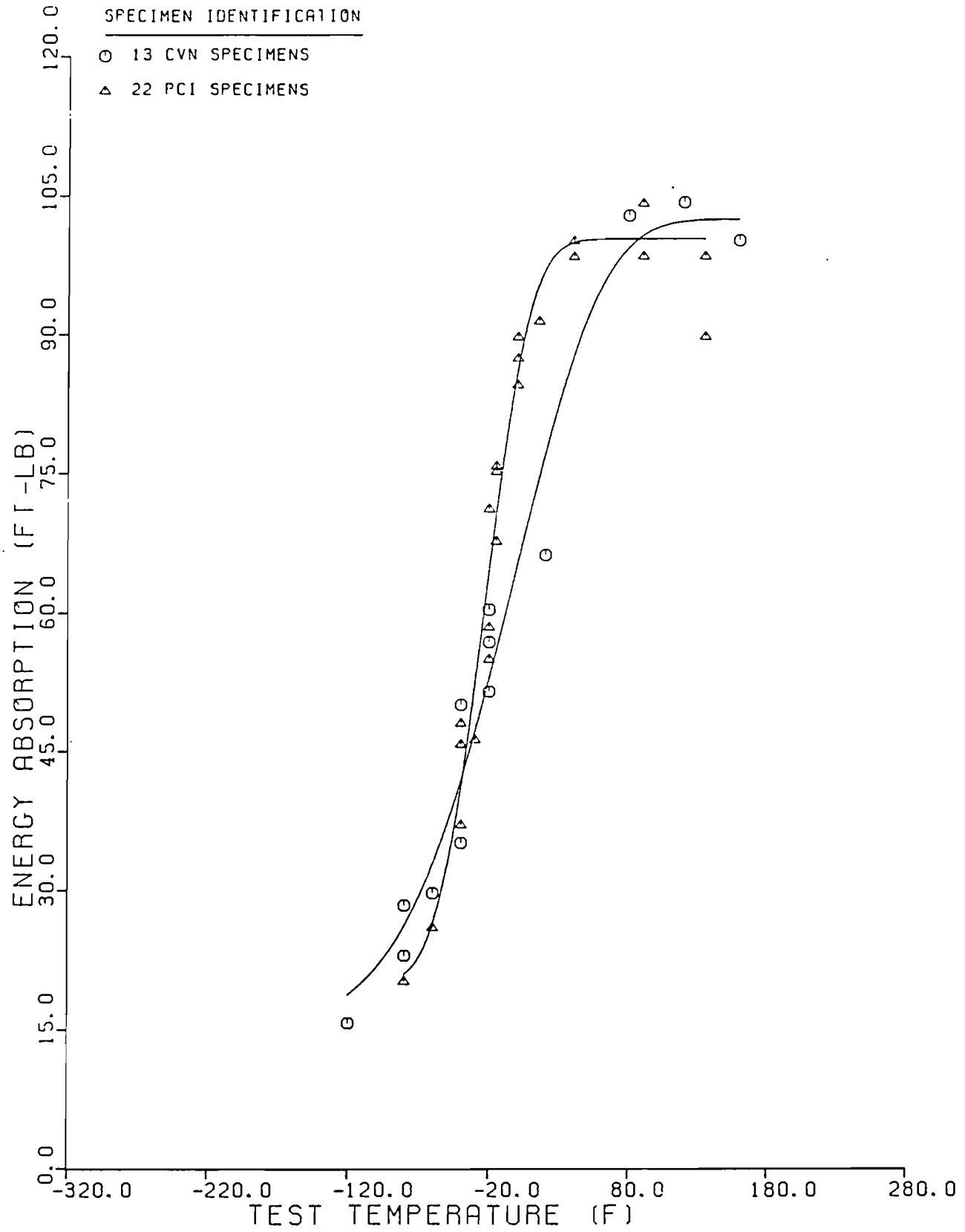

Figure 44. Comparison of Results for CVN and PCI Tests for Plate U.

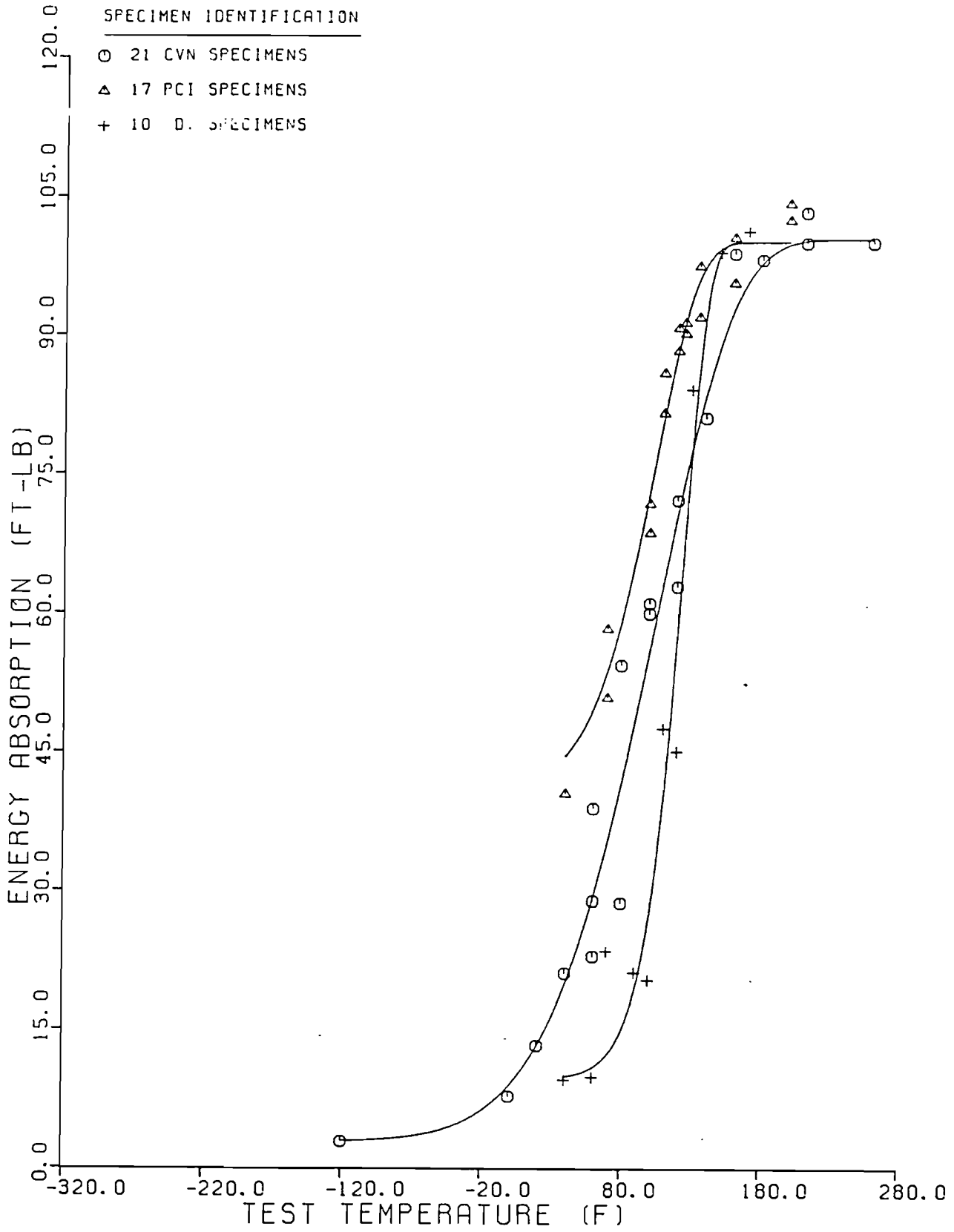

Figure 45. Comparison of Results for CVN, PCI, and DT Tests for Plate S.